3S'15

SYMPOSIUM ON SURFACE SCIENCE 2015

Les Arcs 1800, France
March 22 – 28, 2015

CONTRIBUTIONS

EDITORS
Fabien Cheynis, Stefano Curiotto, Frédéric Leroy,
Pierre Müller - CINaM, Marseille, France
Gilles Renaud - INAC, Grenoble, France

Omicron

Forging Links with Science!

For Decades!

Multi-Module-Cluster-System consisting of:

- *Oxide MBE*
- *Metal MBE*
- *Topological Insulator MBE*
- *Superconducting Material Sputtering*
- *Magnetic Material Sputtering*
- *Surface Analysis*

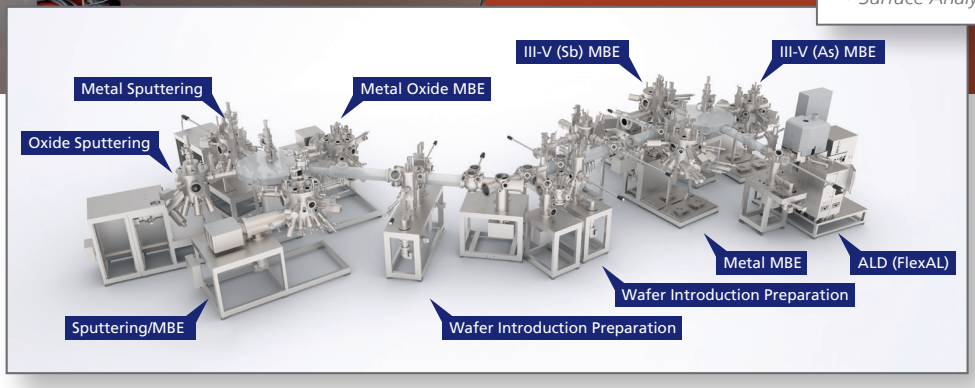

For further information:
sales@omicron.oxinst.com
www.omicron.de

OXFORD INSTRUMENTS
The Business of Science®

Sponsors

The Business of Science®

Limburger Str. 75,
65232 Taunusstein,
Germany
www.oxford-instruments.com

Ankvarnasgatan 14, Uppsal
75308 Sweden
www.vgscienta.com

84 rue de LEVIS 75017 Paris
http://www.neyco.fr

3S'15

SYMPOSIUM ON SURFACE SCIENCE 2015

Les Arcs 1800, France
March 22 – 28, 2015

CONTRIBUTIONS

EDITORS
Fabien Cheynis, Stefano Curiotto, Frédéric Leroy,
Pierre Müller - CINaM, Marseille, France
Gilles Renaud - INAC, Grenoble, France

Organizing Committee:

F. Cheynis, CINaM, Marseille, France
S. Curiotto, CINaM, Marseille, France
F. Leroy, CINaM, Marseille, France
P. Müller, CINaM, Marseille, France
G. Renaud, INAC, Grenoble, France

International Advisory Committee:

A. Arnau, Donostia, Spain
F. Aumayr, Vienna, Austria
E. Bauer, Tempe, USA
H. Daimon, Nara, Japan
U. Diebold, Vienna, Austria
C. Draxl, Berlin, Germany
P. M. Echenique, Donostia, Spain
R. Fasel, Dübendorf, Switzerland
T. Koshikawa, Osaka, Japan
E. Lundgren, Lund, Sweden
D. Menzel, Munich, Germany
K. Morgenstern, Hannover, Germany
P. Müller, Marseille, France
F. Netzer, Graz, Austria
W. D. Schneider, Lausanne, Switzerland
G. Thornton, London, UK
P. Varga, Vienna, Austria

Preface

We welcome all participants and accompanying persons to the 28th Symposium on Surface Science (3S'15).
This symposium belongs to a series of conferences on Surface Science founded in 1993. This year we are happy to host the 3S in the French Alps for the 8th time and more especially in Les Arcs for the 3rd time.
The Symposium on Surface Science seeks to promote effective exchange among scientists working on surface physics and chemistry. In that purpose scientific communications cover many aspects of Surface Science from its fundamental aspects to the most recent applications. In order to facilitate fruitful scientific exchanges, a large amount of time is devoted to informal discussions after each session.
This year the scientific program is divided into several sessions respectively dedicated to 2D materials, Graphene, Molecules at Surfaces, Oxides, Alloys, Surface Reactivity, Electronic Transport, Atomic Probe Microscopies, Spectroscopy and Catalysis. The complete program is built from 63 communications given by scientists from 10 different countries.
The organization committee specially thanks the 3S'15 sponsors as well as all the participants for their scientific contributions.
We hope that all participants will find gathered conditions to experience a friendly and lively meeting full of fruitful scientific discussions and will enjoy the beautiful landscape of Les Arcs 1800.

The organizing committee

History

1983 Obertraun, Austria
1985 Obertraun, Austria
1988 Kaprun, Austria
1990 La Plagne, France
1991 Obertraun, Austria
1992 La Plagne, France
1993 Kaprun, Austria
1994 Les Arcs, France
1995 Kaprun, Austria
1997 Aussois, France
1998 Park City, USA
1999 Pamporova, Bulgaria
2000 Kananaskis Village, Canada
2001 Furano, Japan
2002 St. Christoph/Arlberg, Austria
2003 La Plagne, France
2004 St. Christoph/Arlberg, Austria
2005 Les Arcs 1800, France
2006 St. Christoph/Arlberg, Austria
2007 Les Arcs 2000, France
2008 St. Christoph/Arlberg, Austria
2009 St. Moritz, Switzerland
2010 St. Christoph/Arlberg, Austria
2011 Baqueira Beret/Lleida, Spain
2012 St. Christoph/Arlberg, Austria
2013 Åre, Sweden
2014 St. Christoph/Arlberg, Austria

SYMPOSIUM ON SURFACE SCIENCE 2015

Les Arcs 1800, France
March 22 – 28, 2015

Time Schedule

Monday 23rd March, 2015

Session I: 2D materials

08:20 – 08:40 **H. Dil** 12
Spin structures of polar and ferroelectric materials

08:40 – 09:00 **G. Le Lay** 14
Silicene and Germanene: from monolayers to multilayers

Session II: Graphene

16:20 – 16:40 **V. Repain** 16
Grain boundaries in graphene on SiC(000-1)

16:40 – 17:00 **Y. Coraux** 18
Epitaxial graphene on metal hybrid systems

17:00 – 17:20 **C. Bichara** 20
Interdependency of Subsurface Carbon Distribution and Graphene-Catalyst Interaction

17:20 – 17:40 **G. Renaud** 22
Graphene on Ir structure by synchrotron X-rays

17:40 – 18:00 **D.W. van Baarle** 24
Direct, in situ evidence of various nucleation, ripening and growth mechanisms of graphene on metal surfaces

18:00 – 18:20 **S. Günther** 26
Properties and commensurability of moiré patterns formed by hexagonal coincidence lattices

18:20 – 18:40 **P. Roncin** 28
Atomic and topographic corrugations of graphene on 6H-SiC(0001) derived from Grazing Incidence Fast Atom Diffraction

Tuesday 24th March, 2015

Wednesday 25th March, 2015

Thursday 26th March, 2015

Session IX: Atomic Probes

Session X: Spectro/Transport

Friday 27th March, 2015

Session XI: Catalysis/Reactivity

Monday

Spin structures of polar and ferroelectric materials

S. Muff[1,2], G. Landolt[2,3], J. Krempasky[2], A. Santander-Syro[4], N. Plumb[2], M. Radovic[2], S. V. Eremeev[5,6], E. V. Chulkov[6,7], J. Minar[8], and J. H. Dil[1,2]

[1]*Institut de Physique de la Matière Condensée, Ecole Polytechnique Fédérale de Lausanne, CH-1015 Lausanne, Switzerland*
(corresponding author: Hugo Dil: hugo.dil@epfl.ch)
[2]*Swiss Light Source, Paul Scherrer Institute, 5232 Villigen, Switzerland*
[3]*Physik-Institut, Universität Zürich, 8057 Zürich, Switzerland*
[4]*CSNSM, Université Paris-Sud and CNRS/IN2P3, 91405 Orsay cedex, France*
[5]*Institute of Strength Physics and Materials Science, Russian Academy of Sciences, Siberian Branch, Tomsk, 634021 Russia*
[6]*Tomsk State University, Tomsk, 634050 Russia*
[7]*Donostia International Physics Center (DIPS) and CFM, Centro Mixto CSIC-UPV/EHU, Departamento de Fisica de Materiales, UPV/EHU, 20080 San Sebastian, Spain*
[8]*Department of Chemistry, Ludwig Maximillian University, 81377 Munich, Germany*

For spintronics applications nowadays mainly topological insulators are considered as important materials although many topological insulators are made up of technologically difficult materials. Furthermore, for most applications a tuneable spin- and electronic structure is required, or in the ideal case the spin texture should be inverted. Tuneable and technologically easily implemented materials are mostly found on the trivial side of the distinction of material classes. Although topological insulators might play a role in spintronics applications, we should not let trivial Rashba systems out of sight. In this respect especially materials with strong polar properties are expected to play an important role.

Here we will give an overview of our recent results on the determination of the spin texture of several polar and even ferroelectric materials, both with 2D and 3D band structures. In these types of materials the Rashba-type spin splitting is expected to be enhanced due to the strong local electric fields. Furthermore, the sign of the spin helicity is predicted to be coupled to the local electronic polarization and can thus be switched by an external electric field.

The technological relevance of Rashba systems has previously been limited by the fact that any spin signal of the surface is overshadowed by spin degenerate bulk bands. Here we will show two approached to overcome this serious limitation. The first approach is based on the formation of a Rashba split 2DEG on a truly insulating substrate. By spin- and angle-resolved photoemission (SARPES) we have found that the 2DEG formed at the

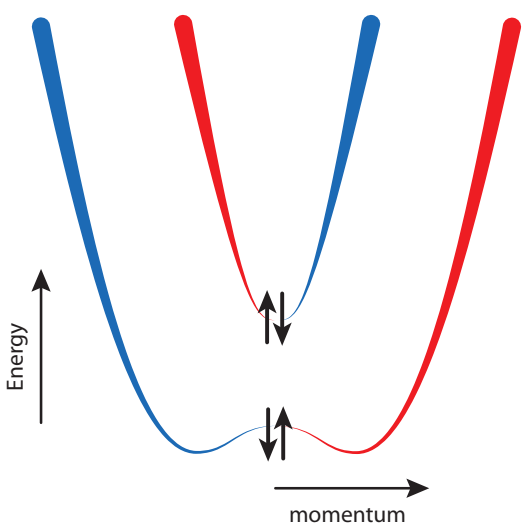

Schematic spin structure of the 2DEG at the surface of $SrTiO_3$

surface of bulk insulating $SrTiO_3$ shows a giant Rashba-type spin splitting [1]. As schematically shown in the figure, due to the presence of magnetic ordering a gap is opened at the Dirac point in this system and combined with the known superconductivity below 250 mK this could create a 2D platform for Majorana physics. It will be shown that the recopy for the formation of such a spin polarized 2DEG can be extended to ferroelectric $BaTiO_3$ [2].

The second approach to reduce the influence of spin degenerate bulk bands on the spin signal is to actually induce a similar spin splitting in these bulk states. In order to achieve this the inversion symmetry in the crystal has to be broken. It will be shown that for BiTeI and BiTeCl this results in a spindle torus shaped 3D Fermi surface [3,4] whereby in the latter we could for the first time follow the spin texture as a function of k_z [5]. Although highly polar, the spin structure in these materials can't be switched as it is intrinsically coupled to the atomic stacking order. To achieve such a switching a ferroelectric materials is needed. Here it will be shown that thin GeTe films are ferroelectric and that both the bulk and surface states of this material exhibit a Rashba-type spin splitting which is directly coupled to the ferroelectric polarization [6].

[1] A. F. Santander-Syro et al. Nature Materials, 13, 1085–1090 (2014).

[2] S. Muff et al. manuscript in preparation.

[3] G. Landolt et al. Physical Review Letters 109, 116403 (2012).

[4] G. Landolt et al. New Journal of Physics 15, 085022 (2013).

[5] G. Landolt et al. submitted to Physical Review Letters.

[6] J. Krempasky et al. submitted to Nature Materials

Silicene and Germanene: from monolayers to multilayers

G. Le Lay
PIIM-CNRS Aix-Marseille Université, Marseille, France
E-mail: guy.lelay@univ-amu.fr

As emergent novel two-dimensional (2D) materials beyond graphene, silicene and germanene, its silicon and germanium based counterparts, artificially created since they do not exist in nature, have attracted enormous interest since 2012 after publication of our seminal paper on the epitaxial synthesis of the archetype 3 × 3 reconstructed monolayer silicene phase in perfect coincidence with a 4 × 4 cell on a silver (111) template [1].

In proper growth conditions at about 200-220°C, 3 × 3 monolayer silicene on 4 × 4 reconstructed Ag(111) (in short 3 × 3 / 4 × 4 silicene) can cover 95% of the substrate surface [2]. However, in most circumstances, 3 × 3 / 4 × 4 silicene co-exists at slightly higher growth temperatures with another rotated silicene phase, namely, ~2% stressed ($\sqrt{7} \times \sqrt{7}$)R(±19.1°) reconstructed silicene in coincidence with $\sqrt{13} \times \sqrt{13}$R(±13.9°) Ag(111) supercells -in short $\sqrt{7} \times \sqrt{7}$ / $\sqrt{13} \times \sqrt{13}$ silicene- existing in four different domains, as imposed by symmetry [3]. Too high substrate temperatures lead, instead of real silicene growth, to the formation of a silicon induced highly disordered ($2\sqrt{3} \times 2\sqrt{3}$)R(±30°) silver superstructure at the verge of dying [4,5].

We have just synthesized in 2014 monolayer germanene, predicted to be a robust 2D topological insulator at nearly room temperature, on a gold (111) substrate as large, nearly flat, $\sqrt{3} \times \sqrt{3}$ reconstructed domains coinciding with Au(111) ($\sqrt{7} \times \sqrt{7}$)R(±19.1°) supercells (in short $\sqrt{3} \times \sqrt{3}$ / $\sqrt{7} \times \sqrt{7}$ germanene), among other two-dimensional structures, still to be characterized in more details [6].

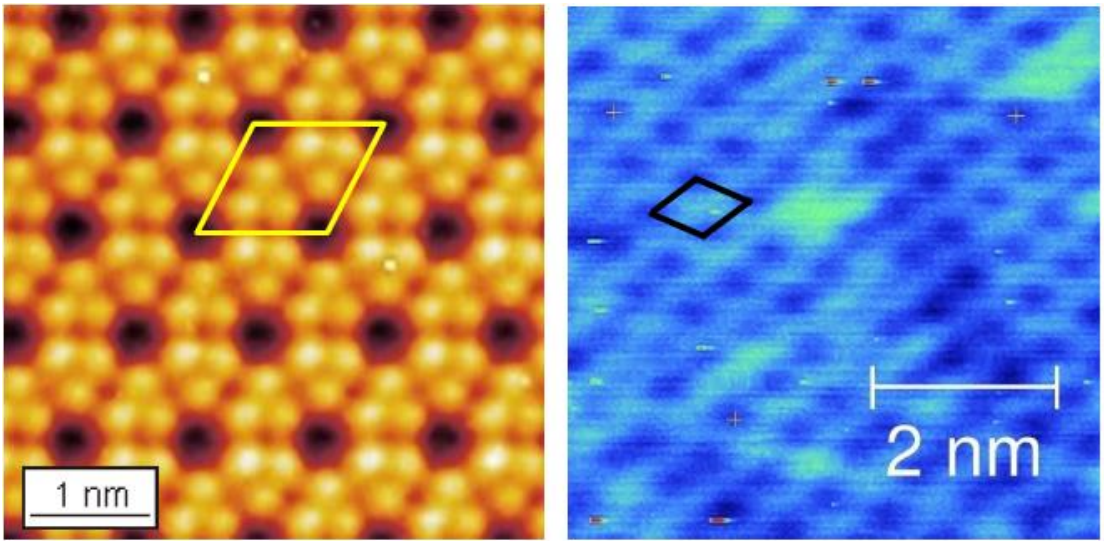

Fig. Scanning tunnelling microscopy images of the archetype 3 ×3 / 4 ×4 monolayer silicene phase (left formed on Ag(111and of the √3 × √3 / √7 × √7 monolayer germanene phase (right) formed on Au(111).

Multilayer germanene has also been obtained upon further epitaxial growth on Au(111), but is still an infant [7].

Starting from bilayer silicene, multilayer silicene, already mature, possesses a unique $\sqrt{3} \times \sqrt{3}$ superstructure formed either on the initial 3×3 / 4×4 silicene phase or on the rotated $\sqrt{7} \times \sqrt{7}$ / $\sqrt{13} \times \sqrt{13}$ ones [8]. Its in-plane lattice parameter is ~4% compressed with respect to that of the prototypical Si(111)$\sqrt{3} \times \sqrt{3}$R(±30°) phase obtained, the other way around, by depositing silver onto a silicon (111) substrate. Strikingly, $\sqrt{3} \times \sqrt{3}$ silicene hosts massless Dirac fermions with a very high Fermi velocity, about a third of that of free standing graphene [9,10], and has a sheet resistance comparable to that of graphite thin films consisting of nano grains [11]. Even more impressive is the stability of multilayer silicene in air: just the very top layers are oxidized, preserving the integrity of the rest of the film underneath [12].

Following the first realization of a Field Effect transistor [13], contradicting a risky prediction by Nobel laureate Andrei Geim [14], this last results is particularly promising for the fabrication of future silicene devices, and, most probably, germanene ones [15].

References

[1] P. Vogt, P. De Padova, C. Quaresima, J. Avila, E. Frantzeskakis, M. C. Asensio, A. Resta, B. Ealet and G. Le Lay, Phys. Rev. Lett. 108, 155501 (2012).
[2] Y. Fukaya, I. Mochizuki, M. Maekawa, K. Wada, T. Hyodo, I. Matsuda and A. Kawasuso, Phys. Rev. B 88, 205413 (12013).
[3] A. Resta, T. Leoni, C. Barth, A. Ranguis, C. Becker, T. Bruhn, P. Vogt and G. Le Lay, Nature Scientific Reports 3, 2399 (2013).
[4] Z.-L. Liu, M.-X. Wang, C. Liu, J.-F. Jia, P. Vogt, C. Quaresima, C. Ottaviani, B. Olivieri, P. De Padova and Guy Le Lay, APL Materials 2, 092513 (2014).
[5] G. Le Lay, S. Cahangirov, L. Xian and A. Rubio, IEEE, 3M-NANO 2014 Proceedings, in press.
[6] M. E. Dávila, L. Xian, S. Cahangirov, A. Rubio and G. Le Lay, New Journal of Physics 16, 095002 (2014).
[7] M. E. Dávila and G. Le Lay, in preparation.
[8] E. Salomon, R. El Ajjouri, G. Le Lay and T. Angot, J. Phys.: Condens. Matter 26 (2014) 185003.
[9] P. De Padova, J. Avila, A. Resta, I. Razado-Colambo, C. Quaresima, C. Ottaviani, B. Olivieri, T. Bruhn, P. Vogt, M. C. Asensio and G. Le Lay, J. Phys.: Condens. Matter 25, 382202 (2013).
[10] P. De Padova, P. Vogt, A. Resta, J. Avila, I. Razado-Colambo, C. Quaresima, C. Ottaviani, B. Olivieri, T. Bruhn, T. Hirahara, T. Shirai, S. Hasegawa, M. C. Asensio and G. Le Lay, Appl. Phys. Lett. 102, 163106 (2013).
[11] P. Vogt, P. Capiod, M. Berthe, A. Resta, P. De Padova, T. Bruhn, G. Le Lay and B. Grandidier Appl. Phys. Lett. 104, 021602 (2014).
[12] P. De Padova, C. Ottaviani, C. Quaresima, B. Olivieri, P. Imperatori, E. Salomon, T. Angot, L. Quagliano, C. Romano, A. Vona, M. Muniz-Miranda, A. Generosi, B. Paci and G. Le Lay, 2D Materials 1, 021003 (2014).
[13] L. Tao, E. Cinquanta, D. Chiappe, C. Grazianetti, M. Fanciulli, M. Dubey, A. Molle and D. Akinwande, Nature Nanotechnol., in press.
[14] A. K. Geim and I. V. Grigorieva, Nature 499, 419 (2013).
[15] G. Le Lay, Nature Nanotechnol., submitted.

Grain boundaries in graphene on SiC(000-1)

J. Lagoute[1], Y. Tison[1], V. Repain[1], C. Chacon[1], Y. Girard[1], S. Rousset[1], F. Joucken[2], R. Sporken[2], F. Gargiulo[3], O. Yazyev[3]

[1] *MPQ, UMR 7162 Université Paris Diderot/CNRS, Paris, France*
[2] *Research Center in Physics of Matter and Radiation, Université de Namur, Namur, Belgium*
[3] *Institute of Theoretical Physics, EPFL, Lausanne, Switzerland*

E-mail: vincent.repain@univ-paris-diderot.fr

Grain boundaries are intrinsically present in graphene samples produced by various synthetic methods. Understanding the structural and electronic characteristics of the grain boundaries is important to master the properties of graphene. Here we report on a comprehensive study by scanning tunneling microscopy (STM) of the properties of grain boundaries in graphene samples grown on SiC(000-1). We investigated several grain boundaries characterized by different misorientation angles measured between the adjacent domains. The STM topographies reveal that the grain boundaries can be either flat and periodic or more disordered and buckled. By investigating a collection of grain boundaries characterized by different misorientation angles, the topographic images reveal a transition between a flat and a buckled regime. The grain boundaries appear buckled for small angles while they are flat for large angles, the transition occurring around 19°. In addition to topographic images, scanning tunneling spectroscopy (STS) was performed to measure the local density of electronic states. In particular we investigated the properties of the 33° grain boundary that is the most stable structure as predicted by ab-initio calculations. Localized electronic states were measured above the Fermi level in this particular structure. This signature is characteristic of the studied grain boundary as evidenced by the comparison with other grain boundaries.

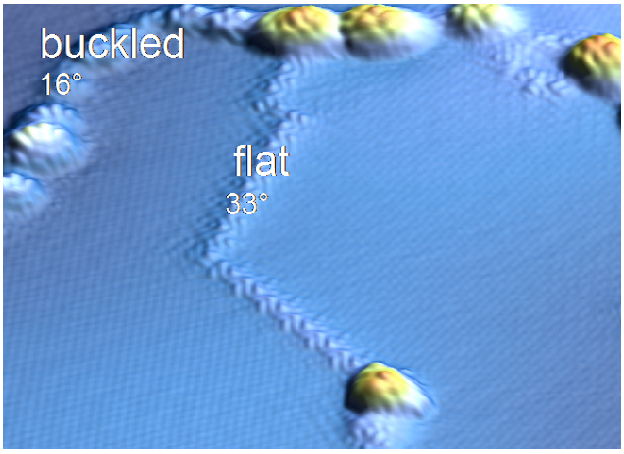

Figure 1 : STM image of buckled and flat grain boundaries in graphene

This study provides fundamental understanding of the properties of graphene samples that contain grain boundaries which may open opportunities for tailoring electronic properties of graphene.

Reference

[1] Y. Tison, J. Lagoute, V. Repain, C. Chacon, Y. Girard . F. Joucken, R. Sporken, F. Gargiulo, O. V. Yazyev, and S. Rousset, Nano Lett. 14, 6382 (2014)

Epitaxial graphene on metal hybrid systems

S. Vlaic[1,2], A. Artaud[3], C. Tonnoir[3], A. Kimouche[1,2], B. Delsol[4], B. Gilles[4], B. Santos[5], A. Locatelli[5], A. T. N'Diaye[6], G. Chen[6], A. K. Schmid[6], L. Magaud[1,2], B. Canals[1,2], N. Rougemaille[1,2], C. Chapelier[3], J. Coraux[1,2]

[1] *CNRS, Inst NEEL, F-38042 Grenoble, France*
[2] *Univ. Grenoble Alpes, Inst NEEL, F-38042 Grenoble, France*
[3] *CEA-INAC/UJF-Grenoble 1, 17 rue des martyrs, 38054 Grenoble cedex 9, France*
[4] *Elettra-Sincrotrone Trieste S.C.p.A., S.S: 14 km 163.5 in AREA Science Park, I-34149 Basovizza, Trieste, Italy*
[5] *SIMAP, Grenoble INP, 1130 rue de la Piscine, BP 75, F-38402 Saint-Martin-d'Hères, France*
[6] *National Center for Electron Microscopy, Lawrence Berkeley National Laboratory, One Cyclotron Road, Berkeley, California 94720,* United States
E-mail: johann.coraux@neel.cnrs.fr

Not only are transition metals convenient platforms for preparing large-area or nanostructured graphene [1], but also they can be exploited for assembling high quality epitaxial hybrid systems. Such systems allow for manipulating the properties of graphene and/or the material contacted to it, as well as inducing novel properties. With the help of in situ scanning tunnelling microscopy (STM) down to very low temperature, low-energy electron microscopy (LEEM, with/without spin-polarized electrons), density functional theory calculations and kinetic Monte Carlo simulations, we explore two such hybrid systems, two of which we we will address in this contribution. They combine graphene with ultrathin ferromagnetic films, and superconducting thin films, respectively.

Cobalt films were prepared by intercalation between graphene and its growth substrate, iridium. We investigated the processes governing intercalation, with special attention paid to the role of point defects, curved regions, and edges of graphene (see Figure (a)). We put in evidence and unconventional growth behaviour in confined epitaxial growth, below the graphene cover [2]. The study of the magnetic properties of the system revealed that the magnetic properties of cobalt are strongly influenced by the graphene/cobalt interface, which pulls the magnetization of the ultrathin film perpendicular to its surface [3]. This strong effect in such an air-protected system offers perspective in view of designing novel spintronics junctions.

Graphene was prepared on rhenium thin films by chemical vapour deposition and temperature-induced surface segregation of carbon, yielding a variety of graphene extensions, from the smallest sizes (see Figure (b)) – graphene clusters comprising several carbon rings – to full coverage. We found that growth proceeds through the formation of graphene nanoclusters of "magic" sizes [4]. Extended graphene sheets exhibit a strong, spatially modulated interaction with rhenium which translates into sizeable variations of the electronic density of state [5]. As a result the electronic transparency of the graphene-rhenium interface is high, which we find results in superconductivity induced in graphene by proximity at low temperature [5]. Such junctions hold promise for the exploration of unconventional superconductivity expected in electron gases hosting Dirac-like quasiparticles such as graphene.

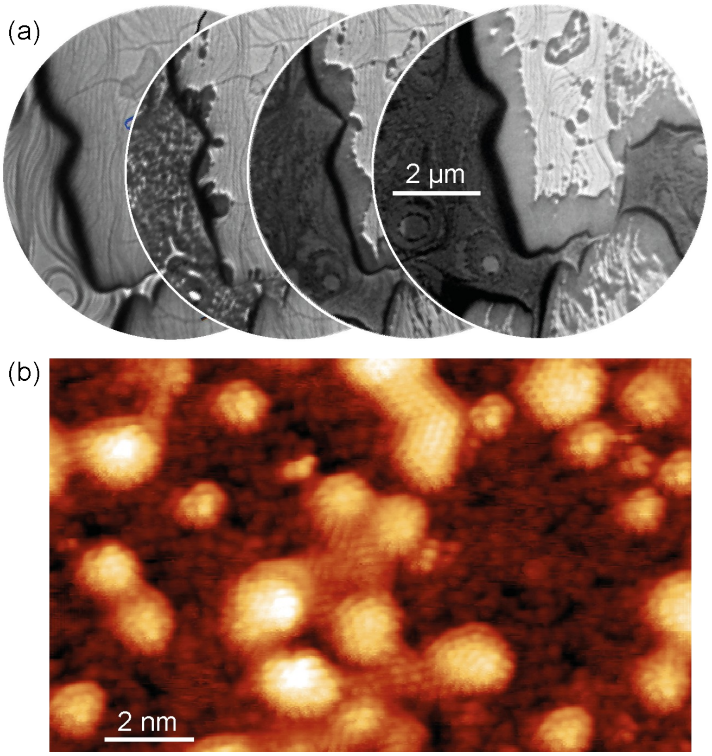

Fig. (a) Series of LEEM images as a function of time as cobalt intercalation proceeds (from left to right) under graphene from its edges. (b) STM topograph of the surface of Re(0001) covered with graphene clusters of well-defined size ("magic") and graphene patches.

Acknowledgements

We acknowledge financial support from ANR through projects NMGEM, NANOCELLS, and SUPERGRAPH, as well as from EU through NMP project GRENADA.

References

[1] H. Tetlow, J. Posthuma de Boer, I. J. Ford, V. V. Vvedensky, J. Coraux, L. Kantorovich, Phys. Rep. 542, 195 (2014)
[2] S. Vlaic, A. Kimouche, J. Coraux, B. Santos, A. Locatelli, N. Rougemaille, Appl. Phys. Lett. 104, 101602 (2014) – S. Vlaic, N. Rougemaille, A. Kimouche, L. Magaud, B. Canals, B. Santos, A. Locatelli, J. Coraux, submitted
[3] J. Coraux, A. T. N'Diaye, N. Rougemaille, C. Vo-Van, A. Kimouche, H.-X. Yang, M. Chshiev, N. Bendiab, O. Fruchart, A. K. Schmid, J. Phys. Chem. Lett. 3, 2059 (2012)
[4] A. Artaud et al., submitted
[5] C. Tonnoir, A. Kimouche, J. Coraux, L. Magaud, B. Delsol, B. Gilles, C. Chapelier. Phys. Rev. Lett. 111, 246805 (2013)

Interdependency of Subsurface Carbon Distribution and Graphene-Catalyst Interaction

H. Amara[1], R. Weatherup[2], F. Ducastelle[1], S. Hofmann[3], C. Bichara[3]

[1] *LEM, ONERA-CNRS, Châtillon, France*
[2] *Department of Engineering, University of Cambridge, Cambridge, United Kingdom*
[3] *CINaM, CNRS, Marseille, France*
e-mail: bichara@cinam.univ-mrs.fr

Growing graphene on a metal surface is one possible way to obtain high quality graphene, with a controllable number of layers. The synthesis usually relies on a chemical vapor deposition of a carbon bearing gas on the surface of a metal such as Ir, Cu, or Ni. We investigate the case of graphene on Ni that is of particular interest because the role of carbon solubility in subsurface layers is both difficult to investigate experimentally and important to understand to produce high quality graphene.

To study the interaction of carbon with nickel at the atomic level, we have developed a tight binding model [1] implemented in a Grand Canonical Monte Carlo code. It has been used to study the nucleation and growth of carbon nanotubes in CVD processes [2]. With the same approach, we investigate the CVD synthesis of graphene on Ni (111) and correlate our results to experimental data [3]. We identify thermodynamic conditions (temperature and carbon chemical potential) to obtain a graphene monolayer. Moreover, depending on the growth conditions, we show that variable amounts of carbon atoms can be found in the subsurface layers, while the first subsurface layer shows a tendency for carbon depletion when graphene covers the Ni surface. With the support of in situ, time-and depth-resolved X-ray photoelectron spectroscopy (XPS), we discuss how this lower stability of carbon close to the surface can be used to control the number of layers [3].

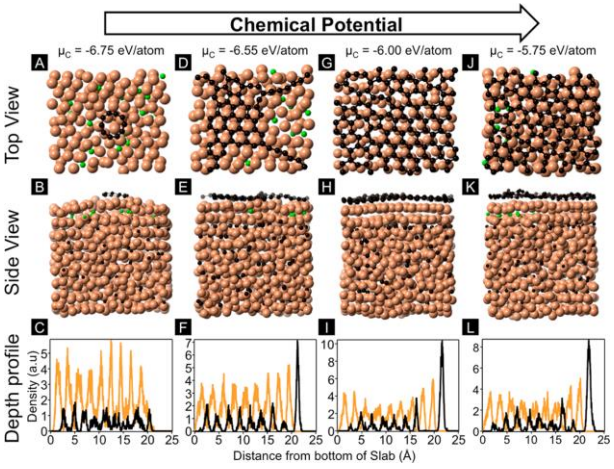

Top views (A, D, G, J), side views (B, E, H, K), and depth profiles (C, F, I, L) of the equilibrium structures obtained from GCMC simulations performed at 1000 K for different C chemical potentials, [μ_C = −6.75 (A−C), −6.55 (D−F), −6.00 (G−I), and −5.50 (J−L) eV/atom]. A 10 atom (2 adjacent hexagons) cluster lying flat on the Ni surface was included as a nucleus, resulting in lower chemical potential values required to grow graphene, as compared to Figure 3. The top and side views show Ni atoms in orange and C atoms in black, except those C atoms in subsurface sites, which are green. The depth profiles show the Ni density as an orange line and the C density as a black line.

Acknowledgements

This research was partially supported by the EU FP7 Work Programme under grant Graphene Flagship (no. 604391).

References

1 H. Amara, J.-M. Roussel, C. Bichara, J.-P. Gaspard and F. Ducastelle Phys. Rev. B ***79***, 014109 (2009)
2 M. Diarra, A. Zappelli, H. Amara, F. Ducastelle and C. Bichara Phys. Rev. Lett. **109**, 185501 (2012)
3 R. Weatherup, H. Amara *et al*., J. Am. Chem. Soc. **136**, 13698 (2014)

Graphene on Ir structure by synchrotron X-rays

F. Jean[1], N. Blanc[1], J. Coraux [1], G. Renaud[2]
[1] *CNRS, Institut Néel, Grenoble, France*
[2] *CEA, Grenoble-Alpes University, INAC/SP2M, Grenoble, France*
E-mail: gilles.renaud@cea.fr

The exceptional properties of graphene can be tailored by small structural modification, such as those induced by the epitaxy on a substrate or by defects. A combined CVD/TPG growth of graphene on Ir(111) was claimed to yield graphene of the highest quality. We have demonstrated [1] that the resulting graphene has tiny imperfections such as small biaxial strain, rotations, shears, and the coexistence of commensurate and incommensurate domains (Fig. 1). These deviations from perfection could only be detected by X-ray diffraction. These structural variations are mostly induced by the increase of the lattice parameter mismatch when cooling down the sample from the graphene preparation temperature. Although graphene only weakly interacts with Ir, its thermal expansion was found positive [2], contrary to free-standing graphene, and was found to follow that of Ir over large temperature ranges. (Fig. 2). The detailed atomic structure of graphene was quantitatively determined by Surface X-Ray Diffraction [3]. The graphene undulation is found to be of small amplitude (0.38 Å), and to be in phase with the Ir (0.017 Å) one (Fig. 3). The structure agrees well with recent *ab initio* calculations. The average graphene-iridium distance is 1.5 times the distance between two Ir(111) planes. The structure was also studied during growth and during the creation of defects [4]. Large strains, above 2%, are present in graphene during its growth on Ir(111) and when it is subjected to oxygen etching and ion bombardment (Fig. 4). Our results unravel the microscopic relationship between point defects and strain in epitaxial graphene and suggest new avenues for graphene nanostructuring and engineering its properties through introduction of defects and intercalation of atoms and molecules between graphene and its substrate. The organized growth of metallic nanoparticle on the graphene's moiré

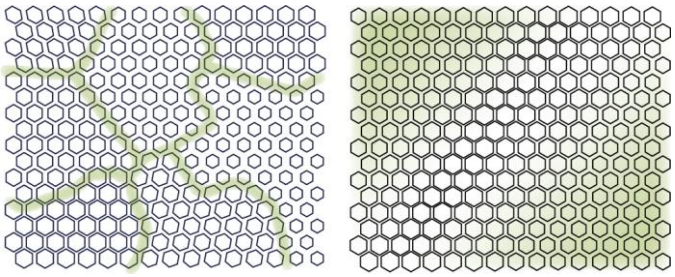

Fig. 1. Graphene deformations mapped onto a regular mesh with hexagons at its nodes, whose shapes represent amplified deformations (strain, rotation, shear), for two cases: left: ~60-nm domains, each having distinct lattice parameter, and right: a domain wall (~100 nm) between two domains having the same lattice parameter.

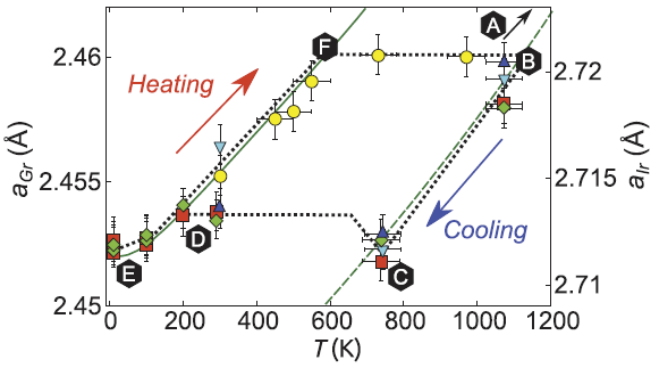

Fig. 2. Graphene lattice parameter aGr (left axis), as a function of temperature . The solid green curve is the evolution of the bulk Ir lattice parameter (right axis) with temperature. The growth is referred to as point A, and measurements began at the lower temperature on point B at 1073 K.

has also been investigated by GISAXS and X-ray diffraction.

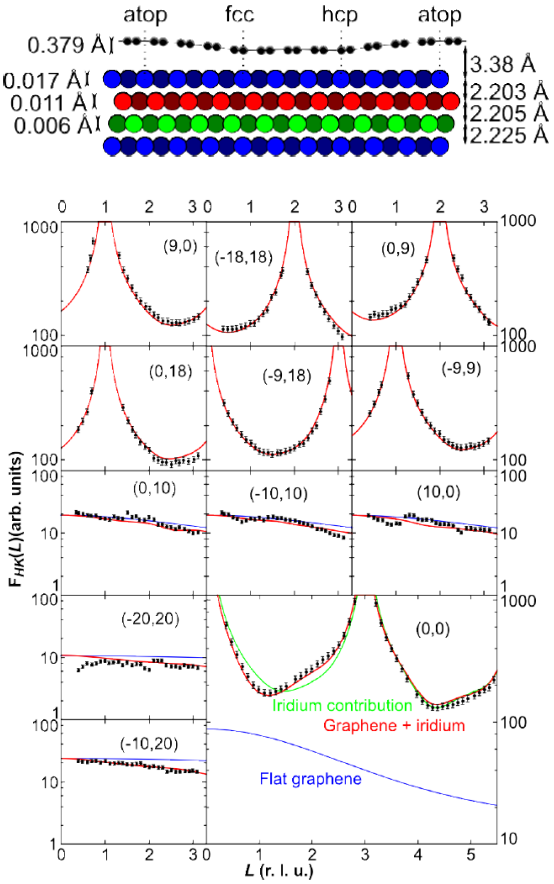

Fig. 4. Top: Schematic side view picture of the atomic structure of graphene on Ir(111). Bottom: Rods from Ir, Gr, moiré, and reflectivity for one ML of graphene on Ir(111), together with best fits.

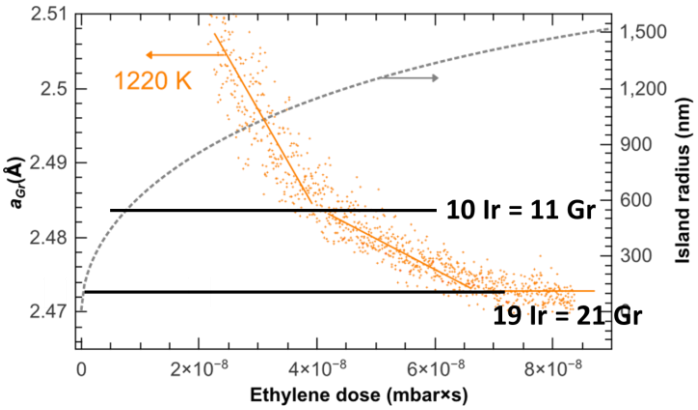

Fig. 3. Graphene deformations mapped onto a regular mesh with hexagons at its nodes, whose shapes represent amplified deformations (strain, rotation, shear), for two cases: left: ~60-nm domains, each having distinct lattice parameter, and right: a domain wall (~100 nm) between two domains having the same lattice parameter.

Acknowledgements

We thank R. Felici and O. Geaymond for their help.
This work was funded thank to French ANR Contract No. ANR-2010-BLAN-1019-NMGEM.

References

[1] N. Blanc et al, Phys. Rev. B 86 (2012) 235439;
[2] F. Jean et al. Phys. Rev. B, **88**, 165406 (2013).
[3] F. Jean et al, submitted
[4] N. Blanc et al, Phys. Rev. Lett. 111 (2013) 085501.

Direct, *in situ* evidence of various nucleation, ripening and growth mechanisms of graphene on metal surfaces

D.W. van Baarle[1], J. Verhoeven[1,2], J.W.M. Frenken[1,2]
[1]Huygens-Kamerlingh Onnes Laboratory, Leiden, The Netherlands
[2]Advanced Research Center for Nanolithography, Amsterdam, The Netherlands

e-mail: baarled@physics.leidenuniv.nl

After the experimental discovery of graphene in 2004, research has created an impressive field of applications of this 2-dimensional material. However, up to now almost no consumer product exists that exploits the unique properties of graphene. One of the hardest barriers that have to be overcome is the unpredictability of the quality of synthesized graphene. Most large-scale production methods of graphene make significant compromises in the quality of the produced graphene, which makes them unreliable.

In our home-built Variable Temperature Scanning Tunneling Microscope (VT-STM), we can perform real-time variable-temperature studies on the nucleation and growth processes of graphene on various substrates. In this manner, both fundamental insight and direct evidence can be obtained of the growth behavior of graphene, with a specific focus on phenomena that lead to either an increase or a reduction of the quality of the synthesized nanolayer. Our results add crucial information and allow us to enter a next level of understanding and prediction concerning the growth process of graphene.

We have selected the system of graphene growth on Ir(111) since this is a well-defined model system, perfect for growth characterization. Although various reports have been published on this system, direct evidence on growth modes and nanometer-scale, spatially resolved observations during growth are lacking. In the experiments reported here, the iridium surface was exposed to hydrocarbons both at room temperature and at elevated temperature, while the surface was monitored with our STM in a temperature window of 300 to 1200K. In this manner, the lowest graphene nucleation temperature, the growth modes and the ripening mechanisms were observed directly.

Additionally, information was obtained on both the preferred graphene orientation and the way in which individual graphene domains coalesc during further high-temperature growth, revealing a major origin of defects in graphene nanolayers.

From our observations, we derive a recipe for mass production of high-quality graphene.

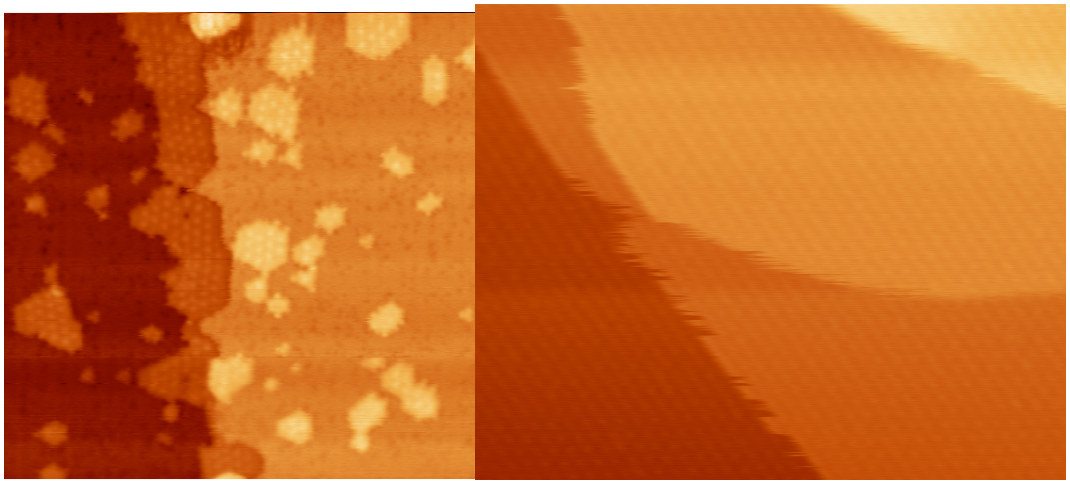

Frames from two STM-movies recorded at elevated temperatures on an Ir(111) surface covered with graphene.
Left: Image from a movie used to follow the ripening mechanism of graphene. Image data: temperature = 1035 K, image width = 75 nm.
Right: Ir(111) surface fully covered with graphene. The three steps in the image are iridium steps underneath the grown graphene. Fluctuations of these steps underneath the graphene are influenced by the direction of the step with respect to both the iridium and the graphene lattice and by the lattice constant of the moiré pattern between the graphene and the metal substrate. Image data: temperature = 1200 K, image width = 85 nm

Properties and commensurability of moiré patterns formed by hexagonal coincidence lattices: applications for metal supported graphene and related materials

Patrick Zeller[1] and Sebastian Günther[2]

[1]Dept.Chemie, Ludwig-Maximilians-Universität München, Butenandtstr.5-13, 81377Munich,Germany
[2]Chemie Department, Technische Universität München, Lichtenbergstr. 4, 85748 Garching, Germany
E-mail: sebastian.guenther@tum.de

After the growth of graphene (g) on transition metal (TM) support surfaces has been identified as one of the promising synthesis routes of this highly wanted material,[1] an old question regained interest: "Which moiré phases are observed when placing hexagonally arranged overlayers on hexagonally packed surfaces?" The same question arises when discussing the properties of other two dimensional materials of hexagonal symmetry, such as hexagonal boron nitride (h-BN), MoS_2, thin metal films, oxide or sulfide phases and similar systems.[2,5] It is also related to the framework of commensurate - incommensurate phase transitions in two dimensions, which is discussed since the 1980ties [6] and involves the solution of so called diophantine equations.[7] The latter is a difficult task and usually the observed moiré patterns are analyzed by trial and error: i.e., two coinciding lattices of a given lattice constant and orientation are plotted one over the other and -if a pattern similar to the experimentally observed one evolves- it is believed that the correct description is found. For certain moiré patterns observed for graphene on hexagonally packed support surfaces an analytical description could be derived,[8-10] but there still exist a variety of other reported moiré patterns for supported graphene which cannot be treated this way.[e.g., 11-13] Thus, a general understanding of the pattern formation including a predictive analytic description is still lacking.

Here, we present a systematic investigation of two coinciding lattices and their spatial beating frequencies that lead to the formation of moiré patterns. We developed a geometric construction that identifies the spatial beating frequencies generated by two coinciding and arbitrarily oriented hexagonal lattices. Analytic expressions for first and higher order beating frequencies present in such patterns are derived and allow the prediction of the size and orientation of the resulting moiré motifs. We can further distinguish between a motif and a potential unit cell of the moiré pattern when adding the constraints of commensurability to our model. In particular, our analysis delivers solvable analytic equations that predict whether or not first or higher order commensurate phases may occur. Their solution can be visualized in so called n-th order commensurability plots. The figure below displays such plots for first, second and third order spatial beating frequencies that are present in moiré patterns. In these plots the left axis represents the lattice constant ratio x of the two coinciding lattices and the horizontal axis the rotational angle φ between the two lattices. The color coding is applied such that darker grey levels correspond to solutions approaching approximate commensurability. Yellow patches indicate areas in the x, φ - parameter space, where true commensurability is reached. If the moiré pattern is commensurate, a unit cell exists that is part of both, the graphene (g)- and the transition metal support (TM)-lattice, i.e. it contains a unit cell vector, which can be indexed by $(m,n)_{TM}$ and $(r,s)_g$ at the same time. These indices relate to four analytic equations. Their solutions are displayed as curves in each plot (red/dark

blue for $(m,n)_{TM}$ and green/light blue for $(r,s)_g$). Where all four curves intersect each other, commensurability is reached, i.e. the moiré pattern has a unit cell vector of the type $(m,n)_{TM}$ and $(r,s)_g$. The right vertical axis displays the g-lattice constant for g-Ir(111) and g-Pt(111) relating to the lattice constant ratio x (left vertical axis). The so called R0°, R14°, R18.5° and R30°- moiré of g-Ir(111) as well as the reported R0°, R19.1°, R23.4° and R30°- moiré of g-Pt(111) are found by our analysis and are correctly indexed. Our approach is universal and can be used for the description of moiré patterns formed not only by supported graphene but by any hexagonally arranged thin layer on any hexagonally packed support surface.

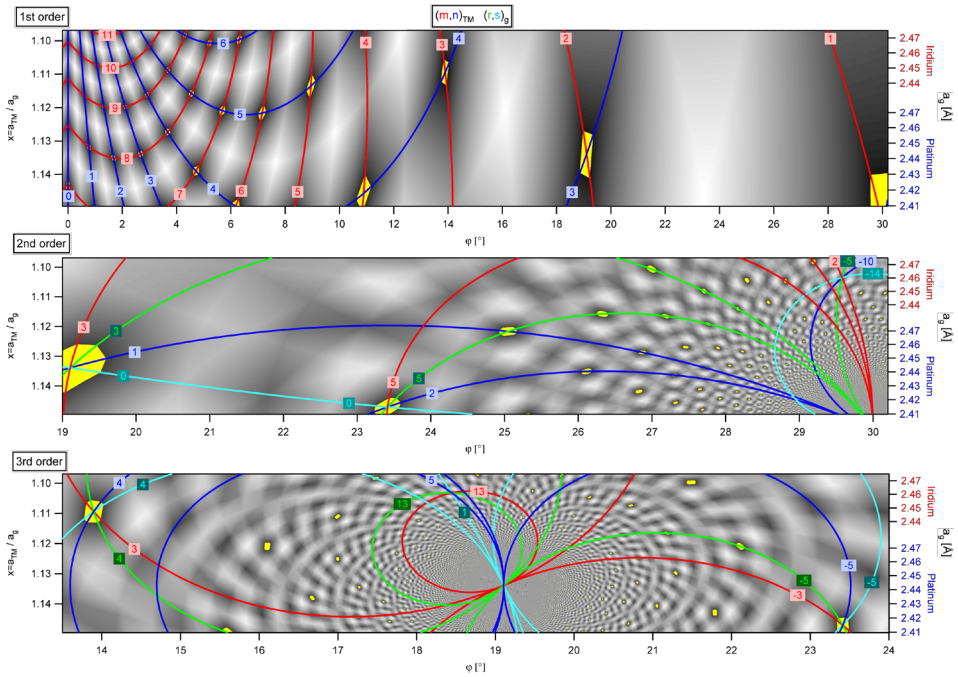

Fig.: Commensurability plots indicating the areas in parameter space (x: ratio of the g- and TM-lattice constant, φ: rotation angle between the g- and TM-lattice) where moiré patterns are commensurate (yellow patches). The right axis displays the g-lattice constant for g-Ir(111) and g-Pt(111) showing that all reported moiré patterns of these systems are correctly predicted and indexed (see text).

Acknowledgements

We acknowledge financial support by the German Research Foundation (DFG) in the framework of the Priority Program 1459 "Graphene".

References

[1] M. Batzill, *Surface Science Reports* **67,** 83-115 (2012).
[2] M. Xu, T. Liang, M. Shi and H. Chen, *Chemical Reviews* **113,** 3766-98 (2013).
[3] C. Günther, J. Vrijmoeth, R.Q. Hwang and R. Behm, *Physical Review Letters* **74,** 754-7 (1995).
[4] K.M. Ostyn and C.B. Carter, *Surface Science* **121,** 360-74 (1982).
[5] T. Wiederholt, H. Brune, J. Wintterlin, R. Behm and G. Ertl, *Surface Science* **324,** 91-105 (1995).
[6] P. Bak, *Reports on Progress in Physics* **45,** 587, (1982).
[7] A. Tkatchenko, *Physical Review B* **75,** 235411 (2007).
[8] A. N'Diaye, J. Coraux, T. Plasa, C. Busse, T. Michely, *New Journal of Physics* **10** 043033 (2008).
[9] J. Coraux, A.T. N`Diaye, C. Busse and T. Michely, *Nano Letters* **8** 565-70 (2008).
[10] K. Hermann, *Journal of Physics: Condensed Matter* **24** 314210 (2012).
[11] P. Merino, M. Švec, A. L. Pinardi, G. Otero and J.A. Martín-Gago, *ACS Nano* **5** 5627-34 (2011).
[12]M. Enachescu, D. Schleef, D.F. Ogletree and M. Salmeron, *Physical Review B* **60,** 16913-9(1999).
[13]E. Loginova, S.Nie, K.Thürmer, N.C.Bartelt, K.F. McCarty, *Physical Review B* 80 085430 (2009).
[14] P. Zeller and S. Günther, *New Journal of Physics* **16,** 083028 (2014).

Atomic and topographic corrugations of graphene on 6H-SiC(0001) derived from Grazing Incidence Fast Atom Diffraction

A. Zugarramurdi[1], M. Debiossac[1], P. Lunca-Popa[1], A. Mayne[1], A. Momeni[1,2], A.G. Borisov[1], Z. Mu[1], P. Roncin[1] , H. Khemliche[1]

[1] Institut des Sciences Moléculaires d'Orsay, CNRS/Université Paris-Sud, F-91405 Orsay, France
[2] Université de Cergy-Pontoise, 33 Boulevard du Port, F-95031 Cergy, France

Abstract
The exceptional properties of graphene and the prospect to use it as the new material for next generation micro- and nano-electronic devices are still waiting for major advances in the production methods in terms of scaling and cost. Current efforts to develop an effective process for producing large samples of high quality graphene could be made easier if characterization techniques, which provide reliable information on sensitive properties such as geometric corrugation, domain size, number of layers and their relative orientation, were able to operate in situ or if possible in real time during the growth process. Supported graphene most often exhibits a Moiré superstructure that originates from local anchoring of the graphene layer onto the substrate. The corresponding corrugation, of geometric origin and which provides a good estimate of the coupling strength between the carbon layer and the substrate, has a strong influence on the graphene properties. For instance the relationship between corrugation and thermal stability of graphene/Re(0001) has been demonstrated [1]. Yet precisely quantifying the corrugation of the Moiré has not become systematically accessible. As an illustration, figures of the superstructure corrugation of graphene grown on Ru(0001) differ substantially whether you consider density-functional-theory calculations [2], STM [3], XRD [4] or Helium Atom Scattering (HAS) [5].

Experiment.

We have used another method: Grazing Incidence Fast Atom Diffraction (GIFAD also called FAD [6 for a review]), to derive *on equal footing* both the atomic and the geometric corrugations with high sensitivity. In terms of interactions, GIFAD is very similar to the HAS technique used by Borca *et al.*[5]. However GIFAD uses helium atoms in the keV energy range in a scattering geometry comparable to that of RHEED; the diffraction pattern is recorded at once on a position sensitive detector and the image captured by a CCD camera. More fundamental, due to grazing geometry, the scattering of the helium atom is spread over all the carbon atoms encountered along it trajectory allowing a *drastic increase* of the Debye-Waller coherence factor [7]. As a result, GIFAD was shown to be able to operate both at high temperatures [8] and at "effective" normal energies much larger than those used in FAD. The clear advantage of using incidence angle θ such that the normal energies $E_\perp = E_0 \sin^2\theta$ above 50-100 meV normal energies, is the helium projectile is hardly sensitive to the polarization forces [9,10] allowing GIFAD to operate just like and AFM in the reciprocal space.

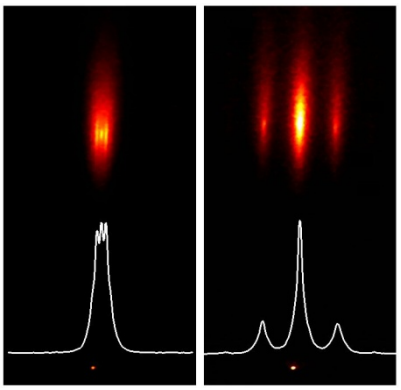

Fig. 1. Diffraction patterns measured with 300 eV He along the armchair (left) and ziz-zag (right) directions. The bottom profile is the horizontal projection of the diffraction pattern.

Figure 1 shows diffraction patterns measured with 300 eV He on a single layer graphene grown on 6H-SiC(0001). The graphene honeycomb six fold symmetry was found to have interesting geometric properties with respect to averaging. Along the zig-zag (right-hand side) direction, the projectile is perpendicular to a C-C bond (blue arrows in fig. 2) allowing high contrast between middle and top of the C-C bond. In this direction, the data (peak separation) indicate a period is 2.13 Å as expected for graphene atomic structure and no clear sign of any moiré structure except for the comparatively broad base of the diffraction peaks. At variance, along the armchair direction (left-hand side in fig.1 and red arrows in fig.2), only the topographic corrugation of the Moiré superstructure is observed. The measured period is 16 Å, it corresponds to the 13x13 phase of graphene, which is commensurate with the $(6\sqrt{3}x\ 6\sqrt{3})R30$ of the SiC(0001) [11]. The fact that atomic and topographic corrugation appear along separate direction is because both structures have hexagonal symmetry but rotated by 30° (fig. 3 and *R30* index) so that they are not clearly visible together in GIFAD.

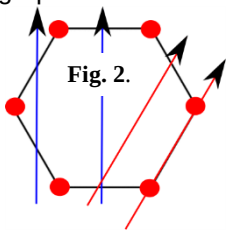

Theoretical description.

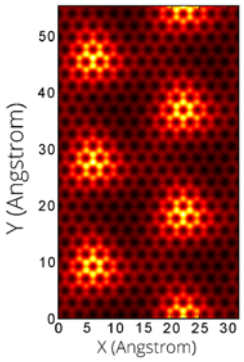

Fig. 3. Constant-height image of the He-graphene potential-map following optimized scaling of data from Varchon *et al* [15] to the experimental diffraction data.

We describe the He-surface interaction using a Lennard-Jones He-C pair-wise potential [12] that has been optimized to reproduce HAS data on graphite. We have considered a graphene layer frozen at its equilibrium position [13] and calculated the diffracted intensities with a close coupling code described in [14]. Without any adjustment, the calculated diffraction probabilities in the zig-zag direction are comparable to the measured values, thus providing confidence on the validity of the He-C interaction potential.

The Moiré structure is introduced by modulating the atom vertical positions on a 13x13 superlattice according to a model-corrugation adjusted to the *ab initio* data reported by Varchon *et al*. [15]. In this case, the calculated diffraction probabilities along the armchair direction do not reproduce the experimental data. However a good agreement is achieved if the Moiré corrugation from Varchon *et al*. is scaled by a factor 0.66 [16]. Figure 3 shows the atomic structure that best fits our diffraction data, the corresponding geometric corrugation is 0.27 ±0.03 Å.

These results demonstrate the capability for GIFAD for resolving the structure of epitaxial graphene. The GIFAD sensitivity, together with its ability to operate at high temperatures makes this technique a good candidate for real time monitoring of graphene growth.

References

[1] E. Miniussi et al. Phys. Rev. Lett. **106**, 216101 (2011)
[2] D. E. Jiang, M. H. Du, and S. Dai, J. Chem. Phys. **130**, (2009) 074705
[3] S. Marchini, S. Günther, and J. Wintterlin, Phys. Rev. B **76**, 075429 (2007)
[4] D. Martoccia *et al.*, New Journal of Physics **12**, 043028 (2010)
[5] Borca *et al*., New Journal of Physics **12**, 093018 (2010)
[6] H. Winter and A. Schüller Prog. in Surf. Science **86**, p169 (2011).
[7] P. Rousseau *et al.*, Journal of Physics. Conf. Series, **133** p.012013 (2008)
N. Bundaleski *et al.*, NIM B, **269**, 11, p 1216–1220 (2011)
[8] P. Atkinson *et al.*, Applied Physics Letters, **105**, p. 021602, (2014)
[9] M. Debiossac *et al.*, Phys. Rev. B, vol. **90**, p. 155308, (2014).
[10] M. Debiossac *et al.* Phys. Rev. Lett, vol. **112**, p. 023203, (2014)
[11] C. Riedl, C. Coletti, and U. Starke, J. Phys. D: Appl. Phys. **43**, 374009 (2010)
[12] W.E. Carlos, and M.W. Cole, Surf. Sci. **91**, 339 (1980)
[13] J.R. Manson, Theoretical Aspects of Atom-Surface Scattering, edited by E. Hulpke, Springer Series in Surface Sciences, Vol.27 (Springer-Verlag, Berlin, 1992)
[14] A. Zugarramurdi, and A.G. Borisov, Phys. Rev. A **87**, 062902 (2013)
[15] F. Varchon, P. Mallet, J.-Y. Veuillen, and L. Magaud, Phys. Rev. B **77**, 235412 (2008)
[16] A. Zugarramurdi et al. Submitted.(2014)

Transmission of slow highly charged ions through graphene and ultrathin carbon nanomembranes

F. Aumayr[1], R. A. Wilhelm[2], E. Gruber[1], R. Ritter[1], R. Heller[2] and S. Facsko[2]

[1] *Institute of Applied Physics, TU Wien, Wiedner Hauptstr. 8-10/E134, 1040 Vienna, Austria*

[2] *Institute of Ion Beam Physics and Materials Research, Helmholtz-Zentrum Dresden-Rossendorf, Bautzner Landstr. 400, 01328 Dresden, Germany*

E-mail: aumayr@iap.tuwien.ac.at

The production of nanostructures by slow highly charged ions (HCIs) on surfaces has been a hot topic in the last years [1]. We have recently discovered that the impact of individual HCIs is able to create permanent nano-sized hillocks on the surface of a CaF2 single crystal [2]. The experimentally observed threshold of the projectile's potential energy necessary for hillock formation could be successfully linked to a solid-liquid phase transition (nano-melting) [1 - 3]. Meanwhile a variety of materials has been found, which is susceptible to nano-structuring by the impact of slow HCI [1]. The nature, appearance and stability of the created structures, however, depend heavily on the properties of the target material and the involved interaction processes (determined by the potential and kinetic energy of the projectiles) [3]. Not in all cases nano-hillocks are formed on the surface but also nano-craters or -holes have been found, e.g. on KBr [4] or PMMA [5].

Starting from a different point as compared to a solid bulk material, in this contribution we present investigations in which freestanding 1nm thick carbon nanomembranes (CNMs) and grapheme sheets are irradiated with individual slow highly charged ions. CNMs are engineered two-dimensional carbon nanolayers, which are produced by cross-linking of an aromatic self-assembled monolayer of biphenyl units with low-energy electrons as described in [6]. The substrate is then subsequently removed and the resulting nanomembrane is transferred onto a TEM grid.

We analyse the charge state and energy loss of projectiles transmitted through the CNMs [7] as well as present transmission electron microscope (TEM) and helium ion microscope (HIM) images of nano-pores produced by impact of individual HCIs [8].

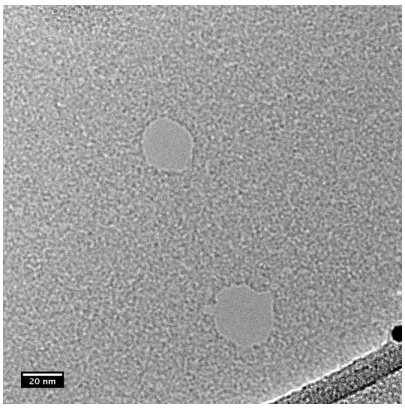

Fig. 1. TEM image of 2 nano-pores in a carbon nanomembrane induced by impact of two Xe^{40+} ions (E_{kin} = 40 keV, E_{pot} = 38.5 keV).

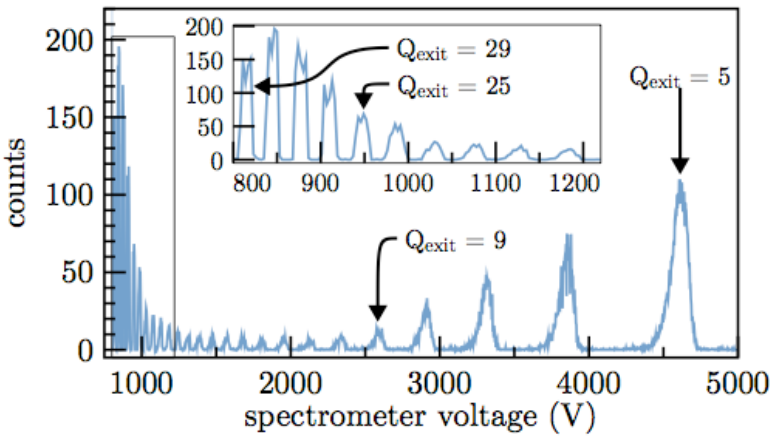

Fig. 2. Charge state and energy loss spectrum of 1050 eV/amu Xe^{30+} ions after passing a 1 nm thick carbon nanomembrane. All charge states below Q = 30 (but larger than Q = 4) are visible, whereas two distinct distributions can be observed. The high exit charge state distribution is magnified in the inset.

CNMs are irradiated with slow highly charged Xe^{q+} ions of various charge states ($20 \leq q \leq 40$) and kinetic energies ($4\ keV \leq E \leq 180\ keV$) at the two source facility of HZDR. After irradiation the CNMs are inspected by high resolution imaging techniques, e.g. transmission electron microscopy (TEM), secondary electron microscopy (SEM), atomic force microscopy (AFM) and He-ion microscopy (HIM) [8]. Above a charge state of 25+ we find nanopores at positions, where the membrane suspends over holes in the TEM grid (fig. 1) [8]. Slow HCI are able to produce nanosized pores from 30 nm down to only 3 nm, without creating further visible damage, because of their very localized energy deposition. The number density corresponds well with the incident ion fluence, indicating that every pore is produced by a single ion impact. For a fixed impact energy, the pore diameter increases with the potential energy of the HCI, indicating that bond breaking due to electron exchange and emission processes is the main mechanism for nanopore formation.

The extremely small thickness of this special target offers us a second opportunity - the observation of the projectile right after the interaction process in terms of its energy loss and charge exchange. For this purpose we designed an electrostatic analyser that allows us to determine both quantities experimentally. The measurements show the unexpected result of two distinct exit charge distributions: on the one hand (a) ions with very high charge states (close to the initial one) that loose nearly no kinetic energy and on the other hand (b) very low charged ions that loose a significant amount of kinetic energy (see fig. 2). The energy loss for ions exhibiting large charge loss shows a quadratic dependency on the incident charge state indicating that equilibrium stopping force values do not apply in this case [7].

In addition angle resolved transmission measurements point to a significant contribution of elastic energy loss. The measurements show that the different impact parameter regimes can be separated and thus a particle's energy deposition in an ultrathin solid target may not be described in terms of an averaged energy loss per unit length (for more details see [7]). Similar investigations on graphene have recently started.

Acknowledgements

Financial support from the Deutsche Forschungsgemeinschaft (DFG) (Project No. HE 6174/1-1) and from the Austrian FWF (Project No. I 1114-N20) is acknowledged.

References

[1] Aumayr F, et al. 2011, J.Phys.: Cond.Mat. 23, 393001.
[2] El-Said A S, et al. 2008, Phys. Rev.Lett. 100, 237601.
El-Said A S, et al. 2012 Phys. Rev.Lett. 109, 117602.
[3] Lemell C, et al. 2007, Solid-State Electron. 51, 1398.
[4] Heller R, et al. 2008, Phys. Rev.Lett. 101, 096102.
[5] Ritter R, et al. 2012, EPL 97, 13001.
[6] Turchanin A and Gölzhäuser A 2012, Prog. Surf. Sci. 87, 108.
[7] Wilhelm R A, et al. 2014, Phys. Rev.Lett. 112, 153201.
[8] Ritter R, et al. 2013, Appl. Phys. Lett. 102, 063112.

Tailoring the Mechanics of Carbon Nanomembranes

X. Zhang, C. Naumann[1], A. Beyer[1], P. Angelova[1], H. Vieker, S. Shishatskiy[2], J. Wind[2], A. Gölzhäuser[1]

[1] *Physics of Supramolecular Systems, Bielefeld University, 33615 Bielefeld, Germany*
[2] *Inst. for Polymer Research, Helmholtz-Zentrum Geesthacht, 21502 Geesthacht, Germany*

E-mail: ag@uni-bielefeld.de

Carbon Nanomembranes (CNMs) are extremely thin (0.5 – 3.0 nm), synthetic two-dimensional (2D) layers or sheets with tailored physical, chemical or biological function. With their two opposing surfaces they interface and link different environments by their distinct physical and chemical properties, which depend on their thickness, molecular composition, structure and the environment on either side. Due to their minute nanometer thickness and 2D architecture, they can be regarded as "surfaces without bulk" separating regions with different gaseous, liquid or solid components and controlling any materials exchange between them [1].

The fabrication of CNMs involves the formation of a monolayer of aromatic molecules on a solid surface [2]. This precursor layer is exposed to electrons or UV, which leads to a dehydrogenation, followed by a cross-linking between neighboring molecules. The cross-linked monolayer is released from the surface as a self-supporting CNM with properties that are determined by the precursor molecules [3,4]. Fig. 1 shows Helium Ion Micrographs of CNMs from different aromatic molecules; pyrolysis transforms these CNMs into graphene [3,5]. CNMs can be engineered with a controlled thickness, permeability and elasticity [6].

Here, we demonstrate that CNMs can be utilized as *ballistic membranes*, for the separation of gas molecules (Fig. 2) [7]. In particular it is shown that CNMs made from of cross-linked 4'-nitro-1,1'-biphenyl-4-thiol show a high selectivity for the permeation of carbon dioxide molecules (Fig. 3). We also report on bulge-test experiments that elucidate a correlation between the flexibility of the precursor molecules and the macroscopic mechanical stiffness of CNMs. CNMs made from rigid and condensed precursors like naphthalene and pyrene thiols exhibit higher Young's moduli (15-20 GPa), than CNMs from less condensed oligophenyls (~10 GPa). In CNMs of less densely packed monolayers, the presence of defects and nanopores plays an important role in determining their permeability and mechanical properties.

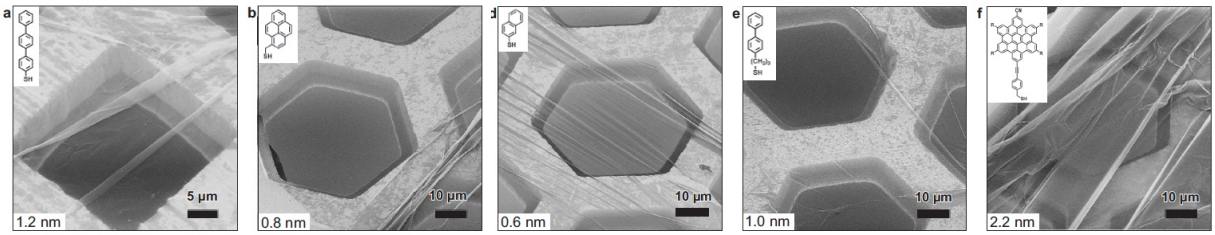

Fig. 1: Helium Ion Micrographs of free-standing carbon nanomembranes from different aromatic molecules. The CNMs are suspended over quadratic (a) and hexagonal (b-f) openings in thin metal grids. The parenting precursor molecule is shown in the upper left insert, the CNM thickness is shown in the lower left insert (from ref. 3).

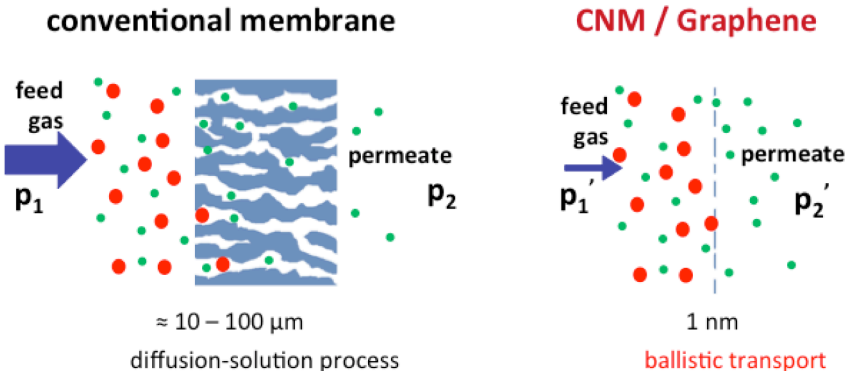

Fig. 2: Schematics of gar permeation through conventional (left) and ultrathin membranes (right). To transport molecules through a thick membrane, a pressure difference is required. When the membrane thickness lies in the range of the molecular size, an energy efficient ballistic transport with a low-pressure difference becomes possible.

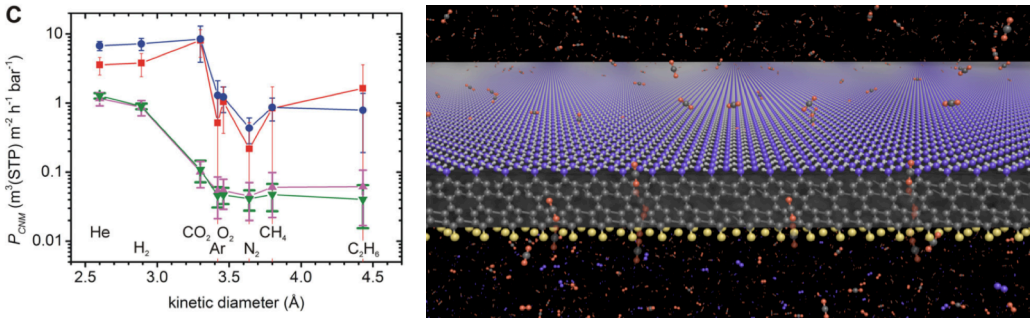

Fig. 3: Permeation of different molecules through ultrathin CNMs (left), schematics of CO_2 permeation through an ultrathin CNM CNMs made from of cross-linked 4'-nitro-1,1'-biphenyl-4-thiol (from ref. 7).

References

[1] D. Anselmetti, A. Gölzhäuser: *Converting Molecular Monolayers into Functional Membranes,* Ang. Chem. Int. Ed., **53**, 12300 (2014).

[2] A. Turchanin, A. Gölzhäuser*: Carbon Nanomembranes from Self-Assembled Monolayers: Functional surfaces without bulk*, Progress in Surface Science, **87**, 108 (2012).

[3] P. Angelova, H. Vieker, N. Weber, D. Matei, O. Reimer, I. Meier, S. Kurasch, J. Biskupek, D. Lorbach, K. Wunderlich, L. Chen, A. Terfort, M. Klapper, K. Müllen, U. Kaiser, A. Gölzhäuser, A. Turchanin: *A Universal Scheme to Convert Aromatic Molecular Monolayers into Functional Carbon Nanomembranes*, ACS Nano **7**, 6489 (2013)

[4] Z. Zheng, C. T. Nottbohm, A. Turchanin, H. Muzik, A. Beyer, M. Heilemann, M. Sauer, A. Gölzhäuser: *Janus nanomembranes: A generic platform for chemistry in two dimensions*, Angew. Chem. Int. Ed. 49, 8493 (2010).

[5] A. Turchanin, D. Weber, M. Büenfeld, C. Kisielowski, M. Fistul, K. Efetov, T. Weimann, R. Stosch, J. Mayer and A. Gölzhäuser: *Conversion of Self-Assembled Monolayers into Nanocrystalline Graphene: Structure and Electric Transport*, ACS Nano, **5**, 3896 (2011).

[6] X. Zhang, C. Neumann, P. Angelova, A. Beyer, and A. Gölzhäuser: *Tailoring the Mechanics of Ultrathin Carbon Nanomembranes by Molecular Design,* Langmuir **30**, 8221 (2014).

[7] M. Ai, S. Shishatskiy, J. Wind, X. Zhang, C.T. Nottbohm, N. Mellech, A. Winter, H. Vieker, J. Qui, K.J. Dietz, A. Gölzhäuser, A. Beyer: *Carbon Nanomembranes (CNMs) supported by polymer: mechanics and gas permeation*, Adv. Mater. **26**, 3421 (2014).

Electronic stopping of slow protons in metals and semiconductors

D. Roth, D. Goebl, B. Bruckner, and P. Bauer

Institut für Experimentalphysik, Abteilung für Atom- und Oberflächenphysik, Johannes Kepler Universität Linz, A-4040 Linz, Austria
(corresponding author: P. Bauer, e-mail: peter.bauer@jku.at)

Despite its long history, electronic stopping of slow H ions in a semiconductor is still a subject of research. While for high ion velocities electronic stopping is well understood [1, 2], the prevailing mechanisms are still unresolved in the regime of low ion velocities $v << v_F$ (v_F being the Fermi velocity), where deceleration occurs due to both collisions with target atoms and due to electronic interactions. By convention, one distinguishes between *nuclear stopping* (repulsive Coulomb interaction between the nuclei) and *electronic stopping* (transfer of energy to the electronic system). The resulting deceleration is described by the *stopping power* $S = -dE/dx$. Alternatively, one introduces the stopping cross section ε related to S via $\varepsilon = (1/n).S$, where n denotes the atomic density of the target.

For projectile velocities $v<<v_F$, only weakly bound conduction and valence electrons can be excited. For a free electron gas (FEG), $dE/dx = Q(Z_1,r_s)v$, where $Q(Z_1, r_s)$ denotes the friction coefficient which depends on the atomic charge of the projectile Z_1 and the Wigner-Seitz radius r_s. Experimentally, deviations from velocity proportionality were observed for metals with finite excitations thresholds, e.g. for the *d*-band in noble metals or the band gap energy, and for insulators with a band gap energy E_g: for transition and noble metals changes in the slope of ε were observed in the velocity range 0.2 a.u. < v < 0.5 a.u. [3]. In contrast, for insulators, electronic stopping has been found to vanish for ion velocities lower than a threshold velocity, v_{th} < 0.1 a.u., [4, 5], even for a large band gap insulator like LiF (E_g = 14 eV, [6]).

In this contribution we present a study of electronic stopping of H ions in elemental semiconductors (Si, Ge) [7, 8] and in binary semiconductors like ZnO and ZnS [8]. Experiments were performed in backscattering geometry relative to copper, and the resulting electronic stopping cross sections are compared to metals of qualitatively different conduction band properties like noble metals (Cu, Ag, Au) and transition metals (Al, Pt, Zn and In) [a]. The friction coefficients are found to behave in a quite different way than expected from collective electronic properties like density of valence/conduction electrons or plasmon energies $\hbar\omega_p$. The corresponding friction coefficients exhibit a variation on a large scale, with the lowest value for ZnO ($\hbar\omega_p$ = 19 eV [9], E_g = 3.4 eV [6]) and the highest value for Ge ($\hbar\omega_p$ = 16 eV [10], and E_g = 0.66 eV [6])). The complete set of results is presented in Fig. 1:

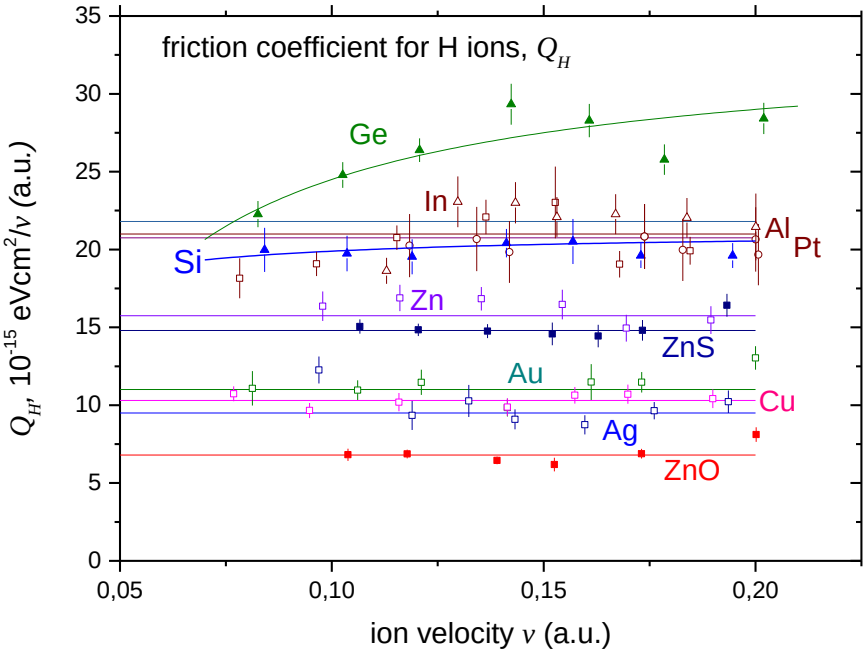

Fig.1: Friction coefficients for electronic stopping of very slow H ions (v < 0.2 a.u.) in selected metals and semiconductors.

In this presentation, the results are set into relation to electronic properties of the valence/conduction electrons, and other possible parameters of importance are discussed (doping, position of the Fermi level, …).

Support by the Fonds zur Förderung der Wissenschaftlichen Forschung (project P22587-N20) is gratefully acknowledged.

[1] J. Tersoff and D.R. Hamann, Phys. Rev. Lett. 50, 1998 (1983); Phys. Rev. B 31, 805 (1985)
[2] M. F. Crommie, C. P. Lutz and D. M. Eigler, Nature 363, 524 (1993)
[3] D. Goebl, W. Roessler, D. Roth, and P. bauer (Phys. Rev. A90, 042706 (2014).
[4] S. N. Markin, D. Primetzhofer, and P. Bauer, Phys. Rev. Lett. 103, 11, 113201 (2009).
[5] D. Primetzhofer, S.N. Markin, and P. Bauer, Nucl. Instr. Meth. B 269, 19, 2063-2066 (2011).
[6] W.H. Strehlow and E.L. Cook, J. Phys. Cehm. Ref. Data, col. 2, p. 163, 1973.
[7] D. Roth, D. Goebl, D. Primetzhofer, and P. Bauer, Nucl. Instr. Meth. B317, 61 (2013).
[8] D. Roth, private communication (2014).
[9] R.L Hengehold, R.J. Almassy, and F.L. Pedrotti, Phys. Rev. B1, 4784 (1970).
[10] T. Aiyama, and K. Yada, J. Phys. Soc. Japan 36, 1554 (1974).

Tuesday

(Thermo)Dynamics of Caged (Supra)Molecules

C.-A. Palma[1], J. Björk[2], F. Klappenberger[1], D. Kühne[1], E. Arras[1], S. Stafström[2] & J.V. Barth[1]

[1] *Physik-Department E20, Technische Universität München, D-85748 Garching, Germany;*
[2]*Department of Physics, Chemistry and Biology (IFM), Linköping University, 58183 Linköping, Sweden*

Artificial molecular switches, rotors, and machines are set to establish design rules and applications beyond their biological counterparts. We exemplify the role of noncovalent interactions and transient rearrangements in the complex behavior of supramolecular rotors caged in a 2D metal–organic coordination network. Combined scanning tunneling microscopy experiments and molecular dynamics modeling of a trimeric rotor species identify key steps in collective rotation events and reconfigurations. We notably reveal that stereoisomerization of the chiral otors entails topological isomerization whereas rotation occurs in a topology-conserving, asynchronous two-step process. In addition, the chemical environment can be instructed to control the system dynamics.

Furthermore, we provide access to single-molecule thermodynamics, by analysing individual molecules at the nanoscopic pores and recording their time-averaged statistical weights using temperature-controlled scanning tunneling microscopy. The obtained patterns represent a real-space equilibrium probability distribution. We associate such distributions with a partition function projection to assess spatially resolved thermodynamic quantities, by means of computational modeling. By *in-silico* customized energy landscapes distinct probability distributions can be encrypted at different temperatures. Such modulation provides pathways to encode and decode information into position-temperature space.

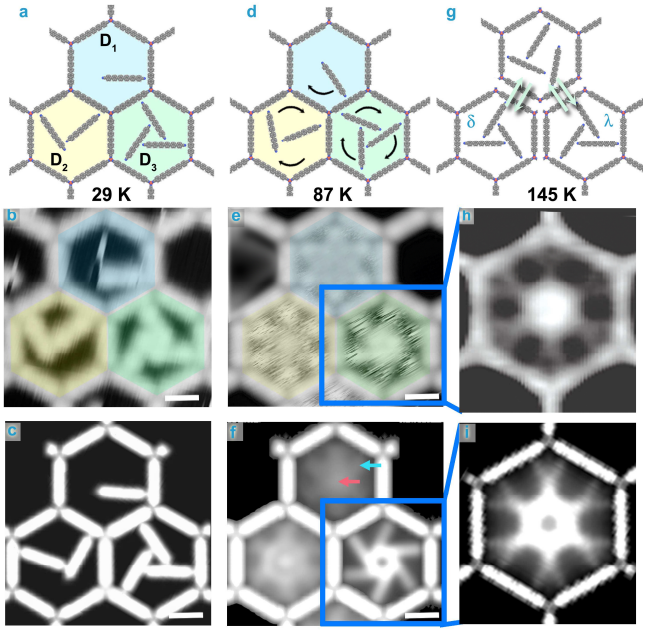

Caged single molecules and supramolecular dynamers in metal-organic network pores on Ag(111). a, b) Scheme for the static state of the molecules and STM image at 29 K. **c)** Rendering of the molecules in the pore by mapping their occupation. **d)** Scheme with multiple intrapore configurations at higher temperatures. **e**) STM at 87 K showing the time-average pattern (TAP) of $\mathbf{D_1}$, $\mathbf{D_2}$ and $\mathbf{D_3}$ (blue, yellow and green hexagons, respectively). **f)** Corresponding TAPs from µs-long MD simulations. Each independent simulation is placed as in the experiment in (e). Arrows indicate the main differences compared to experimental data in (e). **g)** Scheme illustrating chiral inversion of a $\mathbf{D_3}$ propeller structure; different enantiomers are labeled δ and λ. **h)** The STM TAP at 145 K of $\mathbf{D_3}$ shows a 12-branched star resulting from the superposition of two rotating propellers with opposite handedness. **i**) TAP from 0.5 µs-long MD at 450 K. STM parameters U_T=2.0 V, I_T=0.1 nA. Sexiphenyl dicarbonitrile N-to-N length is 30 Å and scale bars are 20 Å. Rendering of the silver substrate is omitted in the models for clarity

References *Rotational and constitutional dynamics of caged supramolecules*, Proc. Nat. Acad. Sci. 107, 21332 (2010); *Topological dynamics in supramolecular rotors*, Nano Lett. 14, (2014). DOI: 10.1021/nl5014162; *Visualization and thermodynamic coding of single-molecule partition function projections*, Nature Comms., to be publ. (2015)

Work supported throug European & Swedish Research Council

Sequential assembly at the liquid-solid interface

B. Karamzadeh[1], T. Eaton[2], I. Cebula[1,3], D. Muñoz Torres[2], M. Mayor[2,4], M. Buck[1]
[1]*EaStCHEM School Chemistry, University of St Andrews, St Andrews,UK*
[2] *Department of Chemistry, University of Basel, Basel, Switzerland*
[3] *present address: School of Chemistry, University of Nottingham, Nottingham, UK*
[4] *KIT Institute for Nanotechnology, Karlsruhe, Germany.*
E-mail:mb45@st-andrews.ac.uk

Supramolecular self-assembly at surfaces involving hydrogen bonding, van der Waals interactions and metal-organic coordination bonding represents a well established, versatile approach for the routine generation of atomically precise nanostructures [1,2]. However, to what extent its opportunities can be harnessed for going beyond the mere generation of patterns and building functional nanostructures is open at present as crucial issues concerning the assembly and stability of increasingly complex systems remain to be addressed.

In our efforts to develop strategies based on solution processing we investigate the sequential assembly of molecules as a means to built more complex structures. Starting point is a bimolecular hydrogen bonded network consisting of PTCDI and melamine (see Fig. 1) which serves as template [3]. Contrasting an approach taken previously where the geometry of the network pores were modified by derivatising a component of the bimolecular network [4], a third molecule is used to partition the pore of the honeycomb network [5]. Owing to the threefold symmetry the pore modifier, which is based on 1,3,5-tri(phenylene-ethynylene) ben-zene (TPEB), adsorbs in two equivalent positions in the hexagonal pore of the supramolecular network as seen from the STM image displayed in Fig. 1. However, in addition to pores where the the molecule is resolved, a sixfold pattern is also observed. Analogous to the dynamic behaviour of a hydrogen bonded trimer in a honeycomb structure [6], this is interpreted to arise from the rotation of the molecule on a time scale fast compared to the temporal resolution of the STM. The fraction of the sixfold pattern varies with the modification of the terminal phenyl ring. For example, introducing an OH group decreases the rate

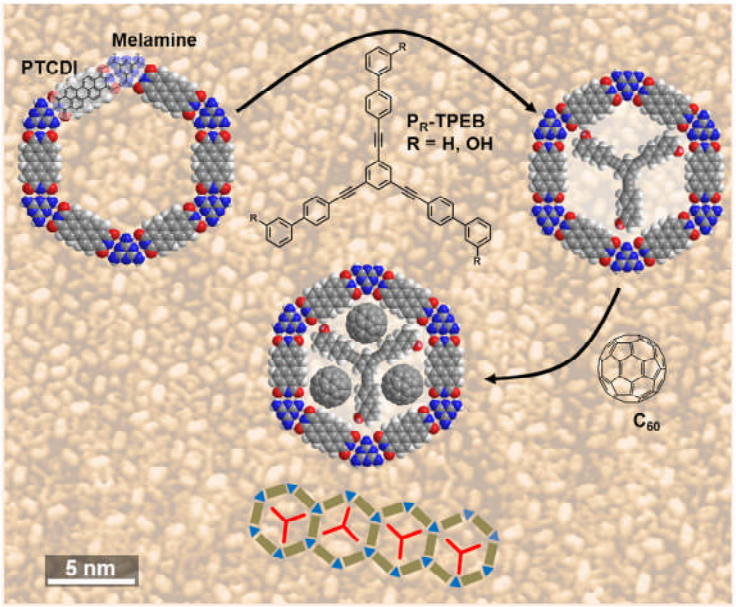

Fig. 1: Scheme of sequential supramolecular assembly using a hydrogen bonded network of PTCDI and melamine as template to direct adsorption of a star shaped molecule (P_R-TPEB). The partitioned pores of the network represent adsorption sites for single fullerene molecules. Background shows STM image of network on Au(111)/mica modified by the star shaped P_{OH}-TPEB molecule. As guide to the eye some of the network pores are marked.

of rotation due to increased interactions of the molecule with the network and/or the substrate.
The trimolecular network structure with the compartmentalised pores acts as a second order template when exposed to a solution of fullerenes. Contrasting the hexagonal pores of the PTCDI-melamine network into which clusters of up to seven C_{60} molecules adsorb [7], the smaller sub-pores can only host single fullerenes.
The studies presented demonstrate two major points. One is consecutive templating as a means to control dimensions down to the isolated molecule level. Notably, the second level of templating introduces additional opportunities for supramolecular assembly as, through variation of the star shaped P_R-TPEB molecules, it should be possible to vary the compartmentation and introduce specific docking sites. The second point is that the stability of the pore modifier is key to the optimisation of the yield and fidelity of such a sequential assembly processes.

Acknowledgements

The work is supported by the Leverhulme Trust.

References

[1] J. Elemans, S. B. Lei, S. De Feyter, Angew. Chem. Int. Ed. 48, 7298 (2009)
[2] J. V. Barth, Annu. Rev. Phys. Chem. 58, 375 (2007)
[3] R. Madueno, M. T. Räisänen, C. Silien, M. Buck, Nature 454, 618-621 (2008)
[4] M. T. Räisänen, A. G. Slater, N. R. Champness, M. Buck, Chem. Sci., 3, 84 (2012)
[5] B. Karamzadeh, T. Eaton, I. Cebula, D. M. Torres, M. Neuburger, M. Mayor, M. Buck, Chem. Commun. 50, 14175 (2014)
[6] D. Kühne, F. Klappenberger, W. Krenner, S. Klyatskaya, M. Ruben, J. V. Barth, Proc. Natl. Acad. Sci. USA 107, 21332 (2010)
[7] J. A. Theobald, N. S. Oxtoby, M. A. Phillips, N. R. Champness, P. H. Beton, Nature 424, 1029 (2003)

Chiral recognition among helical aromatic molecules*

Johannes Seibel,[1] Anaïs Mairena,[1] Manfred Parschau,[1] and Karl-Heinz Ernst[1,2]

[1]*Empa, Swiss Federal Laboratories for Materials Research and Technology*
(corresponding author: K.-H. Ernst, e-mail: karl-heinz.ernst@empa.ch)

[2]*Department of Chemistry, University Zurich, Zürich, Switzerland*

Molecular recognition among chiral molecules on surfaces is of paramount importance in biomineralization, enantioselective heterogeneous catalysis, and for the separation of chiral molecules into their two mirror-image isomers (enantiomers) via crystallization or chromatography. Understanding the principles of molecular recognition in general, however, is a difficult task and calls for investigation of appropriate model systems. One popular approach is thereby studying intermolecular interactions on well-defined solid surfaces, which allows in particular the use of scanning tunneling microscopy (STM). We present an elucidation of chiral recognition of helical hydrocarbons (Fig. 1) at the few-molecule level, in complete monolayers and in multi-layers. This includes lateral separation of the molecules that constitute a dimer with a modified STM tip and the subsequent determination of their handedness with a non-modified tip. Moreover, we will show that a preference between homochiral and heterochiral recognition in monolayers depends strongly on substrate symmetry, but may switch with increasing coverage within the monolayer or during transition from saturated monolayer to multilayer coverage.

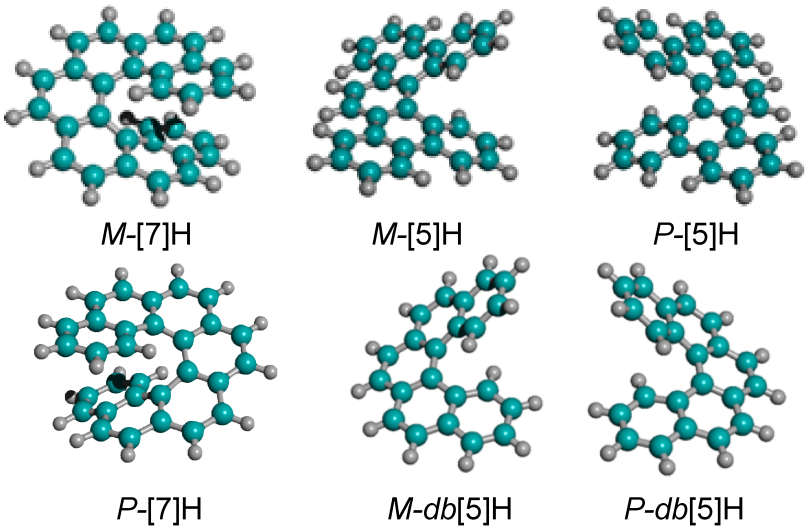

Fig. 1. Structural formulas of the enantiomers of heptahelicene ([7]H), pentahelicene ([5]H), and dibenzo-pentahelicene (db[5]H). The prefixes *P* and *M* stand for *plus* and *minus*, respectively, and denote the sense of helicity of the molecule.

A crucial issue in understanding the nature of chiral recognition among helical molecules is the analysis of their absolute handedness. For [5]H, for example, the sense of helicity is directly deducted from a constant current STM image (Figure 2), and dimers observed on Cu(111) are easily recognized as homochiral. For [7]H on Cu(111), on the other hand, the dimers had to be separated manually and image filtering was needed in order to being able to analyze the helicity of the molecules. In that case, basically all dimers were found to be heterochiral.

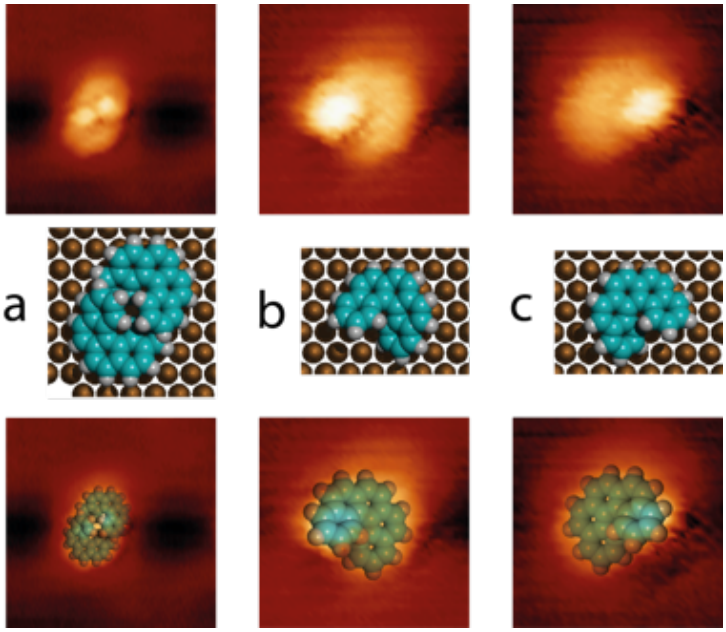

Fig. 2. STM image of a dimer and single molecules of [5]H on Cu(111). The corresponding models and a superposition of both are shown in the lower rows.

For monolayer-self-assembly, the symmetry of the underlying single-crystal substrate was found to play an important role for the fate of lateral separation of enantiomers [1].

Financial support by the Swiss National Science Foundation (SNSF) is gratefully acknowledged.

* Coauthors of parts of results presented in this talk are: Liying Ma (Empa),
Alix F. Tröster, Konstantin Grenader, Andreas Terfort (Goethe Universität, Frankfurt am Main),
Laura Zoppi, Oliver Allemann, Jay Siegel (University Zurich),
Susanne Baumann, Christopher Lutz, Andreas Heinrich (IBM ARC).

[1] J. Seibel, M. Parschau, K.-H. Ernst, *J. Phys. Chem. C 118 (**2014**) 29135–29141*

Controlling porphyrin coordination reactions and assembly on a Cu(111) supported boron nitride monolayer

J.I. Urgel[1], M. Schwarz[1], M. Garnica[1], D. Stassen[2], D. Bonifazi[2], S. Joshi[1], F. Bischoff[1], D. Ecija[1]*, J.V. Barth[1], W. Auwärter[1]

[1] *Physik Department E20, Technische Universität München, Garching, Germany*
[2] *Department of Chemistry and Namur Research College, University of Namur, Namur, Belgium*

E-mail: wau@tum.de

Contemporarily, the combination of atomically thin sheets of sp^2-hybridized boron nitride (BN) or graphene with complex molecules has emerged as a powerful strategy to functionalize surfaces and engineer structural, electronic, magnetic, optical or catalytic properties of such low-dimensional materials [1]. In an ultra-high-vacuum scenario, a variety of model systems based on molecules adsorbed on surface supported BN monolayers were characterized with sub-molecular resolution, exploiting the real space imaging capabilities of scanning tunneling microscopy [2-5].

Here, we focus on porphyrin-based nanostructures assembled on a BN monolayer grown on Cu(111) via chemical vapor deposition. Porphyrin molecules and related tetrapyrrole compounds are ideal building blocks for surface-anchored architectures [6], as they possess an impressive variety of functional properties that have been exploited in both natural and artificial systems. Specifically, metal centers incorporated in the porphyrin macrocycle and tailored peripheral substituents can be used to engineer characteristics of porphyrin arrays on surfaces. The BN/Cu(111) support is a geometrically smooth, but electronically corrugated template featuring coexisting domains of moire-like electronic superstructures with different periodicities up to 13 nm [7]. As exemplified for free-base porphin adsorbates (2H-P, see Figure (a)), the BN/Cu(111) support can have three distinct functions: (i) The electronic moirons of the BN/Cu(111) interface trap 2H-P, steering self-organized growth of arrays with extended molecular assemblies. (ii) The electronic coupling of adsorbates to the underlying metal support is reduced by the BN spacer layer, which allows for a direct

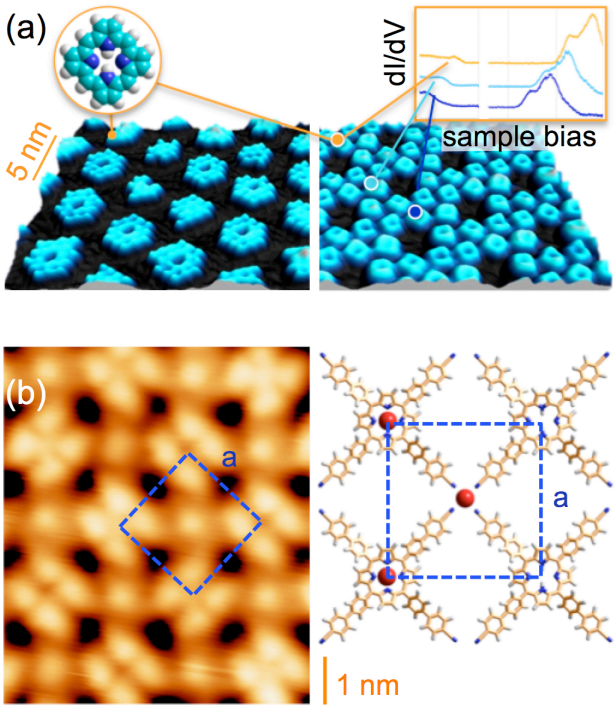

Fig. (a) STM images of porphine (2H-P) on BN/Cu(111) at intermediate (left panel) and high 2H-P coverage (right panel). The tunneling spectra (inset on the top right) reveal shifts of molecular resonances depending on the position on the BN/Cu(111) template (adapted from [4]). (b) Metal-organic coordination network on BN/Cu(111) formed by CN functionalized porphyrins (2H-TPCN) and Co. The assembly features a four-fold coordination motif and contains in-situ metalated TPCN units, i.e. Co-TPCN (see structural models in the right panel).

visualization of frontier orbitals by STM. (iii) The lateral molecular positioning on the superstructured surface determines the energetic level alignment, *i.e.*, the energy of the frontier orbitals, and the electronic gap are tunable.
Furthermore, we will discuss an exemplary surface-confined coordination architecture on BN/Cu(111). It bases on a combination of carbonitrile-functionalized free-base porphyrins (2H-TPCN) and Co atoms (see Figure (b)) on BN/Cu(111) at 350 K. While interactions mediated by the terminal CN groups prevent a trapping of individual TPCN units under the applied experimental conditions, two on-surface complexation reactions of 2H-TPCN can proceed upon exposure to the atomic beam of Co: a metalation reaction occurring with the tetrapyrrolic macrocycle already at room temperature, and the CN-Co coordination governing the formation of metal-organic networks. The latter exhibit a grid-like topology featuring a periodicity of about 2.4 nm. It bases on a four-fold coordination motif and a 1:1 stoichiometry between Co nodes and TPCN. The successful in-situ metalation yielding Co-TPCN directly on the BN sheet is corroborated by scanning tunneling spectroscopy data evidencing a spectral fingerprint of the Co center and comparison to related systems (CoPc/BN/Ir(111) [3]). Though the four-fold linkage to N is characteristic for both the macrocycle center of Co-TPCN and the coordination nodes, there are pronounced differences in their coordination spheres and their electronic properties. Notably, the spectral signatures of Co in Co-TPCN and in the coordination node reveal an upshift of the lowest unoccupied resonance by about 0.5 eV in the latter, which might point to the formation of a mixed oxidation and valence metallic network.

These findings provide perspectives for the assembly of molecular arrays and coordination networks on BN and related systems featuring structural, electronic and magnetic properties unachievable on metallic supports.

Acknowledgements

Work supported by the ERC Consolidator Grant NanoSurfs (615233), the Munich Center for Advanced Photonics (MAP), the Technische Universität München – Institute for Advanced Study and other funding schemes.

* Now at IMDEA Nanoscience (Madrid, Spain)

References

[1] J.M. MacLeod and F. Rosei, Small 10, 1038 (2014)
[2] S. Berner et al., Angew. Chem. Int. Ed. 46, 5115 (2007)
[3] F. Schulz et al., ACS Nano 7, 11121 (2013)
[4] S. Joshi et al., ACS Nano 8, 430 (2014)
[5] T. Dienel et al., ACS Nano 8, 6571 (2014)
[6] W. Auwärter et al., Nature Chem., DOI: 10.1038/NCHEM.2159 (2015)
[7] S. Joshi et al., Nano Lett. 12, 5821 (2012)

Fabricating functional molecular nanoarchitectures from terminal alkyne precursors: the route to novel carbon-based materials.

Florian Klappenberger,[1] Y.-Q. Zhang,[1] B. Cirera,[1] C.-A. Palma,[1] K. Diller,[1] A. Papageorgiou,[1] F. Allegretti,[1] M. A. Öner,[1] I. R. Lahoz,[2] S. Castro-Fernańdez,[2] S. Míguez-Lago,[2] M. Magdalena Cid,[2] J. L. Alonso-Gómez,[2] Björk, J.,[3] Z. Chen,[4] S. Klyatskaya,[4] M. Ruben,[4] and J. V. Barth[1]

[1] *Physik Department E20, Technische Universität München, James-Franck Straße, 85748 Garching, Germany*
[2] *Departamento de Quimica Orgańica, Universidade de Vigo, 36310 Vigo, Spain*
[3] *Department of Physics, Chemistry, and Biology (IFM), Linköping University, 58183 Linköping, Sweden*
[4] *Institute of Nanotechnology, Karlsruhe Institute of Technology, 76344 Eggenstein-Leopoldshafen, Germany*
E-mail: florian.klappenberger@tum.de

The bottom-up construction of two-dimensional (2D) functional molecular nanoarchitectures from precursors featuring multiple terminal alkyne moieties under ultra-high vacuum conditions is reported. The related supramolecular chemistry and the involved covalent reactions are comprehensively understood by the STM+XS approach[1] combining scanning tunneling microscopy/spectroscopy (STM/STS) and X-ray spectroscopic methods with density functional theory (DFT) investigations and all-atom molecular dynamic (MD) simulations allowing to precisely characterize the obtained nanostructures and unraveling the underlying formation mechanisms.

Allene derivatives are famous for their outstandingly strong chiroptical responses.[2] Here, we employed for the first time an allene derivative for the construction of supramolecular architectures under well-defined conditions. The elongated building-block (Figure 1a) features two allene moietes (highlighted in red) and terminal alkynes at both ends and is characterized by an extremely large conformational phase space resulting from rotations around the internal ethynylene groups (angles ϕ_1 and ϕ_2) and flexure of covalent bonds. Surprisingly, in electrospray ionization mass spectrometry of solutions of standard molarity the signal of the supramolecular dimer strongly dominates over the monomer signal. Consistently, in MD simulations we find a pronounced tendency to form dimers of a geometry similar to the one depicted in Figure 1b. The driving forces behind this behavior are antiparallel stacking of the dipolar central pyridine units and the optimization of the van der Waals contact surface between the two tectons, made possible by the complementary conformations leading to a molecular "hug" and termed morphological assembly. After evaporation onto the Ag(111) surface at 200 K and subsequent cooling to cryogenic temperature, regular domains with a rhombic unit cell are observed by STM (Figure 1c). By manipulation procedures it was clarified that four monomers contribute to one unit cell. High-resolution STM images unravel that the different domains belong to two diastereomeric versions of the same architecture each appearing in three 120°-rotated symmetric equivalents. MD simulations demonstrate that the allene derivatives form an upstanding chiral architecture (UCA) with a geometry similar to the one depicted in Figure 1d.[3]

Then the versatile potential of terminal alkynes for the fabrication of novel carbon-based nanomaterials is discussed with special focus on graphdiyne-related scaffolds.[4, 5] Homo-coupling of the reactive moieties (Figure 2a) allows for the synthesis of novel molecular species (Figure 2b) and conjugated 2D polymers (Figure 2c) at relatively low reaction temperatures (300 – 400 K) with volatile H_2 as the only by-product.[6] A profound analysis of the reaction mechanism[7] demonstrates that on the noble metal surface

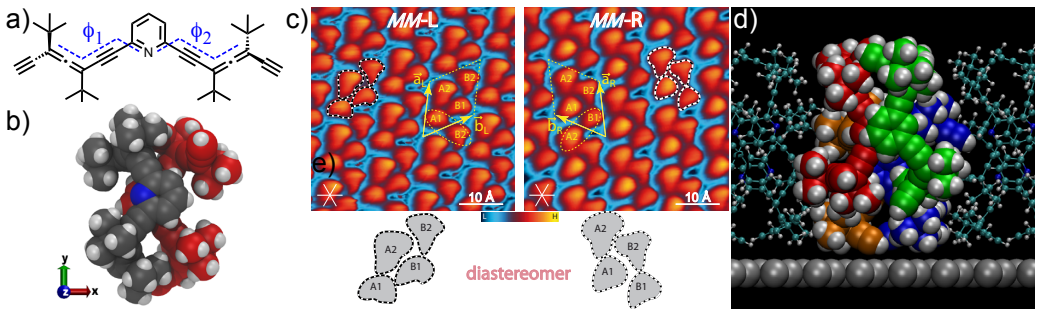

Figure 1: a) Chemical structure of the employed allene precursor. b) Visualization of the supramolecular dimer as obtained from MD simulations. c) On the Ag(111) surface diastereomeric architectures self-assemble whereby the unit cells (highlighted in yellow) consist of four tectons each. d) Rendering of the tentative UCA geometry where the four molecules of a specific unit cell are depicted with van der Waals spheres and the surrounding molecules of the densely-packed architecture are drawn with ball-and-stick models.

the reaction is initiated via a covalently-coupled tautomer and continues via step-wise dehydrogenation in contrast to the established solution pathways for Glaser-type coupling. Next, we demonstrated that the chemo- and regioselectivity of the covalent linkage can be increased by a vicinal surface template. Employing a linear ditopic monomer (DETP) on the stepped Ag(877) surface, monomers align along the step edges (Figure 2d) and as a consequence side reactions were suppressed (Figure 2e). The realized novel hydrocarbon semiconducting molecular wire (Figures 2f,g) represents an extended version of the thinnest possible graphdiyne nanoribbon.[8] The longest polymers produced with our approach exceed 270 Å. According to DFT calculations, the band structure of the nanowires is characterized by approximately cosinus-shaped bands derived from the HOMO and LUMO orbitals, nicely isolated in energy from other bands. The theory is compared to experimental findings from STS and ARPES measurements.

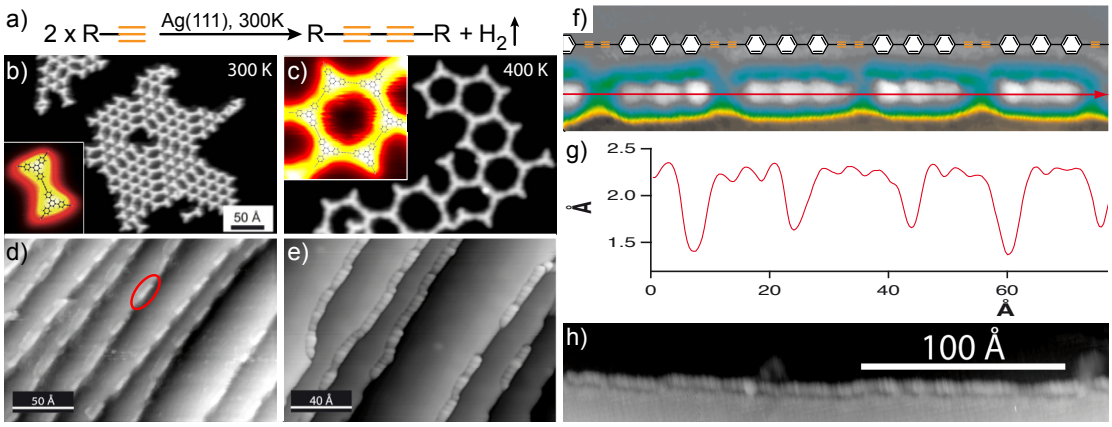

Figure 2: Covalent architectures by terminal alkyne homo-coupling. a) Formal reaction scheme. b) STM image of Ext-TEB on Ag(111) after annealing to 300 K. A mixture of unreacted monomers and covalent dimers (inset) is visible. c) After annealing to 400 K a porous covalent network with irregular shape is present. d) On the vicinal Ag(877) surface, DETP monomers (circled) align with the step edges. e) Molecular wires follow the step edge after annealing to 400 K. f) Zoom-in on a nanowire demonstrating its regularity. The chemical structure of the polymer has been superimposed for comparison. g) Line profile along the red arrow in f). h) Example of an extended-graphdiyne nanowire with a length of more than 27 nm.

Finally, the complex chemistry of the terminal alkyne groups on the more reactive Cu(111) surface is investigated. After adsorption at 200 K, statistically distributed adsorbates are observed having undergone significant conformational adaptation due to strong π-bonding of the functional groups to the substrate. Annealing between 300 and 350 K triggers the formation of dense-packed islands exhibiting room temperature stability. The complementary investigation unravels that deprotonation of the terminal alkyne groups leads to a novel binding motif namely a three-fold ionic C-H$\cdots\pi$ hydrogen bond and theory suggests a network formation energy gain of $\approx$0.3 eV per molecule.[9] The room temperature stable assemblies are explained by the interplay of the relatively weak, but directional hydrogen bonding together with strong surface anchoring via the alkynyl functionalities with mixed σ and π character.

Acknowledgements

The work was supported by the DFG priority program 1459, the European Union via ERC Advanced Grant MolArt (no. 247299), the Chinese Scholarship Council, Xunta de Galicia (IPP contract J.L.A.G.) and Gobierno de España (CTQ2010-18576 and CTQ2011-28831).

References

[1] F. Klappenberger, *Prog. Surf. Sci.* **89**, 1 (2014).
[2] J. L. Alonso-Gomez, P. Rivera-Fuentes, N. Harada, N. Berova, F. Diederich, *Angew. Chem.-Int. Edit.* **48**, 5545 (2009).
[3] Y.-Q. Zhang, M. A. Öner, I. R. Lahoz, B. Cirera, C. A. Palma, S. Castro-Fernandez, S. Miguez-Lago, M. M. Cid, J. V. Barth, J. L. Alonso-Gomez, F. Klappenberger, *Chem. Commun.* **50**, 15022 (2014).
[4] K. Srinivasu, S. K. Ghosh, *J. Phys. Chem. C* **116**, 5951 (2012).
[5] A. L. Ivanovskii, *Prog. Solid State Chem.* **41**, 1 (2013).
[6] Y.-Q. Zhang, N. Kepčija, M. Kleinschrodt, K. Diller, S. Fischer, A. C. Papageorgiou, F. Allegretti, J. Björk, S. Klyatskaya, F. Klappenberger, M. Ruben, J. V. Barth, *Nat. Commun.* **3**, 1286 (2012).
[7] J. Björk, Y.-Q. Zhang, F. Klappenberger, J. V. Barth, S. Stafström, *J. Phys. Chem. C* **118**, 3181 (2014).
[8] B. Cirera, Y.-Q. Zhang, J. Björk, S. Klyatskaya, Z. Chen, M. Ruben, J. V. Barth, F. Klappenberger, *Nano Lett.* **14**, 1891 (2014).
[9] Y.-Q. Zhang, J. Björk, P. Weber, R. Hellwig, K. Diller, A. C. Papageorgiou, S. C. Oh, S. Fischer, F. Allegretti, S. Klyatskaya, M. Ruben, J. V. Barth, F. Klappenberger, *submitted* .

Molecules “pop up”: massive conformational changes during thermally induced self-metalation of 2H-Tetrakis-(3,5-di-tert-butyl)-phenylporphyrin on Cu(111)

Michael Stark[1], Stefanie Ditze[1], Michael Lepper[1], Liang Zhang[1], Hannah Schlott[1], Florian Buchner[1], Michael Röckert[1], Min Chen[1], Ole Lytken[1], Hans-Peter Steinrück[1] and Hubertus Marbach[1]

[1] *Lehrstuhl für Physikalische Chemie II, Universität Erlangen-Nürnberg, Egerlandstr. 3, 91058 Erlangen, Germany*
E-mail: hubertus.marbach@fau.de

Based on a combined scanning tunneling microscopy and X-ray photoelectron spectroscopy study we discuss pronounced changes of the long-range order and the intramolecular conformation during the self-metalation of 2H-5,10,15,20-Tetrakis-(3,5-di-tert-butyl)-phenylporphyrin (2HTTBPP) to CuTTBPP on Cu(111). 2HTTBPP adsorbed on Cu(111) at room temperature forms a peculiar entropically stabilized supramolecular ordered phase: the molecules arrange in alternating rows, with two distinct appearances in STM, which are assigned to concave and convex intramolecular conformations (Fig. 1 a-h) [1,2].

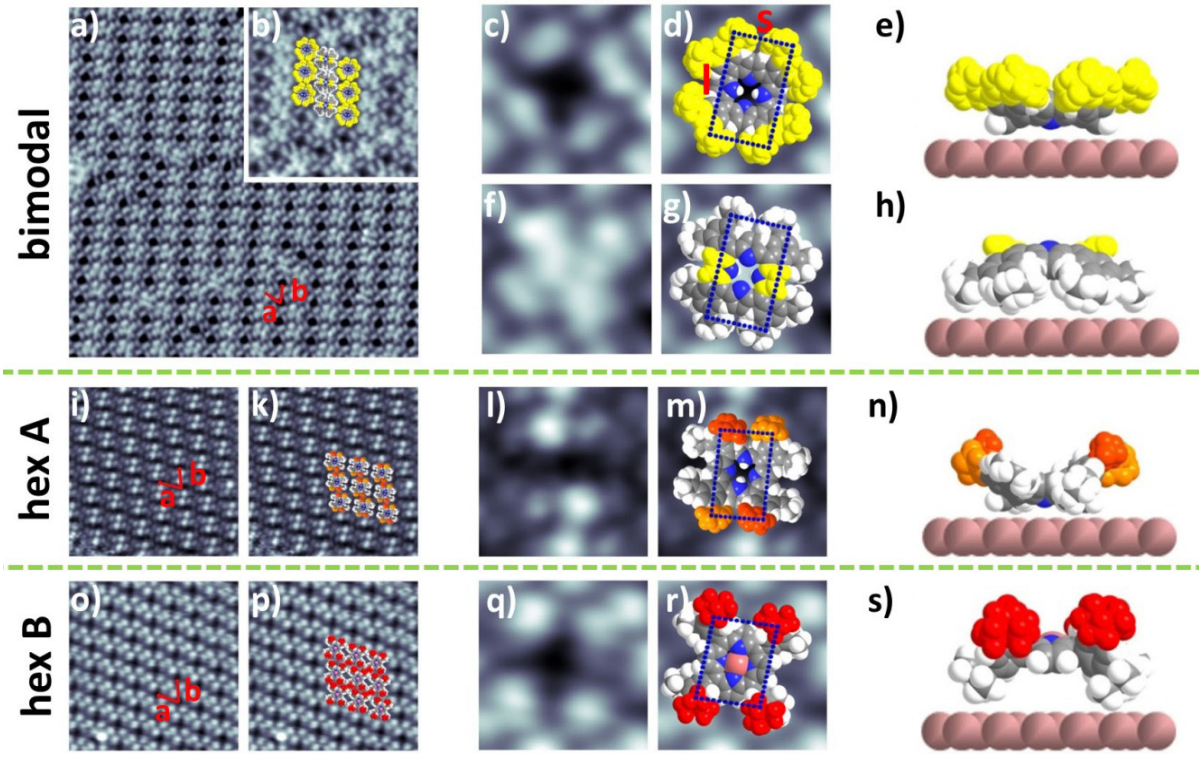

Fig.1 Overview of the observed supramolecular porphyrin phases and the derived molecular models on Cu(111): (a-h) bimodal phase of 2HTTBPP as prepared at room temperature. (i-n) hex A phase of 2HTTBPP after heating to 360 K for 2 minutes. (o-s) representing hex B phase of CuTTBPP after thermally induced metalation reaction. The scanning parameters are: (a) U=+1.3 V, I=30 pA; (b-g) U=+1.8 V, I=25 pA; (i-r), U=+1.8 V, I=30 pA; (a) 35.0x35.0 nm^2; (b, i, k, o, p) 13.5x13.5 nm^2; (c, d, f, g, l, m, q, r) 2.5x2.5 nm^2.

Starting at ~330 K, the initially bimodal supramolecular structure changes to the monomodal "hex A" arrangement with reduced intramolecular symmetry (Fig. 1 i-n). At higher temperatures and/or prolonged heating times, 2HTTBPP undergoes a metalation reaction with Cu substrate atoms to form CuTTBPP in the "hex B" phase (Fig. 1 o-s). Upon metalation, the porphyrin literally "pops up" from the surface, due to a drastically reduced molecule-substrate interaction (Fig. 2) [3]. In summary, we report detailed insights into the thermally induced morphological and chemical transformations of 2HTTBPP on Cu(111). The observed massive structural changes can be conclusively explained by reduced molecule-substrate interactions after metalation [3].

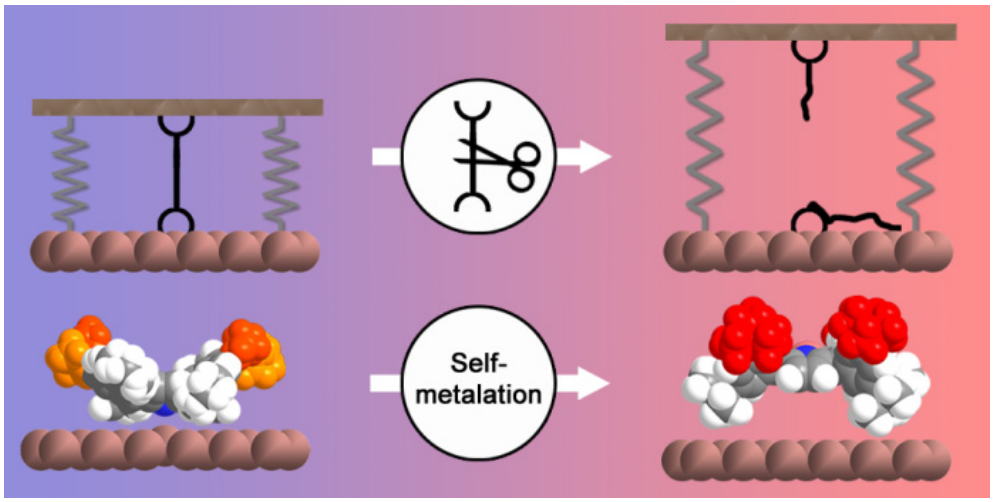

Fig.2 Sketch of the "pop up" mechanism: 2HTTBPP on Cu(111) phase behaves almost like a loaded spring which is hold by the strong attractive interactions of the iminic nitrogens with the Cu substrate and is released upon metalation.

Acknowledgements

This work was funded by the German Research Council (DFG) through research unit FOR 1878/funCOS and the Cluster of Excellence 'Engineering of Advanced Materials' granted to the FAU Erlangen-Nürnberg.

References

[1] S. Ditze , M. Stark, F. Buchner, A. Aichert, N. Jux, N. Luckas, A. Görling, W. Hieringer, J. Hornegger, H.-P. Steinrück and H. Marbach, JACS, 136 (2014) 1609
[2] H. Marbach and H.-P. Steinrück, Chem. Commun., 50 (2014) 9034
[3] M. Stark, S. Ditze, M. Lepper, L. Zhang, H. Schlott, F. Buchner, M. Röckert, M. Chen, O. Lytken, H.-P. Steinrück and H. Marbach, Chem. Commun., 50 (2014) 10225

Molecular seesaw: s-triazine on Pt(111)

S.N. Filimonov[1], W. Liu[2], A. Tkatchenko[2]
[1] *Department of Physics, Tomsk State University, 634050 Tomsk, Russia*
[2] *Fritz-Haber-Institut der Max-Planck-Gesellschaft, D-14195, Berlin, Germany*
E-mail: filimon@phys.tsu.ru

It is well known that in dense arrays of organic molecules adsorbed on inorganic surfaces molecules may undergo spontaneous changes of their adsorption geometry as a result of subtle interplay of the molecule-surface and intermolecular interactions. For isolated adsorbed molecules appearance of multiple adsorption states is much less anticipated due to the absence of intermolecular interactions which might stabilize or destabilize different adsorption structures. An important exception is bistable adsorption of organic molecules involving a chemically bound and a physically bound (precursor) adsorption states [1]. The precursor state is commonly treated as a weakly bound, short living and quickly yielding to a more stable chemisorbed state. However, as has been shown by recent theoretical calculations [2,3], relative stability of the physisorbed and chemisorbed states, as well as the transition barrier between these states, might be tuned by changing the molecule constitution or/and the metal substrate.

In the present work we study adsorption of nitrogen-containing benzene derivatives on noble metal surfaces using density functional theory calculations with the PBE+vdWsurf method, which takes into account van der Waals forcers and screening of the dispersive interactions inside the inorganic bulk [4]. Our calculations show that complex interplay of covalent bonding and van der Waals forcers may lead to appearance of multiple adsorption states of isolated adsorbed molecules on metal surfaces. In particular, for s-triazine ($C_3N_3H_3$) adsorbed on Pt(111) four distinct adsorption states are identified by calculations. One of them is a physisorbed state, three other are chemisorbed states characterized by different equilibrium geometry of the adsorbed $C_3N_3H_3$ molecule (Fig. 1).

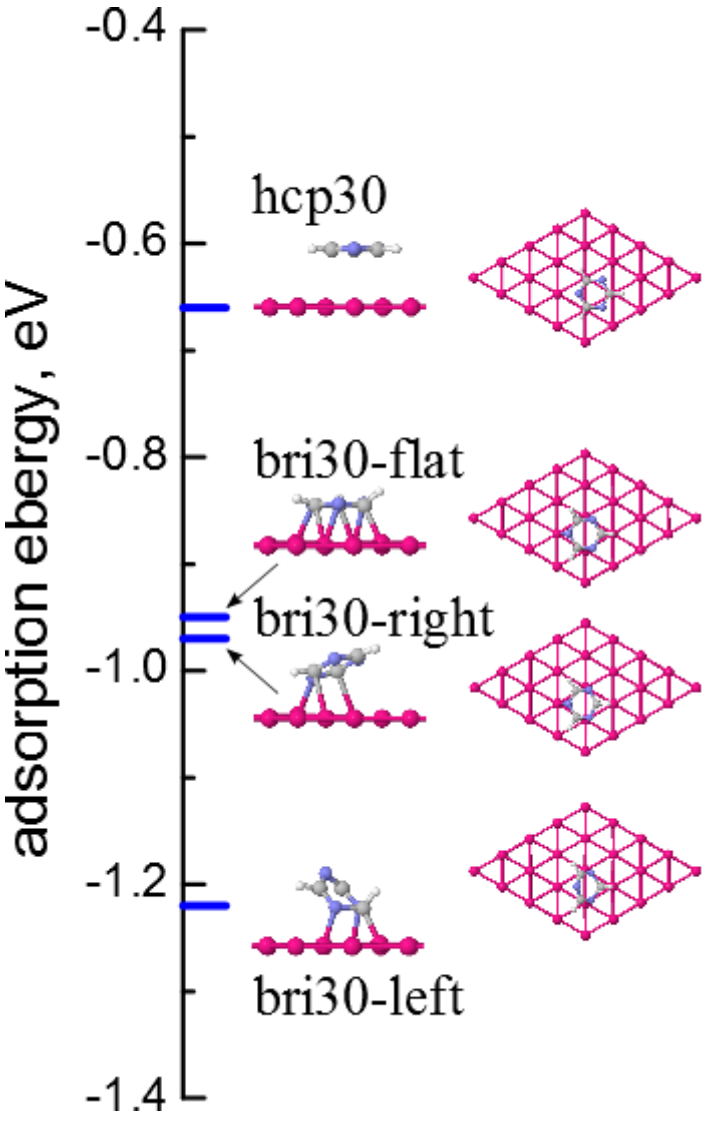

Fig.1 Four adsorption states of s-triazine on Pt(111).

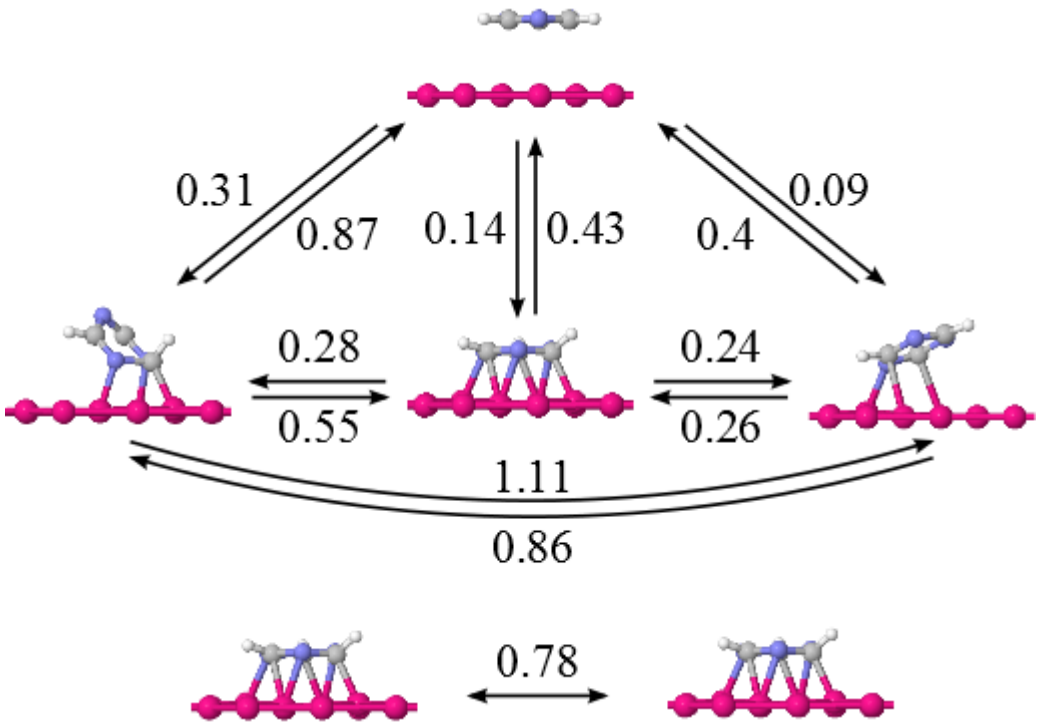

Fig.2 Transition barriers between different adsorption states of s-triazine on Pt(111).

The most stable adsorption state of s-triazine on Pt(111) is the bri30-left state in which two nitrogen atoms and one carbon atom of the molecule are located close to the metal surface presumably forming strong covalent bonds with underlying Pt atoms. The rest atoms of the molecule, including hydrogen atoms, are lifted up from the surface, so that the aromatic ring is strongly distorted and the molecule looks tilted in respect to the surface. In the next stable state, bri30-right, the molecule is tilted in the opposite direction, with one nitrogen and two carbon atoms pointing to the surface. Slightly higher in energy is the brige30-flat state, characterized by a parallel orientation of the aromatic ring to the surface. The fourth state is the physisorbed state in which the molecule is lying flat at the hcp30 adsorption position.

Calculations show, that the physisorption minimum of s-triazine on Pt(111) is rather shallow: the barrier to escape the physisorption state and go to the chemisorbed bri30-right state is less than 0.1 eV. Thereby all three chemisorbed states are well separated by moderate activation barriers of 0.2-0.6 eV (Fig. 2). This should make possible reversible seesaw-like switching of $C_3N_3H_3$ between the chemisorbed states by applying external stimuli such as charge injection, mechanical manipulation etc. A barrier of 0.78 eV for surface diffusion of chemisorbed molecules should enable secure trapping of the target molecule at a particular adsorption site.

Acknowledgements

S.N.F. thanks the Russian Science Foundation for financial support (grant #14-12-00813).

References

[1] D.E. Brown, D.J. Moffatt, R.A. Wolkow, Science 279, 542–544 (1998).
[2] W. Liu, et al., Nat. Commun. 4:2569 (2013, doi: 10.1038/ncomms3569).
[3] R. Peköz et al., J. Phys. Chem. C 118, 6235 (2014).
[4] V.G. Ruiz, et al. Phys. Rev. Lett. 108, 146103, (2012).

Modelling ferro- and antiferromagnetic interactions in two-dimensional metal-organic coordination networks

Marisa N. Faraggi,[1,2] Vitaly N. Golovach,[3,45] Sebastian Stepanow,[6,7] Tzu-Chun Tseng,[7] Nasiba Abdurakhmanova,[7] Christopher Seiji Kley,[7] Alexander Langner,7 Violetta Sessi,[8] Klaus Kern[7,9] and Andres Arnau[1,3,4]

[1]Donostia International Physics Center (DIPC), P. de Manuel Lardizabal 4, E-20018 San Sebastián, Spain
[2] Instituto de Astronomía y Física del Espacio, Conicet, Bs.As. Argentina
[3]Departamento de Física de Materiales, Facultad de Ciencias Químicas, Universidad del Pais Vasco, Apdo. 1072, E-20080 San Sebastián, Spain
[4]Centro de Física de Materiales CFM, Materials Physics Center MPC, Centro Mixto CSIC-UPV/EHU, P. de Manuel Lardizabal 5, E-20018 San Sebastián, Spain
[5] IKERBASQUE, Basque Foundation for Science, E-48011, Spain
[6] Department of Materials, ETH Zürich, Hönggerbergring 64, 8093 Zürich, Switzerland
[7] Max Planck Institute for Solid State Research, Heisenbergstrasse 1, 70569 Stuttgart, Germany
[8] European Synchrotron Radiation Facility, BP 220, 38043 Grenoble, France
[9] Institut de Physique de la Matiére Condensée, École Polytechnique Fédérale de Lausanne, CH-1015 Lausanne, Switzerland
E-mail: andres.arnau@ehu.es

Magnetization curves of two rectangular metal-organic coordination networks formed by the organic ligand TCNQ (7,7,8,8-tetracyanoquinodimethane) and two different (Mn and Ni) 3d transition metal atoms [M(3d)] show marked differences that are explained using first principles density functional theory and model calculations.

We find that the existence of a weakly dispersive hybrid band with M(3d) and TCNQ character crossing the Fermi level is determinant for the appearance of ferromagnetic coupling between metal centers, as it is the case of the metallic system Ni-TCNQ but not of the insulating system Mn-TCNQ. The spin magnetic moment localized at the Ni atoms induces a significant spin polarization in the organic molecule; the corresponding spin density being delocalized along the whole system. The exchange interaction between localized spins at Ni centers and the itinerant spin density is ferromagnetic for sufficiently strong hybridization between both types of electron states.

Based on two different model hamiltonians, we estimate the strength of exchange couplings between magnetic atoms for both Ni- and Mn-TCNQ networks that results in weak ferromagnetic and very weak antiferromagnetic correlations for Ni- and Mn-TCNQ networks, respectively.

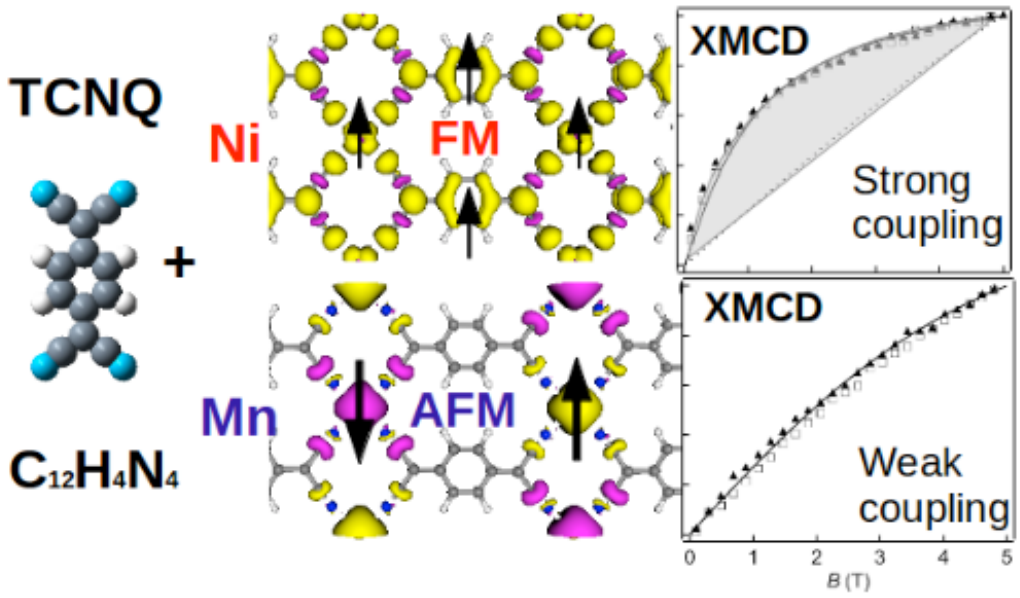

Figure. LEFT PANEL: top view of the TCNQ molecule with N atoms (blue), C atoms (grey) and H atoms (white). CENTRAL PANELS: spin density of Mn-TCNQ (lower panel) and Ni-TCNQ (upper panel) showing localized magnetic moments at Mn sites and delocalized magnetic moments at Ni and TCNQ sites, respectively. RIGHT PANELS: measured XMCD intensities as a function of applied magnetic field (magnetization curves) showing strong deviation from paramagnetic behaviour for Ni-TCNQ (upper panel) and, essentially, no deviation for Mn-TCNQ (lower panel).

Acknowledgements

M. N. F. and A. A. thank MINECO (grant number FIS2010-19609-C02-01) and Eusko Jaurlaritza - UPV/EHU (grant number IT-756-13) for financial support and DIPC for providing us with computational resources of its Computer Center. V. N. G. was supported by the Spanish Ministry of Economy and Competitiveness under Project No. FIS2011-28851-C02-02. We thank the ESRF for the provision of beam time to do the X-ray absorption experiments.

Water Adsorption on the SrO-terminated Surface of Strontium Ruthenates

Ulrike Diebold[1], Bernhard Stöger[1], Daniel Halwidl[1], Michael Schmid[1], Wernfried Mayr-Schmölzer[1,2], Florian Mittendorfer[1,2], Josef Redinger[1,2]

[1] *Institute of Applied Physics, TU Wien, 1040 Vienna, Austria*

[2] *Center for Computational Materials Science, TU Wien, 1040 Vienna, Austria*

E-mail: diebold@iap.tuwien.ac.at

The surfaces of ternary oxides are generally complex, thus surface chemistry studies on well-defined model systems are rare. Here we report a combined STM/DFT study of the Ruddlesden-Popper materials $Sr_{n+1}Ru_nO_{3n+1}$ (n=1, 2). The samples were grown by the group of Zhiqiang Mao [1]. Cleaving in ultrahigh vacuum results in almost perfect SrO-terminated surfaces with micron-sized terraces. Contrary to previous reports [2] the surface quality does not depend on the cleaving temperature, and the only apparent defects are due to impurities in the starting material [3]. The surface is surprisingly reactive, however. For example CO readily reacts, forming a strongly adsorbed carboxylate group [4].

Dosing water on the clean SrO-terminated surfaces at 105 K leads to dissociation of the molecule forming an $(OH)_{ads}$ group and an $O_{surf}H$ group. With STM we observe a locally restricted movement of the $(OH)_{ads}$ around the $O_{surf}H$. Such 'dynamic ion pairs' were predicted in theoretical studies on various alkaline earth oxide [5, 6, 7] and $SrTiO_3$(001) [8]. Annealing leads to diffusion and the formation of 1D chains. At higher coverages various superstructures form that depend on the dosing temperature and amount, as well as the annealing time.

Acknowledgements

We acknowledge support by the ERC Advanced Grant 'OxideSurfaces' and the Austrian Science Fund (Project F45)

References

[1] Z. Qu, *et al.*, Phys. Rev. B 78, 180407 (2008).
[2] Y. Pennec, *et al.,* Phys. Rev. Lett. 101, 216103 (2008).
[3] B. Stöger, *et al.,* Phys. Rev. B 90, 165438 (2014).
[4] B. Stöger, *et al.*, Rev Lett 113, 116101 (2014).
[5] J. Carrasco, F. Illas, F. and N Lopez, Phys Rev Lett 100, 016101 (2008).
[6] X.L. Hu, J. Carrasco, J. Klimeš, and A. Michaelides, Phys. Chem. Chem. Phys. 13, 12447 (2011).
[7] H. Grönbeck and I. Panas, Phys. Rev. B 77, 245419 (2008).
[8] H. Guhl, W. Miller, and K. Reuter, Phys. Rev. B 81, 155455 (2010).

Employing Infrared Reflection Absorption Spectroscopy to Probe Polarons in Photoactive Oxides: TiO_2 and ZnO

Fabian Bebensee, Alexei Nefedov, and Christof Wöll

Karlsruhe Institute of Technology (KIT), Institute of Functional Interfaces (IFG), Herrmann-von-Helmholtz-Platz 1, 76344 Eggenstein-Leopoldshafen, Germany

TiO_2 and ZnO are wide-band gap metal oxides exhibiting various desirable physico-chemical properties, e.g. high photocatalytic and photovoltaic activity. The nature of photo-excitations and their time-dependence are crucial for understanding and ultimately optimizing the photocatalytic activity of these materials. In this context, previous work has mainly focused on the investigation of excitons. A recent study has measured the ultrafast formation dynamics in case of ZnO.[1] It is important to note that charge carriers generated from dissociation of excitons, the crucial step for photocatalytic and photovoltaic activity, may be trapped in polaronic states. Consequently, the polaron binding energy becomes crucial for the photocatalytic activity, as this energy is not available to drive the desired reaction. Yet, only very little work has been devoted to these trap states. Here, we report a novel approach to study polarons in metal oxide single crystals by populating these trap states via UV-light irradiation and then probing them using infrared reflection absorption spectroscopy (IRRAS). We will present results for TiO_2 (cf. [2]) and ZnO, where a number of previously unobserved bands ascribed to polaronic states appear in the IR-spectra upon irradiation and compare them to theoretical work. Exploiting time-resolved IRRAS, we were able to determine lifetimes and binding energies for ZnO.

[1] J.-C. Deinert, D. Wegkamp, M. Meyer, C. Richter, M. Wolf, J. Stähler, *Phys. Rev. Lett.* **2014**, *113*, 057602.

[2] H. Sezen, M. Buchholz, A. Nefedov, C. Natzeck, S. Heissler, C. Di Valentin, C. Wöll, *Sci. Rep.* **2014**, *4*, 3808.

Electron- and Hole-Induced Reactions on Anatase TiO_2(101)

M. Setvin,[1] B. Daniel,[1] T. Simschitz,[1] M. Schmid,[1] U. Aschauer,[2] C. Di Valentin,[3] A. Selloni,[4] U. Diebold[1]

[1] *Institut für Angewandte Physik, Technische Universität Wien, A-1040 Wien, Austria*
[2] *ETH Zurich, Materials Theory, Wolfgang-Pauli-Strasse 27, 8093 Zürich, Switzerland*
[3] *Dipartimento di Scienza dei Materiali, Universita di Milano-Bicocca,Via R. Cozzi 53, 20125 Milano, Italy*
[4] *Department of Chemistry, Princeton University, Frick Laboratory, Princeton, NJ 08544, USA*
(corresponding author: M. Setvin, e-mail: setvin@iap.tuwien.ac.at)

TiO_2 is a prototypical material used in photocatalytic reactions, e.g. in water remediation, photocatalytic water splitting or in the oxidation of organic molecules [1, 2]. Industrially two forms of TiO_2 are used, rutile and anatase. Anatase is preferred in most applications, while fundamental research has mostly been conducted on rutile. Here we study elementary photocatalytic reactions on the anatase TiO_2 (101) surface using Scanning Tunneling Microscopy (STM) combined with Photoemission Spectroscopy (PES) and Density Functional Theory (DFT).

The key processes in photocatalysis are photon absorption, electron-hole pair generation, and transport of the excited charge carriers to reactants at the surface. The exact role of the electrons and holes in the photocatalytic reactions is still intensely debated. Photogenerated holes can directly oxidize adsorbed species, while excess electrons can activate molecular oxygen by forming superoxo or peroxo species chemisorbed at the surface. Here we choose two fundamental photocatalytic reactions to investigate the role of the excited charge carriers: Water splitting and methanol oxidation.

In our experiments the direct splitting of water by holes shows a negligible efficiency. On the other hand, water molecules readily react with adsorbed oxygen molecules. Water can transfer one hydrogen atom to the O_2 molecule, resulting in an OH group and an OOH species. DFT calculations show that the reaction is energetically favorable only when the O_2 molecule carries two excess electrons (peroxo species). The OOH further splits into an OH group and an oxygen adatom. The oxygen adatom incorporates into the surface, forming a so-called $(O_2)_O$ bridging dimer [3]. The $(O_2)_O$ can react with another water molecule, forming two OH groups. Thus the O_2-assisted water decomposition into OH groups is energetically favorable as long enough excess electrons are available. Based on DFT calculations, we discuss the number of electrons required for each reaction step.

Two steps are identified in methanol oxidation. In the first step – transformation to methoxy – hydrogen is again transferred to an adsorbed O_2 molecule in an electron-mediated process. The second step – methoxy to formaldehyde – occurs via direct oxidation by a photoexcited hole.

We compare our results on anatase (101) surface to equivalent reactions reported on the rutile (110), and point out key differences between these two TiO_2 polymorphs.

Acknowledgements

Work supported by the Advanced ERC grant “OxideSurfaces”.

References

[1] M. A. Henderson, Surf. Sci. Rep. **66**, 185 (2011).
[2] A. L. Linsebigler *et al.*, Chem. Rev. **95**, 735 (1995)
[3] M. Setvin *et al.*, Science **341** , 988 (2013)

Engineering polarons at an oxide surface

Geoff Thornton

London Centre for Nanotechnology, University College London,
7-19 Gordon Street, London WC1H 0AJ
Email: g.thornton@ucl.ac.uk

Polarons, that is lattice distortions associated with the stabilisation of electronic states, are thought to play a pivotal role in the physics and chemistry of metal oxides. They are implicated in phenomena as diverse as high-Tc superconductivity, resistive switching and photocatalysis. Although it is difficult to access polarons in the bulk material, in principle they can be probed and manipulated at the surface in order to test models of their formation and properties. Here this is exploited using a form of scanning probe measurement termed current imaging tunnelling spectroscopy (CITS). We employ oxygen-vacancy induced polarons on TiO_2(110) as our model system. By manipulating the lateral positions of O_b-vacs using electrical pulses in STM, we show that the polaron follows the O_b-vac and is therefore not associated with a particular donor centre in the selvedge. Moreover, by forming O_b-vac dimers, trimers and tetramers it is possible to examine the interaction between polarons. We compare these data to the results of theoretical models.

Wednesday

Two-dimensional alloy of immiscible metals on close-packed surfaces

J. Yuhara, M. Yokoyama, T. Ako, T. Matsui
School of Engineering, Nagoya University, Nagoya, Japan
E-mail: j-yuhara@nagoya-u.jp

Over the last few decades, the formation of surface alloys has been studied intensively because of their importance not only for fundamental aspects but also industrial applications. Many of the systems form monolayer surface alloys, even though they are immiscible in bulk. Recently, bimetallic monolayer films of immiscible metals Pb-Sn exhibit two dimensional (2D) ordered alloy of $PbSn_3$ on Rh(111) and Ru(0001) [1,2]. The Pb and Sn monolayer films form 2D hexagonal and rectangular structures, respectively, both on Rh(111) and Ru(0001). The Hume-Rothery rule indicates that a solid solution alloy can be formed when two elements have identical crystal structures and the relative difference in atomic sizes is less than 15% between the two species [3]. A recent study showed that Bi films form hexagonal structure on Rh(111) [4]. Moreover, we have identified that the Sn film also form hexagonal structure on Ag(111). In this talk, we present a detailed study of the 2D system of Pb-Bi and Pb-Sn monolayer films on Rh(111) and Ag(111), respectively, using low-energy electron diffraction, Auger electron spectroscopy, and scanning tunneling microscopy. Atomic resolution STM images showed that the Pb-Bi binary films on Rh(111) formed hexagonal close-packed structure with 2D solid solution alloy [5]. The interatomic distance linearly decreased from 0.359 nm to 0.342 nm as increasing the Pb compositional ratio, which follows Vegard's law [6]. On the contrary, the Pb-Sn films on Ag(111) exhibited 2D alloy of Pb_2Sn at the coverage of 0.5 ± 0.1 ML Pb and 0.25 ± 0.1 ML Sn [7]. Our results imply that 2D alloy seems to follow the Hume-Rothery rule.

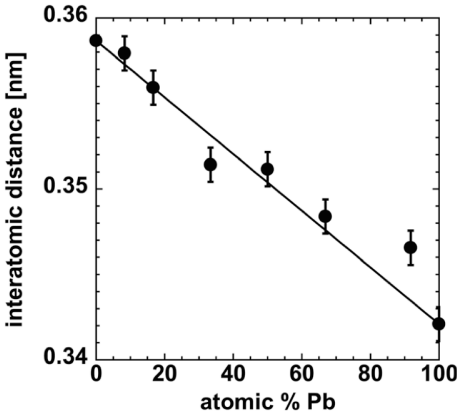

Fig. Nearest neighbor interatomic distance in Pb-Bi 2D films on Rh(111) as a function of Pb compositional ratio.

References

[1] J. Yuhara, M. Schmid, P. Varga, Phys. Rev. B **67** (2003) 195407.
[2] J. Yuhara, Y. Ishikawa, and T. Matsui, Surf. Sci. **616** (2013) 131.
[3] W. Hume-Rothery, R.E. Smallman, C.W. Hayworth, The Structure of Metal and Alloys (The Metals and Metallurgy Trust, London, 1969).
[4] M. Yokoyama, W. S. Liang, W. Chen, A.T.S. Wee, T. Matsui, and J. Yuhara, Surf. Sci. **605** (2011) 844.
[5] J. Yuhara, M. Yokoyama, T. Matsui, J. of Appl. Phys. **110** (2011) 074314.
[6] L. Vegard, Z. Phys. **5** (1921) 17; Z. Kristallogr. **67** (1928) 239; A.R. Denton, N.W. Aschcroft Phys. Rev. A **43** (1991) 3161.
[7] J. Yuhara, T. Ako, Surf. Sci. (2015) in preparation.

Highly ordered Gold-Germanium surface alloy

A.Resta[1], A. Vlad[1] , F. Cheynis[2], Y. Garreau[1,3], A. Coati[1]

[1] *Synchrotron SOLEIL, L'orme des Merisiers BP48, F-91192 Gif Sur Yvette, France*

[2] *CINaM, UMR 7325 Aix-Marseille Université/CNRS, Marseille France*

[3] *Univ Paris Diderot, Sorbonne Paris Cite, MPQ, UMR CNRS 7162, F-75205 Paris 13, France*

E-mail: Resta@synchrotron-soleil.fr

The surfaces of bulk alloys have long been known to be of practical interest for their chemical/physical properties, which differs from the constituent elements in isolation. It has also long been known that the surface composition of such alloys commonly differs from that of the underlying bulk. Nevertheless, our understanding of these chemical and physical phenomena is far from complete, and the application of surface science methods to investigate these phenomena is a manifestation of a general trend to the study of surfaces of increasing complexity. A phenomenon which has been fully recognised far more recently is that of surface alloy formation - the intermixing of substrate atoms and adatoms in the outermost atomic layer, or few atomic layers of a solid, to form a stable ultra-thin alloy phase which may be in equilibrium with an essentially elementally pure substrate, even involving the intermixing of elements which are immiscible in the bulk[1] as the case of gold and germanium[2]. It is in this prospective that we investigate the effect of few percent of germanium mono-layer deposited on the Au(111)22x√3[3-4] clean surface. Beside advancement in fundamental research this subject find application in Gold Germanium junctions which are used for fast alpha particle detection[5]. Moreover recently an article was published on the growth of bi-dimensional germanium layers on Au(111) [6], therefore those information can become useful also in the field of two dimensional materials such as graphene, silicene and many others, that in recent years is attracting more and more researchers[7].

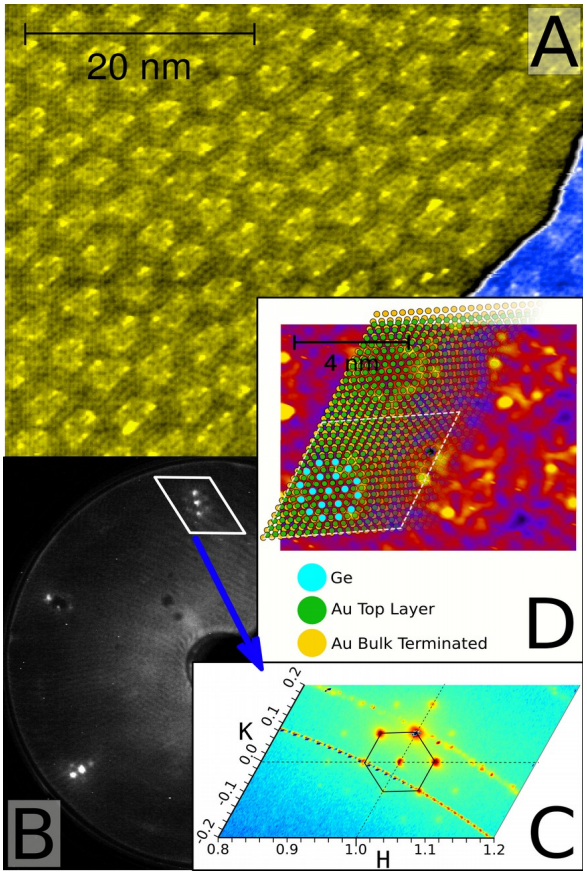

Fig 1: A) Large scale STM image of the ordered alloy [I=13.3nA ,Bias=-0.83V]. B) LEED image of the Au(111) Ge structure [Ekin=65eV] C) Surface X ray diffracion map around the [1 0 0.15] reflection of Au(111) surface, hv=11.8 keV. D) Small scale STM image [I=10.3nA, Bias=-1.15 V]and the current Au(111)16x16 – R0°- 19Ge 270Au atomistic interpretative model.

The aim of this contribution will be to present the surface evolution from the native herring bone (Au(111)22x√3) reconstruction towards a regular array of hexagonal tiles as the content of germanium increase up to few percent. The transition occur first with a sudden change from the herring bone to a 22x22 then smoothly and proportional to the germanium content

towards a 16x16 as probed with surface x-ray diffraction data. The interpretative model (Fig 1D) proposed is consistent with data obtained from Scanning Tunnelling microscope (Fig 1A), Low energy Electron Diffraction (Fig 1B), surface x-ray diffraction (Fig 1C), and high resolution core level spectroscopy.

Acknowledgements

References

[1]2002 Elsevier Science B.V. Surface Alloys, and Alloy Surfaces. D.P. Woodruff, (Editor).
[2]Bulletin of Alloy Phase Diagrams 5 (1984) 602
[3] J.V. Barth, H. Brune, G. Hertl, R.J. Behm. Phys. Rev. B. 42(1990) 9307
[4] Ch, Wöll, S. Chiang, R.J. Wilson, P.H. Lippel. Phys. Rev. B. 39 (1989) 7988.
[5] J.M. McKenzie, D.A. Bromley, IEE Proceedings - Part B: Electronic and Communication Engineering, Vol. 106, (1959), p. 731
[6] M E Dávila, L Xian, S Cahangirov, A Rubio, and G Le Lay. New J. of Physics 16 (2014) 095002
[7] S. Z. Butler., S. M. Hollen, L. Cao, Y. Cui et. Al. ACS Nano 7 (2013) 2898–2926

Dynamics of Au nano-droplets on Si surfaces: self-propelled motion and nanowire formation

S. Curiotto, F. Leroy, F. Cheynis, P. Müller
CINaM, UMR 7325 Aix-Marseille Université/CNRS, Marseille France
E-mail: curiotto@cinam.univ-mrs.fr

Spontaneous migration of droplets involves many processes like 2D ordering, self-assembly mechanisms, mass transport at the nanoscale or growth of nanowires. Understanding the physical mechanisms at the origin of the self-propulsion of nanoparticles on a substrate is a challenge. Since the mobility of a nanoparticle is closely related to its interaction with the underlying surface, the features of the movement depend on the crystallographic orientations and on the nanomorphology of the substrate.

In this work we consider the specific case of droplets grown by deposition of Au on Si substrates with different orientations. Au particles formed on a Si substrate tend to dissolve Si and to become liquid droplets. By Low Energy Electron Microscopy (LEEM) we show that the dynamic behaviour of these droplets depends on the substrate orientation. During Au deposition, only on (001) substrates the droplets grow, spread isotropically and etch deep holes. On other Si orientations the droplets move spontaneously. For instance, on (111) vicinal surfaces, they climb-up and nibble the Si monoatomic steps, leaving a groove in the surface [1]. On Si(110) the droplets spread and move along the [110] direction, dig etch pits in the substrate, and leave behind them a Si nanowire! Comparing the droplet behaviours on the different substrates we show that the morphologies of the growing droplets and of the Si nanowires depend on the shape of the etch pit.

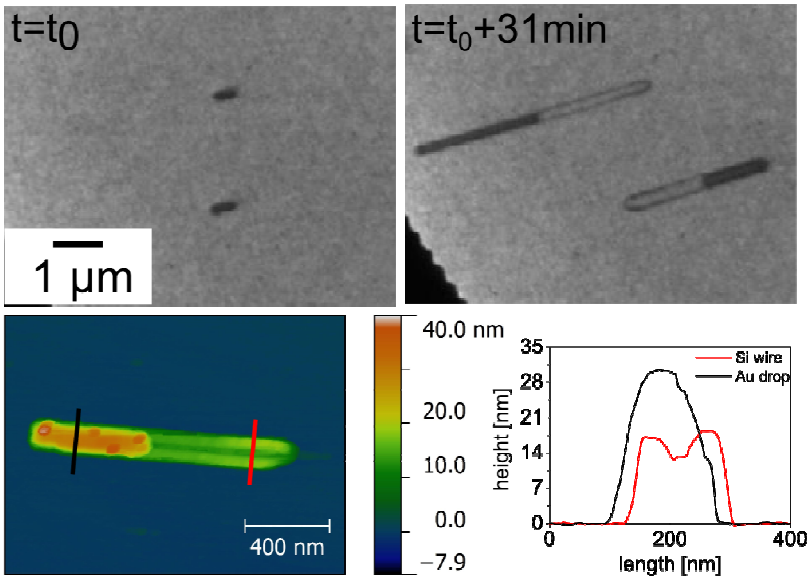

Fig. Top panel: Bright field LEEM images (2eV) of Au-Si droplets moving on Si(110). The black shapes are elongated droplets and have formed a grey Si nanowire behind. Bottom panel: AFM image of an elongated droplet (red-yellow) and the Si wire (green). The profiles of the droplet and of the wire are shown on the left.

Acknowledgements

We thank ANR 13 BS-000-402 grant LOTUS

[1] S. Curiotto, F. Leroy, F. Cheynis, P. Müller, Surface Science 632, 1 (2015).

In-situ study of AuCu NanoParticles Epitaxied on TiO2(110): Synthesis, Structure and Behavior at Low Pressure of Reactant

A. Wilson[1,2], A. Vlad[1], A. Coati[1], R. Bernard[2], Y. Borensztein[2], B. Croset[2], G. Prévot[2], and Y. Garreau[1,3]

[1]*Synchrotron SOLEIL, L'Orme des Merisiers, Saint-Aubin–Boîte Postale 48, 91192 Gif-sur-Yvette cedex, France*
[2]*Institut des NanoSciences de Paris, Université Paris 6, 4, place Jussieu, 75252 Paris cedex 05, France*
[3] *Matériaux et Phénomènes Quantiques, Université Paris Diderot, Sorbonne-Paris-Cité, UMR 7162 CNRS, Bâtiment Condorcet, Case 7021, 75205 Paris Cedex 13, France*
E-mail: garreau@sychrotron-soleil.fr

Specific properties for applications in electronics, optics, magnetism or catalysis can be achieved using materials based on nanoparticles (NPs). The development and characterization of the bimetallic NPs and the understanding of their physical and chemical properties are thus crucial steps for their technological applications. Among them, a promising field is the heterogeneous catalysis: Au NPs have become a paradigm of size effects on the catalytic properties. To improve the catalytic activity of Au-based NPs, a promising method is to use bimetallic NPs that can exploit the synergy between two metals for catalytic reactions. For example, Au-Cu/silica NPs display a better activity for CO oxidation than pure Au or Cu NPs and a better selectivity for preferential oxidation (PROX)[1]. However, the synergies between the two metals and the substrate are not clearly understood.

Scanning tunneling microscopy (STM) and grazing-incidence X-ray diffraction (GIXD) have been used to follow *in situ* the growth and the structure of Au-Cu nanoparticles (NPs) formed on TiO_2(110) by successive metal evaporations [2]. STM observations of the same area of the substrate highlight the strong dependence between the sequence of deposition and the final result. Deposition of Cu first leads to a system where both Au-Cu and pure Au NPs coexist. Deposition of Au first ensures growing mostly bimetallic NPs. GIXD results show that Cu alloys instantaneously with Au NPs at room temperature. Reciprocal space map measurements reveal different epitaxial relationships for crystallized particles and a diffuse ring (see figure) due to the presence of icosahedral NPs that have not specific orientations.

In the presence of oxygen ($PO_2=10^{-7}$ mbar), STM experiments show that Cu NPs of size smaller than 1 nm are unstable [3] but that a small amount of Au (<10%) is enough to ensure their stability. However, GIXD measurements show that the nanoalloys structures are strongly modified during O_2 exposure: the lattice constant of the NPs increases, meaning that Cu segregates at the NPs surface and Au enriches in the core of the NPs. The core-shell configuration obtained is stable at room temperature, even under CO exposure, but annealing above 200°C allows the system to release oxygen and let the Cu diffuse back in the core of the NPs. We also have evidence of a reorganization of small non-oriented NPs toward one specific epitaxial relationship in the presence of a $CO+O_2$ gas phase ($P_{tot} < 10^{-5}$mbar).

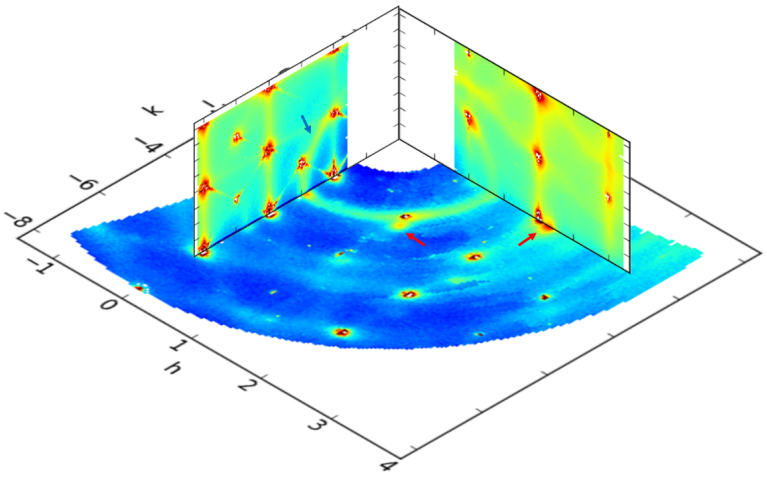

Reciprocal space maps of AuCu NPs grown on TiO_2(110). Maps are represented in reduced units (h//[001]$_{TiO2}$, k//[1-10]$_{TiO2}$). Intense spots for integer numbers of (hkl) are Bragg peaks coming from the substrate. Red arrows point out the spots related to the NPs that present an epitaxial relationship with the subtract. The blue arrow points out the diffuse sphere due to the non-oriented NPs.

References

[1] X. Liu, A. Wang, L. Li, T. Zhang, CY Mou, JF Lee, J. Catal. 2011, 278, 288–296.
[2] A. Wilson, R. Bernard, A. Vlad, Y. Borensztein, A. Coati, B. Croset, Y. Garreau, and G. Prévot Phys Rev.B 90 (2014) 075416.
[3] J. Zhou, Y.C. Kang, and D.A. Chen, J. Phys. Chem. B 107 (2003) 6664–6667.

Sample size dependent active phase

S. Blomberg[1], J. Zetterberg[2], C. Brackmann[2], N. M. Martin[1,*], L. R. Merte[1], C. Zhang[1], M. Shipilin[1], M. Aldén[1], E. lundgren[1], J. Gustafson[1]

[1] *Synchrotron Radiation Research, Lund University, Lund, Sweden*

[2] *Division of Combustion Physics, Lund University, Lund, Sweden*

E-mail: johan.gustafson@sljus.lu.se

The active phase of Pt-metal based CO oxidation catalysts has been thoroughly studied and much debated during the last decades. While several studies have shown that a surface oxide forms when the catalytic activity increases, other studies have shown that the surface is metallic under similar conditions. In a recent high pressure X-ray photoelectron spectroscopy (HPXPS) study, we have shown that the active phase of Pd(100) is strongly dependent on the gas mixture as well as the total pressure [1]. At low total pressures or low O_2:CO partial pressure ratios the surface cannot be oxidized. A higher O_2:CO ratio leads to a higher the oxygen coverage on the active surface, and sufficiently high ratios will oxidize the surface. The same is true for higher total pressures at a constant O_2:CO ratio.

In the present contribution we report on two HPXPS experiments, under similar condition, using two Pd(100) crystals of different size. In both experiments, the chamber was filled with 0.33 mbar O_2 and 0.33 mbar CO at low sample temperature, followed by a stepwise heating and activation. The results are summarized in the top and bottom panels of Fig. 1, respectively. Starting with the C 1*s* spectra to the right in the figure, both experiments are similar. At low temperature the samples are catalytically inactive and the spectra reveal CO on the surface as well as in the gas phase. As the sample temperature is increased, the surface becomes catalytically active and transforms the CO at and near the surface to CO_2. The activity is so high that the only peak that can be found in the spectra is the CO_2 gas phase peak. The amount of CO is below the detection limit both on the surface and in the gas phase.

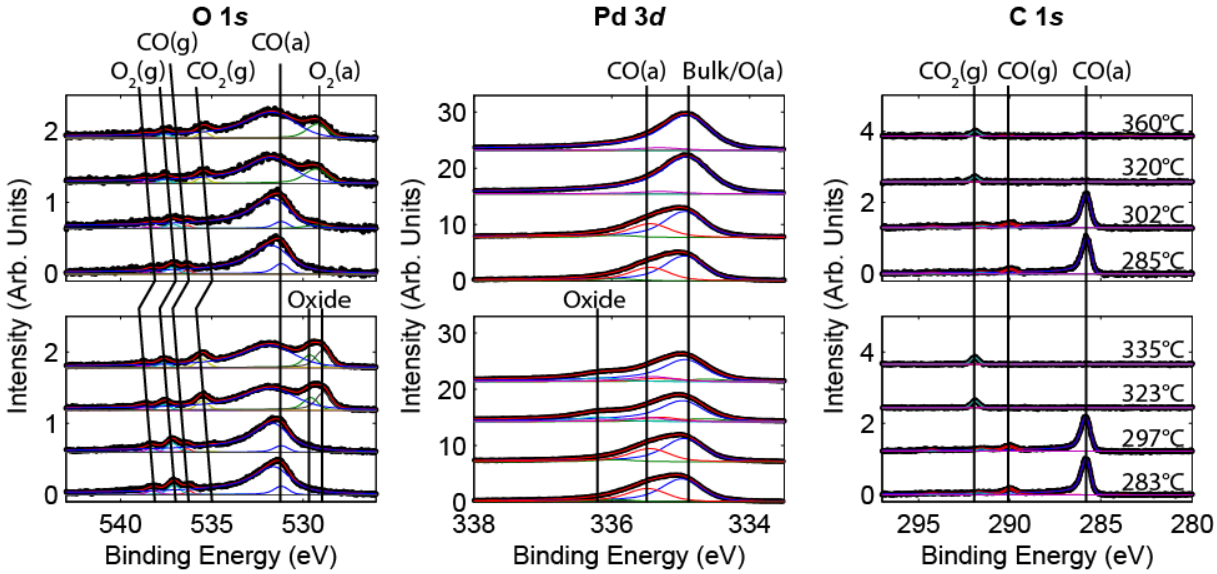

Figure 1 HPXPS data during catalytic activation of Pd(100) in 0.33 mbar O_2 and 0.33 mbar CO. The top panel is from a small crystal (4×4 mm) while the bottom panel is from a larger crystal (9 mm diameter). Both samples become active at around 310°C, as seen from the disappearance of the CO signals and appearance of CO_2 in the C 1*s* spectra. In the active phase, the small sample (top) is covered by chemisorbed oxygen while the large sample (bottom) shows the presence of a surface oxide.

Continuing to the O 1*s* spectra to the left, they coincides with the Pd 3*p* level, which appears as a broad background peak, but show the same trend. At low sample temperatures the surface is catalytically inactive and we find CO and O_2 in the gas phase and CO at the surface, while at higher sample temperatures the gas phase is dominated by CO_2 and instead of CO we find O at the surface. Here we find the difference, though. The top spectra are deconvoluted with a single peak corresponding to (chemisorbed) O on the surface, while the bottom spectra show two O components, which is a fingerprint of an oxide.

This difference is emphasized in the Pd 3*d* spectra in the middle. The CO covered surfaces show two clear components corresponding to surface Pd atoms coordinated to CO and bulk Pd atoms, respectively. In the top panel, the O covered surface shows a single strong component, since bulk Pd and surface Pd coordinated to 1 chemisorbed O atoms have similar binding energies. In the bottom panel, however, the corresponding spectra reveal a component shifted far to higher binding energy, confirming the formation of a surface oxide.

The difference between the two experiments is the size of the samples. The spectra in the top panel of Fig. 1 are from a square crystal of 4×4 mm, while the bottom panel is from a circular crystal with a diameter of about 9 mm.

Using planar laser-induced fluorescence (PLIF), we are able to understand why this apparently minor difference makes such contradicting results. Fig. 2a shows a PLIF image of the CO concentration around a catalytically active 4×4 mm Pd surface in an incoming flow of 50 mbar O_2, 50 mbar CO and 100 mbar Ar. Around the sample the catalytic reaction forms a boundary layer of CO_2, resulting in a depletion of the CO (as well as O_2) concentration. Fig. 2b shows the CO profile over the surface demonstrating that the CO partial pressure varies from 5 mbar over the centre of the sample to 10 mbar at the sample edge. For a larger sample, the partial pressure in the centre will be even more different as compared to near the edge, i.e., the O_2:CO ratio will be higher and the surface is more likely to oxidize.

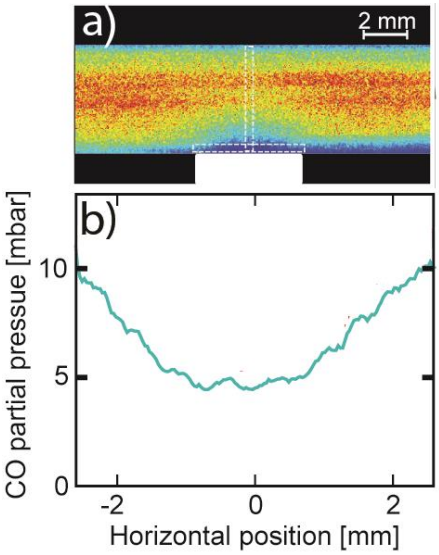

Figure 2 a) PLIF image of the CO concentration above a catalytically active Pd surface. b) Variation of the CO partial pressure over the surface.

Acknowledgements

The authors gratefully acknowledge financial support from the Swedish Researc Council, Swedish Foundation for Strategic Research (SSF), the Crafoord foundation, the Knut and Alice Wallenberg Foundation, and the Anna and Edwin Berger foundation and the European Scientific Research Council (ERC) through the DALDECS program. The work was also supported by the Director, Office of Science, Office of Basic Energy Sciences, of the U.S. Department of Energy under Contract No. DE-AC02-05CH1123

* Now at Competence Centre for Catalysis, Chalmers University of Technology, Göteborg, Sweden

References

[1] S. Blomberg et al., Phys. Rev. Lett. **110**, 117601 (2013).

Surface Chirality of Intermetallic PdGa Single Crystal Catalysts

J. Prinz[1], C. Pignedoli[1], Q. Stöckl[2], H. Brune[3], D. Passerone[1], O. Gröning[1], R. Widmer[1]

[1] *Empa. Swiss Federal Laboratories for Materials Science and Technology, nanotech@surfaces Laboratory, Dübendorf, Switzerland.*

[2] *Empa. Swiss Federal Laboratories for Materials Science and Technology, Nanoscale Materials Science,Dübendorf, Switzerland.*

[3] *Institute of Condensed Matter Physics, Ecole Polytechnique Fédérale de Lausanne (EPFL), Lausanne, Switzerland.*

E-mail: roland.widmer@empa.ch

With its highest technological and economic importance, catalysis is an extremely active research area, which yields in a great impact on the development of new catalyst systems with the aim to produce more efficient and selective chemical processes. Thereby, a key issue is to gain detailed knowledge of the underlying molecular mechanisms which relate the structure, composition, and chemical bonding of the topmost catalytically active surface layer with the reactant.

Recently, intermetallic Pd-Ga compounds were presented as extraordinary selective catalysts for the semi-hydrogenation of acetylene [1], a key process in the polyethylene production. These intermetallic compounds exhibit specific separations of the catalytically active sites [2] and thereby reconcile the usually mutually excluding properties of high activity and concomitant high selectivity. Additionally, the crystal structure of PdGa belongs to the $P2_13$ space group and therefore this system features an intrinsic chirality and polarity [2,3].

As a first step, the stable surface terminations were determined and explored, since they define the activity and selectivity of the catalyst. For this purpose, we investigated the surface atomic and electronic structures of low Miller indexed PdGa single crystals, serving as model catalysts.
In a next step, high-resolution scanning tunneling microscopy (STM) enabled to directly visualize the adsorption geometry and conformational changes in small hydrocarbon molecules upon reaction. In combination with DFT calculations different extent of changes in the adsorption site for the different molecules on the PdGa(hkl) surfaces were discovered [4]. Special emphasis was put on the role of step edges as they are usually most reactive for molecular adsorption and catalytic processes.

As mentioned above, due to its non-centrosymmetric bulk structure of the space group $P2_13$, PdGa exists in two enantiomeric forms A and B, which are denoted as PdGa:A and PdGa:B respectively [3]. All their surfaces are intrinsically chiral and stable due to the intermetallic character. This is markedly different than the common approach for stereochemical processes, where mainly induced chirality is used, such as: i) self-assembled chiral molecular layers, ii) deposition and alteration of chiral inorganic thin films and iii) specific, high index vicinal surfaces exhibiting chiral kink sites at the step edges of atomic terraces.
The advantage of intermetallic PdGa is the significantly higher thermal and chemical stability, and therefore its extended application range for catalyzed chiral reactions compared to surfaces templated with chiral molecular modifiers or auxiliaries. We show that on the Pd_1 terminated PdGa(111) surface, room temperature adsorption of a small prochiral molecule (9-Ethynylphenanthrene, cf. Figure) leads to exceptionally high surface-enantiomeric excess ratios of up to 98%. Our findings [5] highlight the great potential of intrinsically chiral

intermetallic compounds for the development of novel, enantioselective catalysts which can be operated at high temperatures and potentially also in harsh chemical environments.

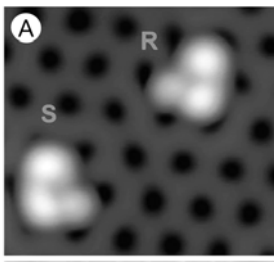

Figure: STM image (3.8x3.5 nm^2, 0.02 V, 2 nA, T = 5 K) of 9-Ethynylphenanthrene adsorbed at room temperature on PdGa:A(111)Pd$_1$. The different adsorbates are identified as clockwise (R) and counterclockwise (S) adsorption conformation.

Our investigations relay mainly on UHV techniques such as STM, X-ray photoelectron spectroscopy and diffraction (XPS and XPD), angle-resolved photoelectron spectroscopy (ARPES), I(V)-Low Energy Electron Diffraction (LEED-I(V)) and atomistic simulations. Thereby, the precise surface stoichiometry and the identification and characterization of relevant adsorption sites were revealed and lead to a better understanding of the materials properties giving rise to a high selectivity towards a specific reaction product and very pronounced surface-enantioselectivity, even though, it remains a challenge to bridge the gaps that were opened by the idealized conditions typically applied in these studies.

Acknowledgements

We gratefully acknowledge funding by the Swiss National Science Foundation under the contract 200021-129511 and support by the Swiss National Supercomputing Center (CSCS).

References

[1] M. Armbrüster, K. Kovnir, M. Behrens, D. Teschner, Y. Grin, R. Schlögl, *J. Am. Chem. Soc.* **132**, 14745 (2010).
[2] J. Prinz, R. Gaspari, C.A. Pignedoli, J. Vogt, P. Gille, M. Armbrüster, H. Brune, O. Gröning, D. Passerone, R. Widmer, *Angew. Chem Int. Ed.* **2012**, 51, 9339.
[3] D. Rosenthal, R. Widmer, R. Wagner, P. Gille, M. Armbrüster, Y. Grin, R. Schlögl, O. Gröning, *Langmuir* **2012**, *28*, 6848
[4] J. Prinz, C. Pignedoli, Q. Stöckl, M. Armbrüster, H. Brune, O. Gröning, D. Passerone, R. Widmer, *J. Phys. Chem. C* **2014**, *118*, 12260; J. Prinz, C.A. Pignedoli, Q.S. Stöckl, M. Armbrüster, H. Brune, O. Gröning, R. Widmer, D. Passerone, *J. Am. Chem. Soc.* **2014**, *136*, 11792.
[5] J. Prinz, O. Gröning, H. Brune, R. Widmer, submitted

Fischer-Tropsch Co(0001) catalyst followed in situ by high pressure STM

V. Navarro and J. W. M. Frenken
Leiden University. Kamerlingh Onnes Laboratory. Leiden. The Netherlands.

Catalysts, as any dynamic system, need to be studied *in situ* in order to understand how they work. These systems have largely been studied with traditional surface science techniques typically operated under vacuum conditions- very different to the real industrial ones. The "pressure gap", difference in pressure between studies in vacuum and the industrial ones, can be up to 13 orders of magnitude. Although the studies in vacuum can be very revealing [1], the "pressure gap" leads to dramatic differences between laboratory and industrial systems. The physico-chemical processes that govern the system might not be the same in both cases.

In our lab we follow catalysts at the atomic scale reproducing the conditions of pressure and temperature used in the industry. We do this by using a scanning tunneling microscope (STM) which works under high pressures (up to 6 bar) and temperatures (up to 320°C) [2, 3]. The STM tip is inside a small gas flow reactor placed in a UHV chamber. Traditional surface science techniques are used to prepare and characterize the samples down to the atomic level, before exposing them to reaction conditions. We can visualize the structural changes on the surface of the catalyst *during* the reaction. Simultaneously we use mass spectrometry to detect the gaseous products of the reaction to be able to correlate them with the structural changes.

As a model catalyst, we have used a single crystal of cobalt to study the Fischer-Tropsch synthesis. This catalytic reaction produces hydrocarbons of different lengths like octanes, used as fuel, from a mixture of CO and H_2. This reaction is of extreme industrial relevance but the fundamental mechanisms are still not known [4]. We have got some insight into the catalyst in action. We have observed several changes on the very dynamic cobalt surface at the atomic scale during the reaction. Among others, islands with internal periodicity grow on the surface until completely covering it. We believe that those are the longer molecules produced during the reaction that self assemble on the surface forming a regular pattern.

References:

1- G. Ertl. *Angewandte Chemie International Edition*, **52**, 1, 52–60, (2013).
Y.D.Yin, *et al*., Science, **304**, 5671. 711 (2004). R. Schaub, *et al*.. Phys. Rev. Let. **87**, 26 (2001).
2- B.L.M. Hendriksen, *et al*., *Topics in Catalysis*, **36**, 1–4 (2005).
3- C.T. Herbschleb at al. Submitted (2014).
4- J. Wilson *et al*., J. *Phys. Chem.* **99**, 7860 (1995).

Substrate dependent reactivity of FeO ultra-thin films

L.R. Merte[1], S. Ataran[1], M. Shipilin[1], S. Blomberg[1], J. Gustafson[1], F. Zhang[2], J. Choi[2], J. F. Weaver[2], C. Heard[3], H. Grönbeck[3], E. Lundgren[1]

[1]*Div. of Synchrotron Radiation Research, Lund University, SE-22100 Lund, Sweden*
(Corresponding author: E. Lundgren, email: edvin.lundgren@sljus.lu.se)
[2]*Department of Chemical Engineering, University of Florida, Gainesville, Florida, USA*
[3]*Department of Applied Physics and Competence Centre for Catalysis,*
Chalmers University of Technology, Göoteborg, Sweden

Recently, monolayer-thick FeO films have gained significant attention in surface chemistry and catalysis. In particular FeO films grown on the Pt(111) surface have been studied in detail [1-4] and it has been reported, most intriguingly, that the formation of an O-Fe-O trilayer phase displays a higher activity than the Pt(111) surface itself for CO oxidation under semi-realistic conditions [4]. It has been suggested that, due to the loosely bound top-most oxygen atoms in the O-Fe-O layer, the reaction proceeds via an Eley-Rideal mechanism; The CO solely interacts with the top-most oxygen forming CO_2. In fact, this promotional effect appears also to be operative for Pt nanoparticles supported on iron oxide surfaces, as these may become spontaneously encapsulated by an O-Fe-O layer of the same type [5,6] as on Pt(111).

Clearly, these observations are interesting, not only from a fundamental point of view but also from an application point of view and an atomistic design approach to novel catalysts. In particular, it is of interest to study the influence of the substrate on the chemical properties on ultra-thin FeO films, and if possible to use a different substrate than Pt for FeO catalysis, due to its known efficiency in oxidation catalysis and high cost.

Previous studies on a variety of substrates have shown that FeO grows preferentially with a hexagonal (111)-like orientation. This common structure is stabilized in a polar state by charge transfer from the film to the surface, and hence the films' electronic and chemical properties should be tunable to some extent by changing the metal substrate.

With the aim of elucidating the effects of the substrate on the chemical properties of ultra-thin FeO films, we have investigated the growth of FeO on Ag(100) as well as the reactivity of the FeO film towards NO adsorption. We present a detailed structural study of the growth of FeO ultra-thin films on the Ag(100) surface combining STM, LEED, XPS, NEXAFS and DFT calculations. We show that it is possible to produce a well-ordered FeO(111)-type monolayer on an Ag(100) surface by reactive deposition and annealing. The FeO(111) monolayer exhibits a p(2x11)/c(2x12) unit cell due to coincidence of the hexagonal overlayer and square substrate lattices, and line defects having locally square atomic coordination are formed due to excess oxygen in the film. The monolayer structure is expanded laterally compared to similar films grown on Pt surfaces, which is attributed to weaker interactions with the

substrate. By varying the substrate temperature and the oxygen pressure, we show that it is also possible to grow FeO(100) grains and multilayer Fe and O layers.

Armed with this structural information we have studied the NO adsorption and desorption on the FeO ultra-thin films on Ag(100) using LEED, IRAS and TPD and compare the adsorption properties with those found for FeO films on Pt(111), see Fig. 1. In Fig. 1a are shown NO TPD from Pt(111) (red line) and from FeO(111)/Pt(111) (black line) after NO saturation adsorption at 85 K. It is clear that while a significant amount of NO adsorb on Pt(111), only a fraction adsorb on the FeO(111)/Pt(111), which has been attributed to NO adsorption on defects on the FeO(111) film. In the case of the FeO(111)/Ag(100) the situation is reversed as can be seen in Fig. 1b revealing no NO adsorption on the Ag(100) at 85 K while almost a full monolayer adsorb on the FeO(111)/Ag(100) system. Thus, despite their clear structural resemblance, the FeO(111) films on Pt(111) and Ag(100) has completely different reactivity towards NO adsorption. The reasons for these differences will be discussed in the contribution.

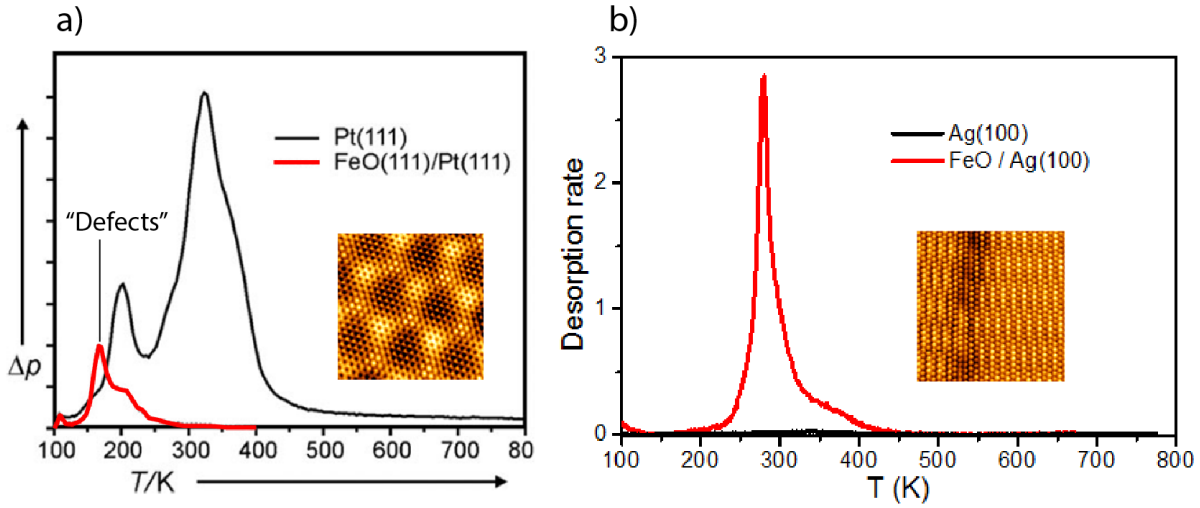

Figure 1 Comparing the reactivity of FeO(111) films on Pt(111) and Ag(100). a) Temperature Programmed Desorption (TPD) spectra from NO adsorbed on Pt(111) (black line) and on FeO(111)/Pt(111) (red line) [7]. A significantly larger amount of NO is found to adsorb on Pt(111) as compared to on FeO(111)/Pt(111). The NO adsorbed on the FeO(111)/Pt(111) has been attributed to adsorb on defects [7]. The inset show an STM image from the FeO(111)/Pt(111) surface. b) TPD spectra from NO adsorbed on Ag(100) (black line) and on FeO(111)/Ag(100) (red line). While no NO adsorb on the clean Ag(100) surface, close to a ML of NO is found to adsorb on the FeO(111)/Ag(100). The inset show an STM image from the FeO(111)/Ag(100).

References

[1] L. Giordano *et al.*, J. Phys. Chem. C **114**, 21504 (2010).
[2] H. Zeuthen *et al.*, J. Phys. Chem. C **117**, 15155 (2013).
[3] L. Giordano *et al.*, Phys. Rev. B **76**, 75416 (2007).
[4] J. Goniakowski, and C. Noguera, Phys. Rev. B **79**, 155433 (2009).
[5] Z.-H Qin *et al.*, J. Phys. Chem. C **112,** 10209 (2008).
[6] M. G. Willinger *et al.*, Angew. Chem. Int. Ed., **53,** 5998 (2014).
[7] Y. Lei *et al*., ChemCatChem **3**, 671 (2011).

Atomically dispersed and oxide-supported platinum in fuel cell catalysis: from surface science to in-situ spectroelectrochemistry

J. Libuda[1], O. Brummel[1], A. Bruix[2], Y. Lykhach[1], I. Matolínová[3], A. Neitzel[1], F. Faisal[1], T. Skála[3], N. Tsud[3], M. Vorokhta[3], V. Stetsovych[3], K. Ševčíková[3], J. Mysliveček[3], I. Khalakhan[3], R. Fiala[3], M. Václavů[3], K.C. Prince[5], F. Illas[2], V. Matolín[3], K.M. Neyman[2,4]

[1] Dept. of Chemistry and Pharmacy, Universität Erlangen-Nürnberg, Germany
[2] Dept. Química Física and IQTCUB, Universitat de Barcelona, Spain
[3] Dept. of Surface and Plasma Science, Charles University Prague, Czech Republic
[4] Institució Catalana de Recerca i Estudis Avançats (ICREA), Barcelona, Spain
[5] Sincrotrone Trieste, Basovizza-Trieste, Italy
E-mail: joerg.libuda@fau.de

Platinum is among the most versatile elements in catalysis, but it is rare and its high price limits large-scale applications. Conventional catalysts, for example in fuel cell technology, utilize only a small fraction of the Pt content, i.e. those atoms located at the catalyst surface. To improve the noble metal efficiency, new strategies are required to increase the dispersion of the precious metal. Ideally the metal should be atomically dispersed and exclusively located within the outermost surface layer of the material. We show that such atomically dispersed Pt surface species can be prepared with exceptionally high stability. Using density-functional calculations we have identified a specific structural element, a ceria "nanopocket", which binds Pt^{2+} so strongly that it withstands sintering and bulk diffusion.[1]

UHV experiments on model catalysts confirm the theoretically predicted stability (see [1] and Fig. 1). These surface science models are prepared by simultaneous co-deposition of Ce and Pt in an oxygen atmosphere onto an ordered $CeO_2(111)$ support. Under the applied conditions, Ce is known to form CeO_2 NPs.[2] We expect that the Pt should be incorporated into these oxide particles during their growth and can be trapped as Pt^{2+} on their {100} nanofacets. Indeed, scanning tunneling microscopy (STM) studies confirms the growth of three-dimensional partially facetted islands (see schematic representation in Fig.1). Synchrotron radiation photo-electron spectroscopy (SRPES) reveals the absence of any metallic Pt and the presence of ionic Pt in the oxidation states +2 and +4.

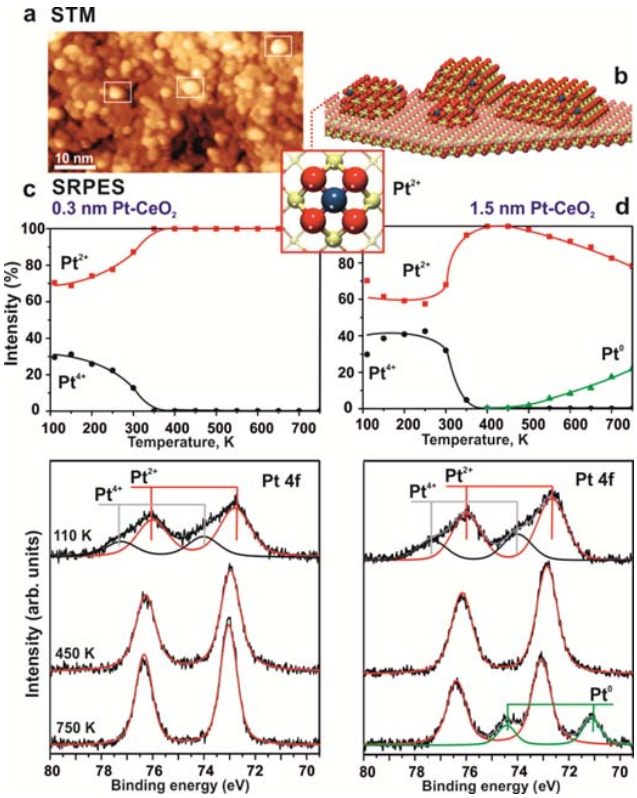

Fig. 1: (a) STM image obtained from Pt-CeO_2 nanoparticles grown on $CeO_2(111)$ in UHV, followed by annealing to 750 K. (b) Schematic structure model of the model catalyst. (c, d) Pt 4f core level spectra as a function of the annealing temperature (the nominal thickness of the Pt-CeO_2 codeposit is 0.3 nm and 1.5 nm.[1]

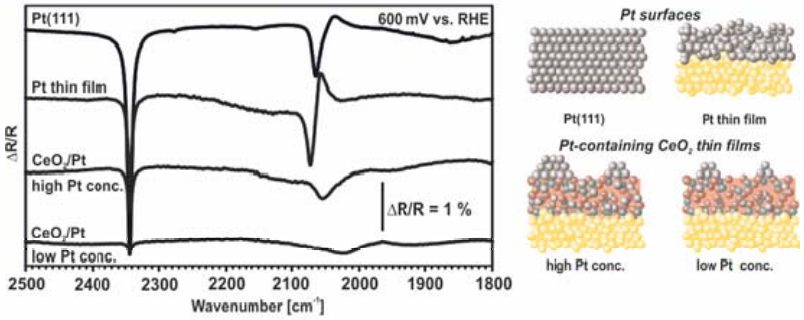

Fig. 2: LPSIRS (Linear Potential Scan Infrared Spectroscopy) during methanol oxidation (1 M MeOH in 0.1 M $HClO_4$) on Pt(111), polycrystalline Pt, and Pt-CeO_2 thin films at differrent Pt concentration.

Upon heating, the Pt^{4+} decomposes, but Pt^{2+} remains stable and anchored to the surface up to the highest temperatures that can be reached on our model surface (~ 750 K). Recent SR-PES studies have shown that similar preparation methods can be used to prepare atomically dispersed species of other metals as well (e.g. Ni and Pd). The latter, however show a thermal behaviour that is very different from that of Pt.

Interestingly, highly porous coatings of Pt-CeO_2 show very promising properties as electrocatalysts in proton exchange membrane fuel cell technology, in specific an outstanding noble metal efficiency.[3]. To explore the related reaction mechanisms we have studied the reactivity and adsorption behaviour of Pt-CeO_2 thin films towards H_2, CO, and CH_3OH both in UHV and under electrochemically controlled conditions.[4] UHV studies suggest that hydrogen activation requires traces of metallic Pt to be present at the surface, whereas CH_3OH activation is facile, even in the absence of any metallic Pt. The chemical state of the Pt species under electrochemical conditions is monitored by Linear Potential Scan Infrared Spectroscopy (LPSIRS) during methanol oxidation in acidic solution (0.1 M $HClO_4$). In Fig. 2, a comparison is shown between the spectra of the CO stretching frequency region for (i) Pt(111), (ii) polycrystalline Pt thin-films, and (iii, iv) Pt-containing CeO_2 thin-film electrodes with different Pt concentration. Before the IR measurement the samples were cleaned by flame annealing or potential cycling and, subsequently, were characterized by cyclic voltammetry (CV). Interestingly, the Pt-doped CeO_2 electrodes show a strong red shift and a broadening of the signal, which depend on the Pt concentration. This observation suggests that, even for low Pt concentration, a fraction of the Pt^{2+} is reduced to Pt^0 and stabilized on the CeO_2 in form of very small aggregates.

Acknowledgements

The authors acknowledge financial support by the EU (FP7 NMP, ChipCAT No. 310191), COST Action CM1104, the Spanish MINECO (CTQ2012-34969, CTQ2012-30751, FIS2008-02238), MICINN (BES-2009-021571), Red Española de Supercomputación, the Czech Science Foundation (P204/10/1169, 13-10396S), the Alexander von Humboldt Foundation, the Deutsche Forschungsgemeinschaft (DFG, Excellence Cluster "Engineering of Advanced Materials"), and Czech Ministry of Education (Materials Science Beamline, LG12003).

References

[1] A. Bruix, Y. Lykhach, I. Matolínová, A. Neitzel, T. Skála, N. Tsud, M. Vorokhta, V. Stetsovych, K. Ševčíková, J. Mysliveček, K. C. Prince, S. Bruyère, V. Potin, F. Illas, V. Matolín, J. Libuda, K. M. Neyman, Angew. Chem. Int. Ed. 53, 10525 (2014).

[2] G. N. Vayssilov, Y. Lykhach, A. Migani, T. Staudt, G. P. Petrova, N. Tsud, T. Skála, A. Bruix, F. Illas, K. C. Prince, V. Matolín, K. M. Neyman, J. Libuda, Nature Materials 10, 310 (2011).

[3] V. Matolín, R. Fiala, I. Khalakhan, J. Lavková, M. Václavů, M. Vorokhta, Int. J. Nanotechnol. 2012, 9, 680.

[4] A. Neitzel, Y. Lykhach, T. Skála, N. Tsud, V. Johánek, M. Vorokht, D. Mazur, K. C. Prince, V. Matolín, J. Libuda, Physical Chemistry Chemical Physics 16, 24747 (2014).

Posters

$Co_{1.5}Fe_{1.5}Ge$ and Co_2MnSi Half-Metal Magnetic behavior tested by spin- and symmetry-resolved photoemission

A. Neggache (1,2), T. Hauet (1), F. Bertran (2), P. Le Fèvre (2), T. Devolder (3), A. Bataille (4), F. Porcher (4), A. Vlad (2), A. Coati (2), Y. Garreau (2), S. Andrieu(1)*

(1) Institut Jean Lamour, Université de Lorraine / CNRS, Vandoeuvre France
(2) Synchrotron SOLEIL, CNRS, Saint Aubin, France
(3) Institut d'Electronique Fondamentale, Université Paris-Saclay, Orsay, France
(4) Laboratoire Léon Brillouin, IRAMIS, CEA Saclay, Gif sur Yvette, France
* Corresponding author : stephane.andrieu@univ-lorraine.fr

In a magnetic spin-valve or tunnel junction, a crucial parameter to get both large magnetoresistance (MR) and a good Spin Transfer Torque (STT) efficiency is the spin-polarization of the magnetic electrodes. So-called "Half-Metallic" Magnetic (HMM) materials are of interest for such devices due to the existence of a pseudo-gap at the Fermi level E_F for minority spins [1]. A first consequence is that large MR values are expected using this kind of materials. Recently, MR enhancements have been observed by different research groups using materials with Heusler-like structure such as $Co_{2-x}Fe_{1+x}Ge$ [1] and Co_2MnSi [2], suggesting HMM behavior. A second consequence is due to the lack of minority spin state at E_F in such materials that should lead to very low damping. Combining both properties in a device is a challenge for decreasing the critical current necessary to switch the magnetization of a magnetic layer using STT. Up to now, many Heusler alloys are claimed to get this HMM property [3], often by using indirect method like transport measurements. Nevertheless, understanding the transport properties in a device by considering only the density of state (DOS) at E_F is often a complex task since it is not the only ingredient involved in the process. Many others phenomena may affect the electronic transport properties like scattering processes in spin valves or complex tunnelling process through the barrier in Magnetic Tunnel Junctions (MTJs). Here we used spin-resolved photoemission fully integrated in k as a direct method to test the HMM behaviour of such materials. The possibility (i) to get the symmetry of the electronic states by tuning the photon E-field polarization and (ii) to distinguish bulk and surface/interface states using Angle-Resolved PhotoEmission Specroscopy (ARPES) are also used [4] to compare the photoemission spectra (PES) with calculated DOS using *ab initio* calculations.

Here we focus on two systems, (i) $Co_{1.5}Fe_{1.5}Ge$ for which a significant increase of the GMR was observed in spin valves [1], and (ii) Co_2MnSi for which very large TMR values were observed in MgO-based MTJs [2]. The origin of the large MR observed in spin-valve with $Co_{1.5}Fe_{1.5}Ge$ [1] is attributed to a large spin polarization at E_F. In a related study, *ab initio* calculations were performed and the importance of chemical ordering was examined [5]. While the chemical ordering between Fe and Ge is not crucial since any disorder between them does not destroy the pseudo-gap, any substitution between Co and Fe or Ge sites destroys it. These calculations also suggest that $Co_{1.5}Fe_{1.5}Ge$ is a good choice of alloy, because the reduced number of Co atoms decreases the probability of substitutional disorder between Co and Fe or Ge sites. Concerning Co_2MnSi, the very large TMR values observed at 4.2K in MgO-based MTJs associated with a strong TMR variation with temperature [2] are strong experimental results in favour of a HMM behaviour.

To test these expectations, $Co_{1.5}Fe_{1.5}Ge(001)$ films (noted CFG in the following) were prepared by MBE. As shown by electron diffraction, the proper Fm-3m crystalline structure is obtained accompanied with chemical ordering. The chemical ordering was studied by a combination of X-Ray diffraction in our lab and at SOLEIL on SIXS beamline, and neutron

diffraction at the LLB neutron reactor. Such layers were studied by spin- and symmetry-resolved photoemission on the CASSIOPEE beamline at the SOLEIL synchrotron [4] and compared to a regular equimolar FeCo(001) bcc film. The layers were prepared in a connected MBE chamber. In the reference FeCo layer, the spin polarization is found negative at E_F as expected (fig.1a). In the CFG film, the polarization becomes close to zero around E_F, meaning that, strictly speaking, CFG is not HMM. However, adding Ge into CoFe alloys leads to a strong majority spin contribution with $\Delta 1$ symmetry just below E_F. The polarization thus becomes positive below E_F (fig.1b), opposite to the behavior of FeCo alloys.

The situation strongly differs for Co_2MnSi (noted CMS in the following). An energy gap is actually observed in the minority spin channel (noted spin-gap in the figure), as predicted theoretically. However, this spin gap is not centered around E_F but is below E_F. As a consequence a 100% spin polarization is observed in CMS, but not at E_F. However, one should note that decreasing a little bit E_F should lead to high spin polarization. To do so, we increased the Mn content by growing $Co_2Mn_{1+x}Si$. This was motivated by Liu *et al* work [2] who reported that the largest TMR values observed in CMS-MgO based MTJs were not obtained for the exact 2;1;1 stoichiometry but by increasing x. Our SR-PES experiments perfectly explain their results. The increase of Mn content clearly leads to a decrease of the Fermi energy in our PES spectra (fig.1c). The minority spin DOS is then observed to decrease, whereas E_F crosses the $\Delta 1$ majority spin band described above. The spin polarization thus increases up to around 75% (at remanence) for x around 1.2. Finally we will show that this spin polarization is slightly reduced when depositing MgO on top of the CMS layer, but is still high (60%). All these results make CMS a very good candidate for spintronic devices.

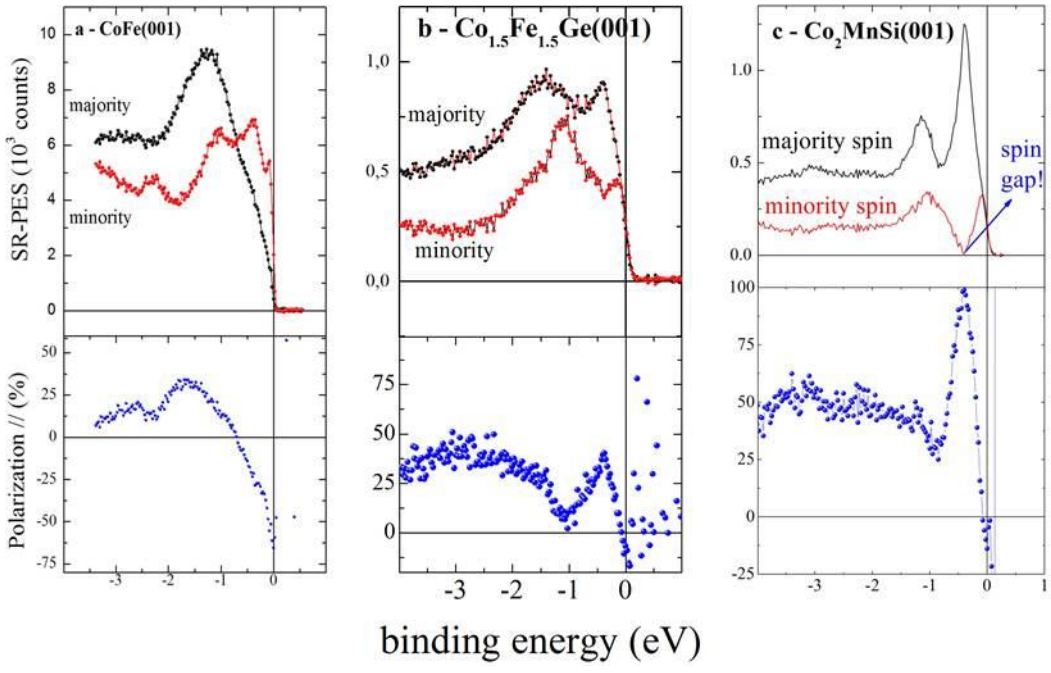

FIG1a-c : SR-PES fully integrated in k measured at 80K and at remanence for (a) bcc FeCo(001), (b) CFG Heusler alloy and (c) CMS Heusler alloy. Note the majority spin DOS increase and the minority spin DOS decrease at E_F for CFG and CMS compared to CoFe.

[1] - S. Maat, M. J. Carey, J. R. Childress, *Appl. Phys. Lett.* **93**, 143505 (2008)
[2] – Hong-xi Liu *et al*, App. Phys. Lett., 101, 132418 (2012)
[3] – T. Graf, C. Felser, S. S. P. Parkin, *Progress in Solid State Chemistry* **39**, 1 (2011)
[4] – F. Bonell *et al*, *Phys. Rev. Lett.* **108**, 176602 (2012)
[5] - H. Lee & al, *Appl. Phys. Lett.* **95**, 082502 (2009)

Theoretical Engineering of Electronic Structure of Topological Insulator Systems

E.V.Chulkov[1,2,3*], T.V.Menshchikova[4], M.M.Otrokov[1,4], and S.S.Tsirkin[1,4]

[1]*Donostia International Physics Center (DIPC), 20018 Donostia - San Sebastián, Basque Country, Spain*
[2]*Departamento de Física de Materiales, UPV/EHU, Apdo. 1072, 20080 Donostia – San Sebastián, Spain*
[3]*CFM - MPC, Centro Mixto CSIC - UPV/EHU, 20018 Donostia - San Sebastían, Spain*
[4]*Tomsk State University, pr. Lenina 36, 634050, Tomsk, Russian Federation*

[*]*E-mail: evguenivladimirovich.tchoulkov@ehu.es*

Spin-orbit interaction underlies many bulk and surface phenomena with intriguing potential applications. It plays especially important role in the surface electronic structure leading to massless states on a surface of many narrow gap semiconductors (topological insulators) [1-9]. Topological insulators (Tis) exhibit robust Dirac-like surface states protected by time-reversal symmetry. Breaking time-reversal symmetry causes splitting of the topological surface state at the Dirac point thus making the surface insulating. Here we present and discuss recent results for complex topological insulator systems that include pristine TIs and topological insulators with overlayers, and TIs under external electric field. We show that overlayers and external electric field can be used to tune the Dirac cone position in the energy gap of TIs and distribute the charge density of this state over the overlayer [8].

[1] K. Kuroda et al., Phys. Rev. Lett. **105**, 076802 (2010)
[2] S.V. Eremeev et al., Phys. Rev. B **83**, 205129 (2011)
[3] T.V. Meshchikova et al., JETP Lett. **93**, 15 (2011)
[4] S.V. Eremeev et al., Nature Commun. **3**, 635 (2012)
[5] K. Miyamoto et al., Phys. Rev. Lett. **109**, 166802 (2012)
[6] D. Niesner et al., Phys. Rev. B **86**, 205403 (2012)
[7] T. Okuda et al., Phys. Rev. Lett. **111**, 206803 (2013)
[8] T.V. Meshchikova et al., Nano Lett. **13**, 6064 (2013)
[9] G. Landolt et al., Phys. Rev. Lett. **112**, 057601 (2014)

Grain boundaries in two-dimensional monolayer silica

S. Mathur[1,2], S. Vlaic[1,2], E. Hadji[3], P. Pochet[3], J. Coraux[1,2]
[1] *CNRS, Inst NEEL, F-38042 Grenoble, France*
[2] *Univ. Grenoble Alpes, Inst NEEL, F-38042 Grenoble, France*
[3] *CEA-INAC/UJF-Grenoble 1, 17 rue des martyrs, 38054 Grenoble cedex 9, France*
E-mail: johann.coraux@neel.cnrs.fr

The study of two-dimensional (2D) crystals, i.e. crystalline materials of ultimate thinness, has been considerably extending much beyond graphene in the past few years. Monolayer silica, a crystalline oxide exhibiting a honeycomb structure, is part of this family of materials. It is a model platform for the surface science study of the structural, electronic, and catalytic properties of thicker silica, one of the most widespread support in catalytic system of industrial significance. Besides the monolayer has optimum atomic surface-to-volume ratio, and hosts a variety of stable point defects of well-defined structure [1], both features holding promise in view of highly active catalytic systems.

Large defect densities are found in the monolayer silica samples thus far presented in the literature. A large fraction of these defects are grain boundaries between 2D crystalline domains. While in other 2D crystals, like graphene, the size of crystalline domains can reach centimetre scales, in monolayer silica domains have much smaller sizes, of the order of 10 nm. With the help of in situ reflection-high energy electron diffraction and scanning tunnelling microscopy (STM), we have explored the formation of the domains in monolayer silica on Ru(0001) [2]. We have unveiled that the multi-domain structure in silica is inherited from the oxygen reconstruction phase which is used as a growth intermediate prior to silicon deposition. We also have resolved the structure of the antiphase grain boundaries, which consist of heptagons and pentagons accommodating Ru-Ru nearest neighbour distance in-plane shifts (Figure).

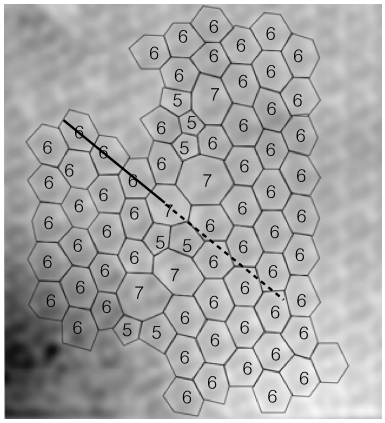

Fig.: STM topograph revealing the honeycomb structure of monolayer silica on Ru(0001) around an antiphase grain boundary. The hexagonal pores (marked '6') are 0.54 nm-large.

Acknowledgements

We acknowledge financial support from ANR through projects NANOCELLS and a PhD grant from LANEF-Grenoble.

References

[1] B. Yang, J. A. Boscoboinik, X. Yu, S. Shaikhutdinov, H.-J. Freund, Nano Lett. 13, 4422 (2013)
[2] S. Mathur, S. Vlaic, E. Hadji, P. Pochet, J. Coraux, submitted

Spectroscopic fingerprints of work-function-controlled phthalocyanine charging on metal surfaces

D. G. de Oteyza[1,2], P. Borghetti [1,2], A. El-Sayed [2,3], E. Goiri [1,2], C. Rogero [1,2], J. Lobo-Checa[1,2], L. Floreano[4], E. Ortega[1,2,3]

[1] *Donostia International Physics Center, San Sebastian, Spain*
[2] *Centro de Fisica de Materiales (CSIC-UPV/EHU), San Sebastian, Spain*
[3] *Dpto. Fisica Aplicada I, Universidad del Pais Vasco, San Sebastian, Spain*
[4] *CNR-IOM, Laboratorio Nazionale TASC, Trieste, Italy*
E-mail: d_g_oteyza@ehu.es

The electronic character of a π-conjugated molecular overlayer on a metal surface can change from semiconducting to metallic, depending on how molecular orbitals arrange with respect to the electrode's Fermi level. Molecular level alignment is thus a key property that strongly influences the performance of organic-based devices. In this work we report how the electronic level alignment of copper-phthalocyanines on metal surfaces can be tailored by controlling the substrate work function. We even show the way of finely tuning it for one fixed phthalocyanine-metal combination without the need of intercalating substrate-functionalizing buffer layers. Instead, the work function is trimmed by appropriate design of the phthalocyanine's supramolecular environment [1], such that charge transfer into empty molecular levels can be triggered across the metal-organic interface [2]. These intriguing observations are the outcome of a powerful combination of surface-sensitive electron spectroscopies, which further reveal a number of characteristic spectroscopic fingerprints of a lifted LUMO degeneracy associated with the partial phthalocyanine charging.

Acknowledgements

This work was supported by the Spanish Grants No. MAT2010-21156-C03-01, PIB2010US-00652, and the Basque Government Grant No. IT-621-13. We acknowledge funding from the European Community's Seventh Framework Programme (FP7/2007-2013) under Grant No. 226716.

References

[1] A. El-Sayed, P. Borghetti, E. Goiri, C. Rogero, L. Floreano, G. Lovat, D. J. Mowbray, J. L. Cabellos, Y. Wakayama, A. Rubio, J. E. Ortega, D. G. de Oteyza, ACS Nano 7, 6914 (2013)
[2] P. Borghetti, A. El-Sayed, E. Goiri, C. Rogero, J. Lobo-Checa, L. Floreano, J. E. Ortega, D. G. de Oteyza, ACS Nano doi:10.1021/nn5060333

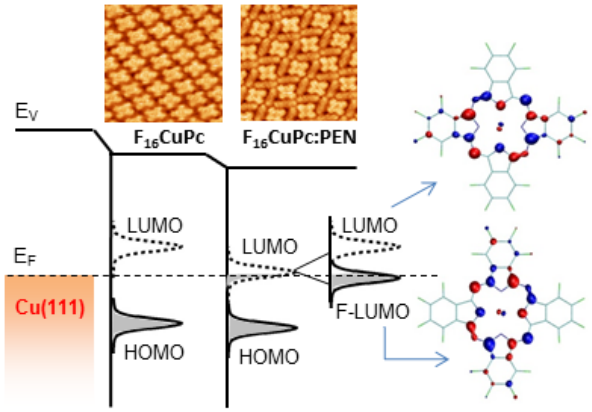

Fig.1 Schematic energy level representation of F_{16}CuPc molecular orbitals at the interface to a Cu(111) substrate. A comparison is made between monolayers of pure F_{16}CuPc and of F_{16}CuPc:PEN blends in a 1:2 ratio (as displayed in the constant current STM images above). The larger interface dipole in the blend draws the LUMO level tail below the Fermi level, causing a partial charge transfer and a Jahn-Teller splitting of the originally degenerate LUMO levels displayed on the right.

Site-specific observation of charge carrier dynamics in organic solar cell materials by time resolved XPS

T. Arion[1], S. Neppl[2], F. Roth[1], A. Shavorskiy[2], H. Bluhm[2], Z. Hussain[3], O. Gessner[2], W. Eberhardt[1,3,4]

[1] *Center for Free-Electron Laser Science/DESY, Notkestraße 85, D-22607 Hamburg, Germany*
[2] *Chemical Sciences Division, Lawrence Berkeley National Laboratory, Berkeley, California, USA*
[3] *ALS, Lawrence Berkeley National Laboratory, Berkeley, California, USA*
[4] *Institute of Optics and Atomic Physics, TU Berlin, Straße des 17. Juni 135, D-10623 Berlin, Germany*

Organic solar cells are viewed to have a large potential as flexible low cost materials systems for photovoltaic (PV) power generation. An additional advantage of organic PV systems is that they may be produced by low cost printing techniques or deposition from solution, rather than vacuum deposition techniques. One major drawback of organic PV, however, is the relatively low conversion efficiency, which so far remains less than 10%. In part this is due to intrinsic recombination processes of electron-hole pairs generated by the absorption of light. If one succeeds to suppress this recombination, the yield of photogenerated charges may be significantly improved. Empirically, this has been accomplished by admixture of C_{60} into the organic photoreceptor film [1-4]. Since C_{60} has a very high electron affinity, it is capable of accepting an electron from the organic photoreceptor, while the hole remains in the organic system and thus the recombination process is strongly suppressed.

While it has been demonstrated by photoelectron spectroscopy that this charge transfer is energetically enabled [2-4], very little information is available about the various steps and time dependence of this crucial charge transfer process. In many light harvesting systems, for example those in solar fuel generation or photosynthesis, charge transfer processes are key steps for the entire process.

XPS is known to be a local probe of the charge configuration around specific atoms (ESCA). Time resolved XPS[5], accordingly, offers the unique opportunity to investigate the relevant timescales for charge transfer processes following a short pulse excitation by a laser from the perspective of specific atomic sites. The C 1s XPS lines of CuPC and C_{60} are separated in energy (Fig. 1) and thus enable us to detect the arrival of charges at the C_{60}, following laser excitation of the CuPC chromophore in a site-specific fashion.

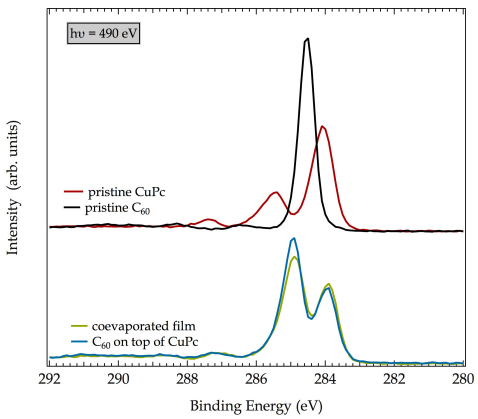

Fig. 1 Photoemission spectra of a pure Cu- PC film and a pure C_{60} film (top) as well as a co-evaporated film (about 1:1 mixing ratio) and a C_{60} film on top of CuPc (bottom), recorded at a photon energy of 490 eV.

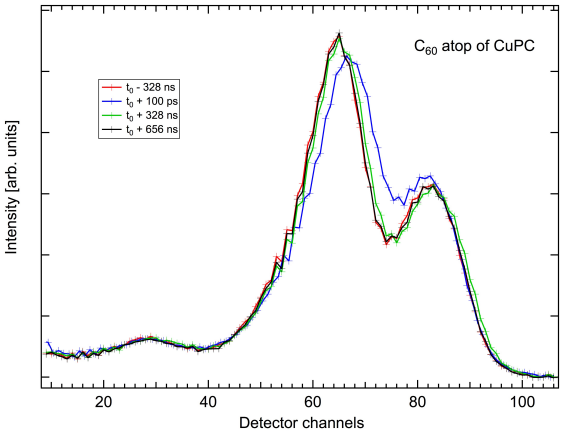

Fig. 2: Time resolved XPS spectra for a C_{60} film deposited on top of a CuPc film. The spectrum recorded 100 ps after the excitation pulse (blue) clearly shows a shift of the C 1s emission from C_{60}, while the CuPc photoemission line remains unshifted for all time delays. At a pump-probe delay of 328 ns the sample has relaxed back to the ground state.

Upon laser excitation the composite film clearly shows a time dependent shift of the core level spectrum, which is completely reversible (Fig. 2), while pure films of CuPc and C_{60} do not change under the same illumination conditions (not shown here). Based upon a component analysis of the time resolved spectra, we will be able to shed new light onto the time scales of excitation and transport of charges in these model systems for organic photovoltaics.

The experimental technique of time resolved XPS certainly can be applied to other systems where charge localization is of specific interest, as for example organics in perovskites. More general, any spectroscopic technique involving excitation or decay processes of core holes is capable of delivering this type of information on timescales down to the single digit fs timescale (6)

References

1. 1.N. Sariciftci, A.J. Heeger, Int. J. Mod. Phys. **B8**, 237 (1994)
2. C. Schlebusch, B. Kessler, S. Cramm, W. Eberhardt, Synth. Metals **77**, 151 (1996)
3. B. Kessler, Appl. Physics **A67**, 125 (1998)
4. A. Wilke, T. Mizokuro, R-P. Blum, P. Rabe, N. Koch, IEEE J. of selected Topics in Quantum Electronics **16**, 1732 (2010) and references therein
5. S. Neppl *et. al*., Faraday Discuss. **171**, 219 (2014).
6. W. Eberhardt, E.W. Plummer, C.T. Chen, W.K. Ford, Austral. J. of Physics **39**, 853 (1986)

Growth of silicon-germanium quantum dots

T.Frisch

Institut Non Lineaire de Nice, Université de Nice Sophia Antipolis, UMR CNRS 7735, Valbonne, France

E-mail: thomas.frisch@inln.cnrs.fr

I will present the physics of the growth of quantum dots on a strained semi-conductor film [1]. In particular, I will describe theoretical results on the mechanism of coarsening of self-organized silicon-germanium islands.

Using the method of continuum elasticity, we have shown that islands form on a wetting layer and that the islands coarsen with time [2].

We have also investigated the role of the anisotropy of the surface energy and we have shown that anisotropy alter strongly the coarsening mechanism [3].

Finally, we have studied the existence of an isolated localized island and we have shown that the transition from a flat film to an unstable film is similar to a fist-order transition [4].

References

[1] J.N. Aqua, I. Berbezier, L. Favre, T Frisch, A. Ronda, Physics Reports 522, 59-189, (2013)
[2] J.N. Aqua, A. Gouyé, A. Ronda, T. Frisch, I. Berbezier, Physical Review letters 110, 096101, (2013)
[3] J.N. Aqua, T. Frisch, Physical Review B 82, 085322, 21 (2010)
[4] T. Frisch et al. (in preparation)

State-of-the art ARPES: new concepts for analyzers, detectors and excitation sources

T. U. Kampen, M. Johansson, S. Maehl, O. Schaff
SPECS Surface Nano Analysis GmbH, Voltastraße 5, 13355 Berlin, Germany
E-mail: Thorsten.Kampen@specs.com

Novel materials like graphene or topological insulators show intriguing structural and electronic properties. Topological insulators, for example, are characterized by their particular electronic structure which enables metallic like charge conduction at surfaces of an otherwise insulating material. Angular resolved photoemission spectroscopy (ARPES) is the obvious choice for studying the electronic structure of surfaces, and technological developments in the field of electron spectrometers and laboratory light sources have led to new possibilities in electronic structure determination.

The PHOIBOS series of hemispherical energy analyzers with 100, 150 and 225mm mean radius sets a new standard with the highest resolution and transmission. The modular power supply and detector concept makes them suitable for every aspect of electron spectroscopy: from laser based ARPES measurements at low kinetic energies starting at virtually zero kinetic energy, to quantitative XPS and high energy photoemission spectroscopy. The multi-element transfer lens of the hemispherical analyzer PHOIBOS is optimized for ultimate energy and angular resolution up to highest kinetic energies and can be used for angular or spatially resolved studies. The acceptance angle can be extended with additional pre-lenses to +/- 30°. Different 2D detector concepts are available: a 2D-CCD detector with a Peltier cooled camera, a 2D-DLD detector (one time and two lateral dimensions), and combined 2D/SPIN detectors.

The THEMIS time-of-flight spectrometer series complements the SPECS photoemission spectrometer line and adds a new dimension the ARPES. Here, the combination of the PHOIBOS analyzer series lens design and the proven 2D-DLD detector technology enables most flexible operation, detecting large angular emission cone and energy windows simultaneously. The raw data from the detector (position and flight time for each electron) is precisely transformed into emission angle and energy coordinates in real time.

Energy dissipation in atomic scale friction: Non-locality and memory

S.Yu. Krylov [1,3], J.W.M. Frenken [2,3]

[1] *Institute of Physical Chemistry and Electrochemistry, Russian Academy of Sciences, Leninsky prospect 31, 119071 Moscow, Russia*

[2] *Advanced Research Center for Nanolithography, P.O. Box 41883, 1009 DB Amsterdam, The Netherlands*

[3] *Kamerlingh Onnes Laboratory, Leiden University, P.O. Box 9504, 2300 RA Leiden, The Netherlands*

E-mail: krylov@physics.LeidenUniv.nl

The traditional description of atomic-scale friction in terms of mechanical stick-slip instabilities appears so successful that it obscures the actual mechanisms of energy dissipation. The reason is that the observed friction force in the stick-slip regime is nearly completely determined by the system parameters (flexibility and contact potential corrugation) and it is practically independent of the dissipation rate, provided the latter is constrained to a certain range, the origin of which has never been explained. As was shown in our recent works [1,2], there are at least two hidden problems. First, the mere fact that atomic stick-slip patterns are readily observed in experiments implies that the inherent dissipation rate is close to the characteristic frequency of the measuring system (nearly critical damping). This observation seems to defy common sense, since the inherent dissipation rate is dominated by the characteristic frequency (i.e. by the flexibility and mass) of the measuring system, rather than by the microscopic properties of the tip-substrate contact. Second, the typical value of the dissipation rate needed to explain friction force microscopy (FFM) experiments turns out to be several orders of magnitude higher than we can expect on the basis of data collected for surface diffusion of atomic particles and clusters and related phenomena. All these observations force us to critically reconsider traditional views on frictional energy dissipation.

Traditionally, one assumes that the dissipative force experienced by a slider is simply linear in its velocity $\dot{x}$, with constant damping factor η (the dissipation rate), $F_{\mathrm{diss}} = -M\eta\dot{x}$ (mass M of the moving object is introduced here by formal reasons to provide η with the convenient dimensionality of frequency). In view of the fluctuation-dissipation theorem, this implies that thermal noise is white (δ-correlated) and memory effects can be neglected. To our knowledge, however, the applicability of this approximation to atomic scale friction has never been properly justified. A motivation to neglect memory effects could be found [3] if dissipation was local, i.e. if irretrievable loss of mechanical energy and momentum took place locally, in the slider—surface contact region, but this is not necessarily the case.

In general case, nonequilibrium statistical mechanics dictates (see, e.g., [4]) that the dissipative force can be non-linear in velocity and can depend on its values in previous moments of time, $F_{\mathrm{diss}}(t) = -M\int_{-\infty}^{t}\hat{\eta}(t-\tau)\dot{x}(\tau)d\tau$. The memory function $\hat{\eta}(t-\tau)$ is related with the noise correlation function via the fluctuation-dissipation theorem. If memory effects are important, the usage of the traditional linear approximation implies that the description is coarsened, i.e. averaged over a sufficiently long time interval. This provides a clue to understanding the frequency dependence of the (mean) dissipation rate and its unexpectedly high value. In order to clarify these questions, one has to address an atomistic model of the dissipation process.

We propose an atomistic model of frictional energy dissipation that allows to elucidate the origin of non-locality and memory. Our approach is based on the concept of a dynamical

deformation pattern (DDP). When an (atomically small) object is in contact with the surface, there is local deformation of the substrate lattice. This deformation pattern follows the object upon its motion along the surface. Dynamical deformation of the lattice is an essentially dissipative process, as it is accompanied by the creation of phonons, with their subsequent thermalization. In this picture, energy dissipates not due to motion of the object with respect to the surface, as one could think naively, but due to the motion of the object together with the dynamical deformation pattern with respect to ideal non-deformed lattice. In other words, the dissipation is related with damping of the induced motion of solid atoms which are currently involved into the DDP.

The effective size of DDP can seem very small, since the deformation of the substrate lattice rapidly decays with distance from the contact. Typically (for static deformation), it is inversely proportional to the distance squared. However, the number of solid atoms involved into the process at a certain distance scales as this distance squared. Consequently, these two trends compensate each other. This means that DDP can be—in principal—infinitely large, and its actual effective size should be determined by some more subtle effects. Apparently, this is the system history that determines which atoms of the solid have already been involved into collective motion with the object and which not. This physics is at the origin of the velocity dependent memory function $\hat{\eta}(t-\tau)$.

We show that the effective size of DDP depends essentially on type of motion of the object with respect to the surface. For an oscillator (the FFM tip) in contact with the surface, DDP includes atoms which have been involved in concerted motion during half the period of its vibration. As a consequence, calculations show that the mean dissipation rate turns out to be close to the characteristic frequency, thus giving natural explanations to the paradox of nearly critical damping and unexpectedly high values of the dissipation rate derived from FFM experiments.

Acknowledgements

Supports of the European Commission (Grant ERC-2010-AdG_20100224) and the Foundation for Fundamental Research on Matter (FOM, The Netherlands) are gratefully acknowledged.

References

[1] S. Yu. Krylov and J. W. M. Frenken, Colloid Journal 74, 569 (2012).
[2] D.W.van Baarle, S.Yu. Krylov, M.E.S. Beck, and J.W.M.Frenken, submitted to Nature Nanotechnology.
[3] M.H. Müser, M. Urbakh, and M.O. Robbins, Adv. Chem. Phys. 126, 187 (2003).
[4] P. Hänggi, P. Talkner, and M. Borkovec, Rev. Mod. Phys. 62, 251 (1990).

Reactivity mediated motion of Si particles onto SiO_2

F. Leroy[1], Y. Saito[2], F. Cheynis[1], E. Bussmann [1,*], O. Pierre-Louis[3], P. Müller[1]
[1] *CINaM, UMR 7325 Aix-Marseille Université/CNRS, Marseille France*
[2] *Department of Physics, Keio University, Yokohama, Japan*
[3] *ILM, UMR 5306 Université Lyon 1-CNRS, Villeurbanne, France*
E-mail: leroy@cinam.univ-mrs.fr

Nanoparticles diffusion on surfaces has recently received new attention because of its theoretical interest and potential technological applications. Indeed surface diffusion processes of 3D Nanoparticles on a reactive interface may be a new approach for self-assembling nanoparticles. Recent articles have provided a few examples of spontaneous motion of liquid droplets [1,2] or solid clusters [3,4] on solid surfaces. More specifically, the chemical reactions [5] that occur at the interface between the particle and the underlying substrate can drive nanoparticles towards a variety of non-equilibrium behaviours such as self-propelled motion [3,4] on a surface or the formation of trenches on solid substrates [5,6].

Here we use *in situ* Low Energy Electron Microscopy (LEEM) and Atomic Force Microscopy (AFM) to study the spontaneous motion of 3D silicon nanoparticles onto SiO_2 substrate [7]. We report on the observation of the random walk of solid-state silicon islands during annealing at high temperatures. The Mean Square Displacement (MSD) of the islands exhibits three regimes. At short times, the islands undergo equilibrium diffusion and begin to etch the surface. Then, an unusual size independent diffusion-like behavior is observed with a linear increase of the MSD. This behavior is attributed to a pinning instability of the triple-line. Finally, as etching proceeds pits are formed in the substrate and the islands are self-trapped in their own pits. Kinetic Monte Carlo simulations provide a consistent picture of the mechanisms at play in the experiments.

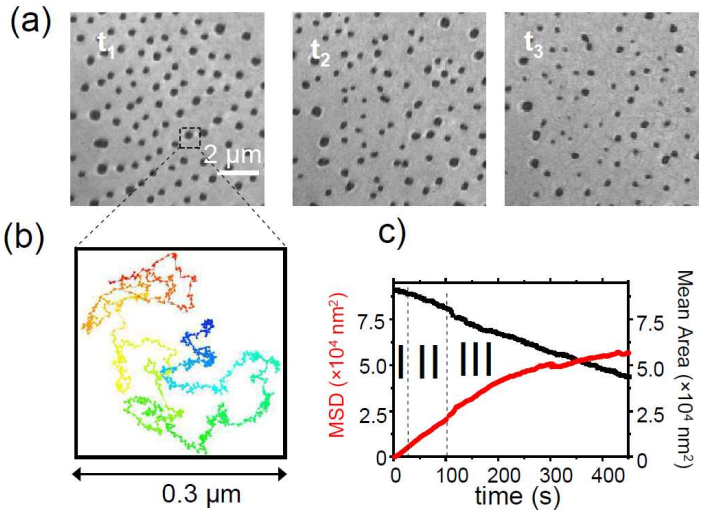

Fig. LEEM images (E = 4.5 eV) of Si/SiO2 islands during annealing ($t_{1,2,3}$ = 0, 15, 30 min; T= 1230 K). (b) Example of trajectory of the center of mass of one Si nanoparticle. (c) Time evolutions of the Mean Square Displacement and mean projected area of Si islands under reaction (T =1280 K).

Acknowledgements

We thank ANR 13 BS-000-402 grant LOTUS and JSPS KAKENHU 23540456
* now at Sandia National Lab (Albuquerque, U.S)

References

[1] J. Tersoff, D. E. Jesson, and W. Tang, Science 324 (2009).
[2] F. D. Dos Santos and T. Ondarçuhu, Phys. Rev. Lett. 75, 2972 (1995)
[3] A. K. Schmid, N. C. Bartelt, and R. Q. Hwang, Science 290, 1561 (2000).
[4] M. L. Anderson *et al.*, Phys. Rev. Lett. 98, 096106 (2007).
[5] U. Denker *et al.*, Phys. Rev. Lett. 94, 216103 (2005).
[6] K. Sudoh and M. Naito, J. Appl. Phys. 108, 083520 (2010).
[7] F. Leroy, Y. Saito, F. Cheynis, E. Bussmann, O. Pierre-Louis, and P. Muller, Phys. Rev. B 89, 235406 (2014)

Imaging of the initial stages of nanoparticle formation in the spark discharge generator

L. Ludvigsson, B. O. Meuller, M. E. Messing
Solid State Physics, Lund University, Box 118, 221 00 Lund Sweden
E-mail: maria.messing@ftf.lth.se

The number of nanoparticle-based products on the market is expected to increase considerably during the coming decades. This forces the industry to have highly meticulous manufacturing of large amounts of nanoparticles using cheap and environmentally friendly methods [1]. For production of metal nanoparticles spark discharge generation is a promising route to fulfill these demands. With a spark discharge generator (SDG) everything from atomic clusters [2] to spherical compact nanoparticles with diameters up to about 100 nm can be formed [3]. In order to optimize the nanoparticle production it is of utmost importance that the fundamental mechanisms taking place during the short discharge is carefully investigated and understood. To improve this understanding we have constructed a customized nanoparticle sampler to enable imaging of the initial stages of particle formation [4].

The leak-tight nanoparticle sampler consists of three main components, the control system, the pneumatics, and the sample holder. The control system enables a sampling time between 1ms up to 70 s and the pneumatic part consist of a piston on which the sample holder is mounted. On the sample holder a strip of silicon is attached which in turn can carry two transmission electron microscopy (TEM) grids. A sampling distance between 5 to 15 mm down stream of the conducting electrodes in the SDG, which evaporate particle material, can be used.

We report on the optimal sampling parameters to enable sampling of single discharge events. Several parameters in the SDG can be adjusted to affect particle formation and we show that the initial stages of particle formation affect the size of the final nanoparticles. Understanding and tuning these parameters can provide a more controlled particle generation and an optimal final product.

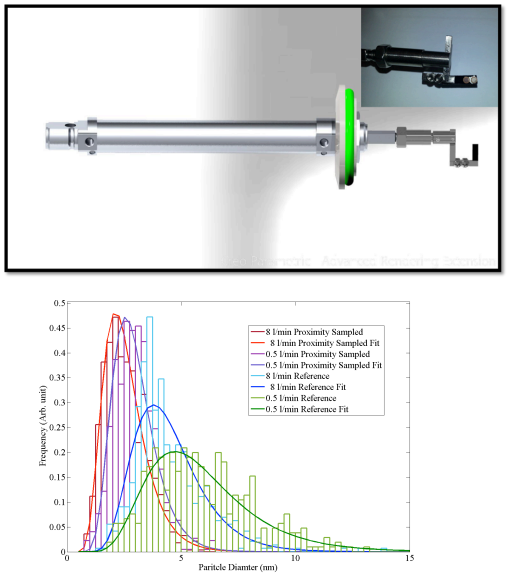

Fig. (top) Piston and holder part of the sampler. (bottom) Size distributions of particles sampled at different conditions.

Acknowledgements

The research leading to these results received funding from the European Union Seventh Framework Programme (FP7/2007-2013) under Grant Agreement n° 280765 (BUONAPART-E).

References

[1] www.buonapart-e.eu.
[2] A Maisser *et al.,* submitted.
[3] M. E. Messing *et al.,* Nanotox. 7, 1052 (2013).
[4] L. Ludvigsson, B. O. Meuller, and M. E. Messing, submitted.

Dewetting mechanisms of Si and Ge crystalline ultra-thin films on amorphous SiO_2: towards dewetting control

F. Cheynis, F. Leroy, S. Curiotto, P. Müller
CINaM, UMR 7325 Aix-Marseille Université/CNRS, Marseille France
E-mail: leroy@cinam.univ-mrs.fr

Solid thin films are used in many technological applications. However, numerous thin films systems are metastable and thus exhibit dewetting instabilities, wherein, during thermal annealing, the 2D film spontaneously agglomerates into compact 3D nanostructures. This so called solid state dewetting is a problem since it complicates the fabrication of thin-film-based devices [1]. However, it can also be used to produce self-assembled nanocrystals [2]. Thus since a few years there is a new craze for understanding solid state dewetting mechanisms (see for instance papers in Ref. [3]).

This poster reports on a synthesis of the results obtained these last years by our team in Marseille [4-10] and partially presented in the last editions of 3S symposia. More precisely the poster is devoted to a complete analysis of the dewetting mechanisms of Si(001)/SiO_2 and Ge(001)/SiO_2 systems (respectively known as SOI and GOI for Silicon On Insulator and Germanium On Insulator). For this purpose we have coupled Low Energy Electron Microscopy (LEEM) and Grazing Incidence Small-Angle x-ray Scattering *in situ* analysis to *ex-situ* Atomic Force Microscopy (AFM) observations.

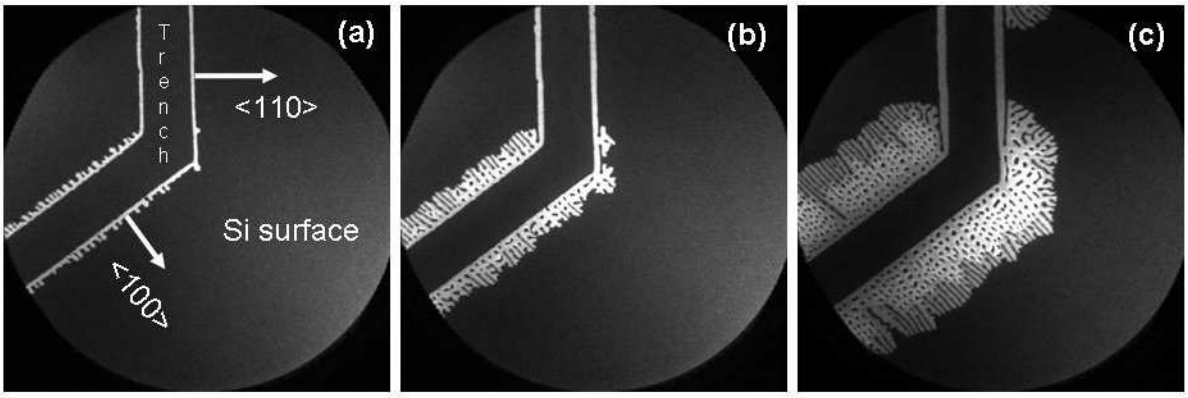

Fig.1: *LEEM sequence of SOI dewetting from artificial edges etched by lithography. Dewetting duration from (a) to (c) is 35 min.*

In both cases, SOI and GOI systems , we report on (i) the dewetting morphology [4] , (ii) the dewetting dynamics [4,5], (iii) the thickening mechanism of the rim that surrounds the dewetted zone [5-6], (iv) the stabilization properties of dewetting fronts [6], (v) the morphology of the 3D islands issued from the dewetting process [7].

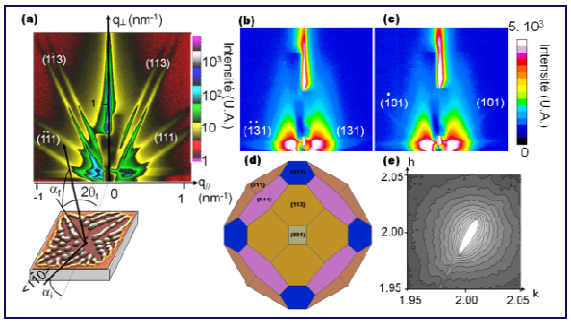

Fig. 2a: *GISAXS study of SOI islands*

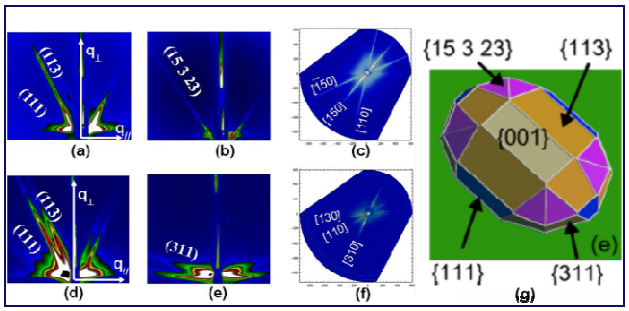

Fig.2b: *GISAXS study of GOI islands*

The comparison between SOI and GOI [8] enables us to clearly understand the influence of the facets on the dewetting instability as well as the origin of the main differences between SOI and GOI dewetting mechanisms that lead to different morphologies, kinetics and orientation of the dewetting zones.

Finally we show that solid state dewetting of SOI can be controlled. For instance it can be kinetically stopped by exposing the Si surface to a partial pressure of oxygen at high temperature (reversible effect) [10] but it can also be enhanced by exposing the surface to Au adsorption [11].

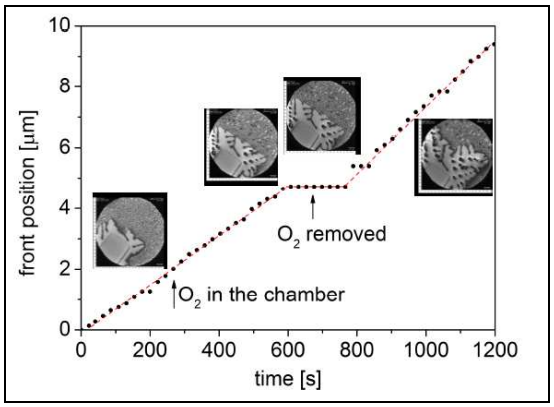

Fig 3: *Dewetting control: dewetting edge position versus time during O_2 exposition*

References

[1] C. Jahan, O. Faynot, L. Tosti, J. Hartmann, J. Cryst. Growth. 280, 530 (2005)
[2] S. Kodambaka, J. Tersoff, M.Reuter, F. Ross, Science 316, 729 (2007)
[3] Trends and perspectives in solid-state wetting, C.R. Acad. Sciences 7, pp 529-635, Editor: O. Pierre Louis (2013)
[4] E. Bussmann, F. Cheynis, F. Leroy, P.Müller, O. Pierre-Louis, New J. Phys. 13, 043017 (2009)
[5] F. Cheynis, E. Bussmann, F. Leroy, T. Passanante, P. Müller, Phys. Rev. B 84, 245439 (2011).
[6] F. Cheynis, F. Leroy, T. Passanante, P.Müller, Phys. Rev. B 85, 195414 (2012)
[7] F. Cheynis, F. Leroy, T. Passanante, P.Müller, Appl. Phys. Lett. 102, 161603 (2013)
[8] F. Leroy, F. Cheynis, T. Passanante, P. Müller, Phys. Rev. B 88, 035306 (2013).
[9] F. Cheynis, F. Leroy, P.Müller, C.R. Physique14, 578 (2013)
[10] S. Curiotto, F. Leroy, F. Cheynis, P. Müller**,** Appl. Phys. Lett. 104**,** 061603 (2014).
[11] F. Leroy et al. in preparation

Formation, stability and atomic structure of the Si(111)-(6×6)Au surface reconstruction

R. Daudin,[1] T. Nogaret,[2] A. Vaysset,[1] T.U. Schülli,[3] A. Pasturel,[2] and G. Renaud[1]

[1] *Univ. Grenoble Alpes, INAC-SP2M and CEA, INAC-SP2M, F-38000 Grenoble, France.*

[2] *Science et Ingénierie des Matériaux et des Procédés, INP Grenoble, UJF-CNRS, 1130, rue de la Piscine, BP 75, 38402 d'Hères Cedex, France*

[3] *Beamline ID01, European Synchrotron Research Facility, 6 rue Jules Horowitz, BP 220 F-38043 Grenoble CEDEX 9, France*

E-mail: gilles.renaud@cea.fr

Au deposits larger than 1 ML on the clean Si(111) surface have been known for a long time to induce, under certain preparation conditions, a (6×6) reconstruction of the previously (7×7) reconstructed surface. Despite intense research on this topic, this reconstruction still remains mysterious and controversial in terms of formation processes and stability. Morevover, the detailed atomic structure of the (6×6) reconstruction has been the matter of debates for years. Solving the structure is all the more important as it has been shown recently to induce an exceptionally marge supercooling of AuSi alloy droplets of the eutectic composition [1]. The conditions of formation of the Au-induced Si-(6×6) reconstruction, its stability as well as its atomic structure have been studied experimentally using Grazing Incidence X-ray Scattering and Surface X-Ray Diffraction *in situ*, in UHV, using the French BM32 beamline setup at the ESRF [2]. This reconstruction is found to form when cooling down eutectic droplets previously obtained by the dewetting of thin gold films deposited at room temperature on a Si(111) substrate. Several experiments show that -1- the system has to be annealed at least at 690 K, i.e. 60 K above the eutectic temperature to form the (6×6) upon subsequent cooling; -2- the (6×6) reconstruction is found to appear around 680 K during cooling; -3- the higher the sample is annealed, the better the reconstruction is defined (i.e. larger domain sizes) (Fig. 1); and -4- the reconstruction can form again after is has been destroyed, even at low temperature (600 K) in the presence of gold liquid droplet that seem to serve as a reservoir; -5- layer-by-layer growth of Si(111) is achieved, even below a pre-existing (6×6) reconstruction, and the reconstruction remains steady during Si deposition at 600 K.

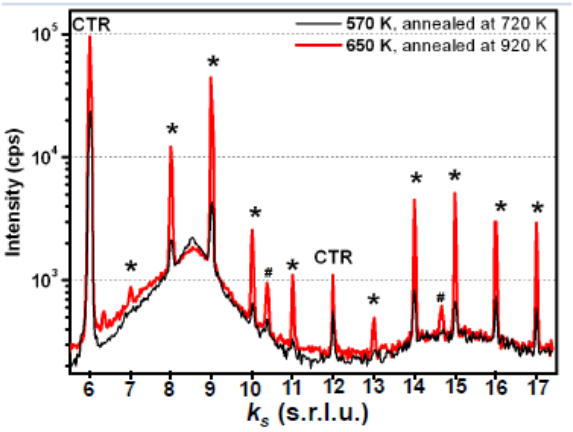

Fig. 1 Radial-scans along the [010] surface direction highlighting the liquid structure factor and the (6×6) signature (stars) for a 30 ML deposit of gold after annealed at different temperatures (720 K and 920 K), and cooling down below Te.

The quality of the reconstruction is found to depend on the annealing temperature (Fig. 1). The formation of the (6×6) reconstruction at low temperature after it has been destroyed by ion bombardment, together with the recovery of the Si surface give evidence of its high stability and highlight the surfactant properties of gold atoms.

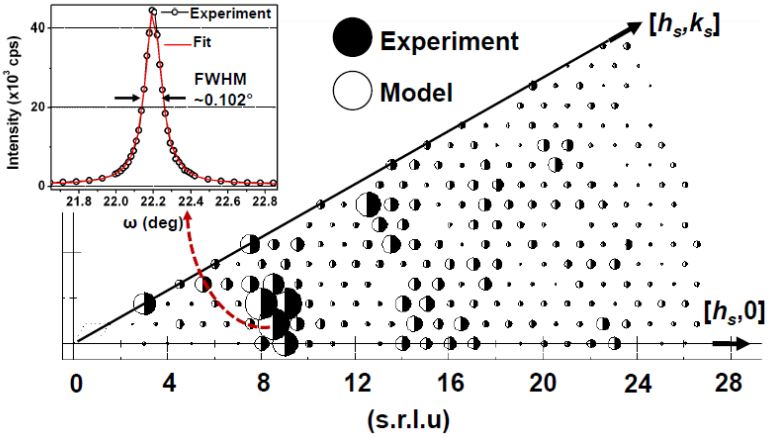

Fig. 2 Experimental structure factors using p3m1 symmetry (in black), together with the final model structure factors (in white), in reconstructed surface reduced units. The area of the circles is proportional to the reflection's intensity. The experimental and model circles are of same sizes (i.e. same intensity) for all reflections illustrating the final agreement χ^2 of 1.3. Inset: rocking-scan performed on the (8,2,0) reconstruction peak.

The determination of the Si(111)-(6×6)Au atomic structure is performed using quantitative surface X-ray diffraction (Fig. 2) with an existing complex model proposed in the literature as a starting structure. The resulting gold structure (Fig. 3) is found to be 1 ML thick and consists in two domains related by a mirror. They are composed of trimer and pentagonal units with special sites presenting a partial occupancy of 0:5. Our experimental dataset does not provide enough accuracy to determine the positions of the Si atoms of the substrate. *Ab initio* calculations were performed to obtain additional information on the stability of the atomic model. They tend to confirm that the Si atoms are only slightly displaced from the bulk position.

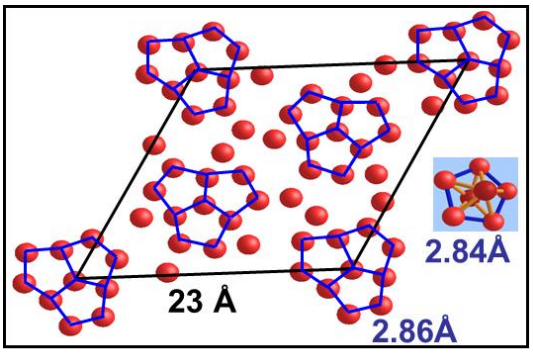

Fig.3 Atpmic structure as refined using SXRD data. Only the Au atoms are shown in red. Trimers of Au pentagons are underlines in blue.

Acknowledgements
The staff of ESRF and of the BM32 beamline is deeply acknowledge.

References

[1] T. U. Schülli, R. Daudin, G. Renaud, A. Vaysset, O. Geaymond, and A. Pasturel, Nature 464, 1174 (2010).
[2] G. Renaud, R. Lazzari, F. Leroy, Surf. Sci. Rep. **64** (2009) pp. 255-380
[3] R. Daudin, T. Nogaret, A. Vaysset, T.U. Schülli, A. Pasturel, and G. Renaud, submitted to Phys. Rev. B

Grazing Incidence Fast Atom Diffraction, A new tool for ultimate epitaxy?

From picometer to micrometer sensitivity on cm scales.

P. Atkinson[1,2], M. Eddrief[1,2], F. Finocchi[1,2], V. Etgens[3],M. Debiossac[4], A. Zugarramurdi[4], A. Borisov[4], M. Mulier[4], B. Lalmi[4], A. Momeni[4,5], H. Khemliche[4] and P. Roncin[4]

[1]Sorbonne Universitées, UPMC Univ. Paris 06, UMR 7588, INSP, F-75005 Paris, France
[2]CNRS, UMR 7588, Institut des NanoSciences de Paris, 4 place Jussieu, F-75005 Paris, France
[3]VeDeCom-Universitée Versailles Saint-Quentin en Yvelines, Versailles, France
[4]ISMO UMR8214 CNRS-Universitée Paris-Sud, Orsay F-91400, France
[5]Univ. Cergy Pontoise, F-95031 Cergy, France

In recent years, the diffraction of fast helium atoms has developed [1-4] as a new technique to probe the surface electronic density of crystalline surfaces. We will present our latest achievements [3,4] obtained inside a Molecular Beam Epitaxy (MBE) chamber installed at the INSP, Paris.

I Dynamic images; Diffraction during growth

GIFAD uses the same geometry as RHEED and most MBE vessels have corresponding ports available. We show that GIFAD works well under MBE growth conditions, and ultra-high resolution images of GaAs surfaces could be obtained even at high substrate temperatures (~ 550°C) while the surface is held under an incident As pressure of ~10^{-5} mbar. In addition, faster, lower resolution images allow changes in the surface to be monitored both during phase transitions and during GaAs growth.

As a striking result, the layer by layer oscillations of the GIFAD signal are well contrasted and comparatively more simple and robust that the equivalent oscillations in RHEED. This is interpreted as due to the fact that the GIFAD intensity grows with the probability for the projectile to undergo specular reflexion. At such grazing angle, this latter is primarily governed by the mean terrace size probed on the length scale of of the helium trajectory (~100 Å). The oscillations phase and period of the oscillations do not depend on the crystalline orientation. A useful consequence is that the maximum of such oscillation is reached at the same moment for all measured diffraction orders and whatever the angle of incidence. The location of a maximum therefore provides an unambiguous measure of the completion of a layer.

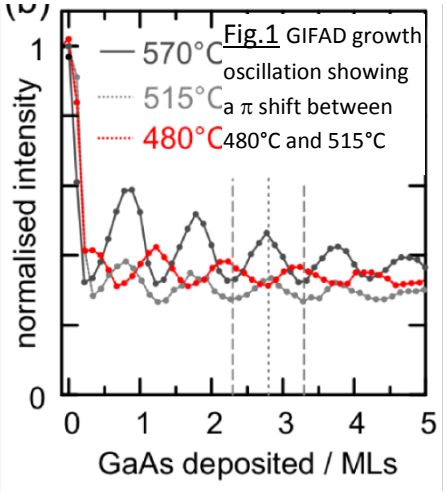

Fig.1 GIFAD growth oscillation showing a π shift between 480°C and 515°C

The phase of the oscillation is also a good indication of the amount of matter needed for the formation of the layers. For instance, at 480°C the GIFAD diffraction image show a surface reconstruction during growth[3]. Figure 1 displays the growth oscillations at various temperatures. The one recorded at 480°C is delayed by half a monolayer indicating that the phase transition taking place is associated with half a layer of Ga to go from an As rich c(4x4) to the (2x4)γ surface reconstruction.

II Static images, ultra-high resolution

The axial channeling approximation [5] indicates that, when the beam is well aligned along a crystal axis, with an angle θ with respect to the surface plane, then the diffraction image can be understood as due to an effective helium atom impinging perpendicular to the surface with an effective energy given by $E_\perp=E_0\sin^2\theta$. This effective particle probes the electronic density profile averaged along the direction of the beam.

With high resolution images (fig.2), it is possible to extract the main feature of the shape of the surface electronic density profile. Using quantum mechanical calculations it is possible to compare the diffraction images with state-of-the-art DFT calculations of the reconstruction. Two conclusions can be derived from such a comparison. First, due to its ability to operate at normal energies $E_\perp$>~100 meV, well above the van der Waals typical energies, GIFAD is actually measuring the electronic density profile of the surface. In this regime, GIFAD is indeed a "helium tipped" AFM operating in the reciprocal space. An overall sensitivity close to 1 pm can be achieved in the vertical dimension together with lateral resolution of 10 pm. Second, at lower normal energies, 1 < $E_\perp$ < 30 meV, the diffraction images are more difficult to analyze because of complex resonances due to the van der Waals interactions between the surface and the helium atoms, which give rise to a shallow potential-well producing bound-states resonances. These resonances allow a very precise determination of the polarization forces, which is an actual issue in DFT. On LiF surfaces, it has been proposed that the measured width of such resonances is a direct measure of the mean surface coherence length (typical size without atomic defect) estimated, in this particular preparation conditions, in the micron scale. It should be emphasized here that the surface illuminated by the beam is quite large; the beam lateral dimension is below ~100 micrometers but the length of the wafer exposed to the beam is ~$100\mu m/\theta$ which rapidly exceeds few cm for θ<1deg. This means that GIFAD is suitable for pre- or post- diagnostic of the surface quality over very large regions.

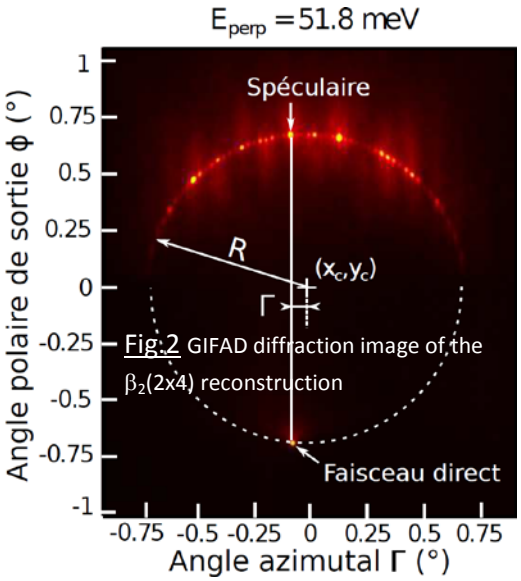

Fig.2 GIFAD diffraction image of the β_2(2x4) reconstruction

In practice though, only the intensity located on the Laue circle and corresponding to perfect elastic diffraction is analyzed so far, leaving plenty of room for future developments such as quantitative measurement of surface atom vibration amplitude, surface temperature, mean terrace size measurements etc…

MBE is a perfect environment for GIFAD! Conversely, GIFAD could help MBE to face the future challenges.

[1] M. Debiossac, A. Zugarramurdi, P. Lunca-Popa, A. Momeni, H. Khemliche, A. Borisov and P. Roncin, Transient quantum trapping of fast atoms at surfaces. Phys. Rev. Lett, vol. 112, p. 023203, (2014)

[1] H. Winter and A. Schüller Fast atom diffraction during grazing scattering from surfaces. Prog. in Surf. Science 86, p169 (2011).

[3] P. Atkinson, M. Eddrief, V. Etgens, H. Khemliche, M. Debiossac, A. Momeni, M. Mulier, B. Lalmi, and P. Roncin, Dynamic grazing incidence fast atom diffraction during molecular beam epitaxial growth of GaAs, Applied Physics Letters, 105, p. 021602, (2014)

[4] M. Debiossac, A. Zugarramurdi, H. Khemliche, P. Roncin, A. Borisov, A. Momeni, P. Atkinson, M. Eddrief, F. Finocchi, and V. Etgens, Combined experimental and theoretical study of fast atom diffraction on the reconstructed GaAs β2(2× 4)(001) surface Phys. Rev. B, vol. 90, p. 155308, (2014).

[5] A Zugarramurdi, AG Borisov - Transition from fast to slow atom diffraction.. Phys. Rev. A 86, 062903 (2012)

Initial time evolution of electronic response at Cu(111) and Ag(111) surfaces

V.M. Silkin[1,2,3], P. Lazić[4], N. Došlić[4], B. Gumhalter[5]

[1]*Donostia International Physics Center, Paseo Manuel de Lardizabal 4, 20018 Donostia/San Sebastian, Basque Country, Spain,*

[2]*Departamento de Fisica de Materiales, Facultad de Ciencias Químicas, Universidad del Pais Vasco/Euskal Herriko Unibertsitatea, Donostia/San Sebastian, Basque Country, Spain*

[3]*IKERBASQUE, Basque Foundation for Science, Bilbao, Spain*

[4]*Institute of Physics, Zagreb, Croatia*

[5]*Institute Rudjer Bošković, Zagreb, Croatia*

E-mail: waxslavas@sc.ehu.es

Screening is a fundamental process which determines dynamical properties of charged Fermi liquids. Of special interest are the dynamical screening properties of inhomogeneous electron gas and their manifestations in spectroscopic measurements, particularly at solid surfaces and interfaces where electronic processes may cause or influence the various phenomena and effects of practical importance. The act of probing the properties of electronic systems by various spectroscopic techniques involves in one way or another nonadiabatic external perturbations that cause transitions of the system from the initial equilibrium into the excited states. These primary transitions give rise to fast deviations from the initial charge density distribution in the system which, in turn, couple to dynamical polarization or screening response of the surrounding electronic density.

In this contribution we present a comparative study of ultrafast screening and evolution of the potentials that govern excited electron and hole dynamics at Cu(111) and Ag(111) surfaces supporting prototype quasi-two dimensional surface bands. The lowest partly occupied state is termed the Shockley surface state and the unoccupied Rydberg-like states detached from the vacuum level are termed the image-potential states. Calculations of energetics [1] and dynamics [2,3] of these states have been based on the assumption of instantaneous creation of image potential $V^{im}(z)$ where z is the electron coordinate perpendicular to the surface. However, assumption of instantaneous $V^{im}(z)$ becomes inapplicable on the ultrashort time scale because surface screening is a dynamical, damped oscillatory process whose cycle duration and attenuation can be identified with the inverse surface plasmon frequency and its width, respectively [4,5]. Thus, upon sudden promotion of a probe charge in front of the surface the formation of its stationary image charge and ensuing potential occur after several such cycles when dephasing processes eliminate the screening transients. Only in that limit the employment of standard static $V^{im}(z)$ can be justified.

We separately analyze the screening of uncorrelated and correlated holes and electrons excited in pre-existent surface state bands and intermediate and emerging screened states, respectively. Special attention is paid to the correlated primary electron-hole states which commence as transient surface excitons [6] and develop in the course of screening into uncorrelated electron and hole in the image potential and surface state bands, respectively [7]. The obtained results enable to establish a consistent picture of ultrafast electron dynamics at surfaces that is verifiable by time resolved pump-probe photoelectron spectroscopies [8].

Acknowledgements

We acknowledge a partial support from the Basque Departamento de Educación, Universidades e Investigación (Grant No. IT-756-13) and the Spanish Ministry of Economy and Competitiveness MINECO (Grant No. FIS2013-48286-C2-1-P).

References

[1] E.V. Chulkov, V.M. Silkin, and P.M. Echenique, Surf. Sci. 437, 330 (1999
[2] P.M. Echenique, R. Berndt, E.V. Chulkov, T. Fauster, A. Goldmann, and U. Höfer, Surf. Sci. Rep. 7-8, 219 (2004).
[3] E.V. Chulkov, A.G. Borisov, J.P. Gauyacq, D. Sanchez-Portal, V.M. Silkin, V.P. Zhulkov, and P.M. Echenique, Chem. Rev. 106, 4160 (2006).
[4] V.M. Silkin, A.K. Kazansky, E.V. Chulkov, and P.M. Echenique, J. Phys.: Condens. Matter 22, 304013 (2010).
[5] R.D. Muiño, D. Sanchez-Portal, V.M. Silkin, E.V. Chulkov, and P.M. Echenique, Proc. Nat. Acad. Sci. USA 108, 971 (2011).
[6] B. Gumhalter, Prog. Surf. Sci. 87, 163 (2012).
[7] V.M. Silkin, P. Lazić, N. Došlić, H. Petek, and B. Gumhalter, submitted to PRB.
[8] X. Cui, C. Wang, A. Argondizzo, S. Garrett-Roe, B. Gumhalter, and H. Petek, Nat. Phys. 10, 505, (2014).

Double photoemission from Ag(001) using a high-order harmonic light source

A. Trützschler[1,2], C.-T. Chiang[1,2], M. Huth[1], F. O. Schumann[1], J. Kirschner[1], and W. Widdra[2,1]

[1] *Max-Planck-Institute for Microstructure Physics, Halle, Germany*
[2] *Institute of Physics, Martin-Luther-Universität Halle-Wittenberg, Halle, Germany*
E-mail: wolf.widdra@physik.uni-halle.de

Electron correlations play a fundamental role in physics ranging from the binding between atoms to magnetism and superconductivity [1]. However, its quantification is challenging, experimentally as well as theoretically. One of the most direct experimental means is provided by double photoemission spectroscopy (DPE), where a pair of correlated photoelectrons is emitted simultaneously upon absorption of a single photon [2]. Due to low cross sections as well as typically low spectrometer acceptance angles, such experiments are highly demanding [3]. Here we present an efficient momentum-resolved time-of-flight setup for electron-electron coincidence spectroscopy using a high-order harmonic generation (HHG) light source with a tunable photon energy of 14 to 40 eV and MHz repetition rate [4-6].

For the Ag(001) surface, the two-dimensional kinetic energy distribution of photoelectron pairs excited by a photon of 25 eV is shown in Fig. 1(a). It demonstrates a high coincidence count rate in the lower left triangular with kinetic energies below 10 eV. In addition, three horizontal and vertical features between 13 and 17 eV are visible, which are attributed to accidental photoelectron pairs excited by two independent photons in the same light pulse. To separate such accidental from the true coincidence events, we determine the accidental background in an independent experiment at two order of magnitude higher HHG photon flux but otherwise identical setup. Under high flux conditions, the accidental events dominate the spectra. These spectra are used for background subtraction in subsequent low-flux experiments. This is illustrated in Fig. 1(b) for the line scan in Fig. 1(a) along the diagonal line (arrow). Clearly, the reference data for accidental pairs (black) describes accurately the raw data (red) above a sum energy of 13 eV. Below this energy, the true pairs are uncovered by the background-corrected data (blue).

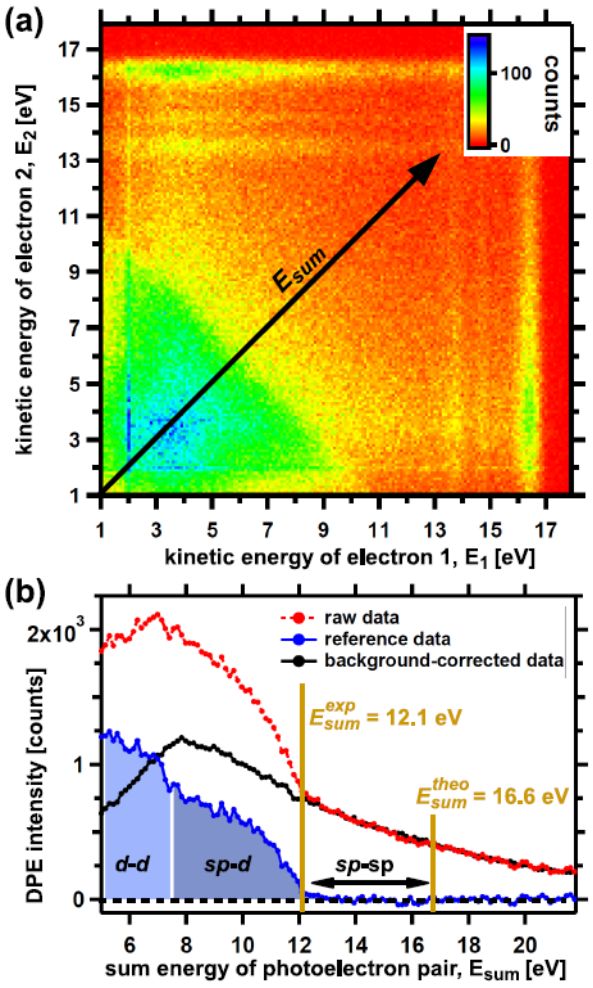

Fig.1: (a) Double photoemission spectrum from Ag(001) at a photon energy of 25 eV. (b) Line scan along the sum energy direction in (a).

Similar to this line scan, the background-corrected two-dimensional kinetic energy distribution is depicted in Fig. 2 where all features from accidental pairs are largely reduced. The data demonstrate clearly that the dominant DPE signal is restricted to the triangular region that is limited by a maximal sum energy of 12.1 eV (black solid line). Between a sum energy of 7.5 (marked by the dot-dot-dashed line) and 12.1 eV, a nearly constant plateau in the DPE intensity is present. It demonstrates a *broad energy sharing* between an electron originating from the Ag d band and an electron from the sp band. On the other hand, their sum energy is a good quantum number as inferred from the sharp coincidence cut-off at 12.1 eV.

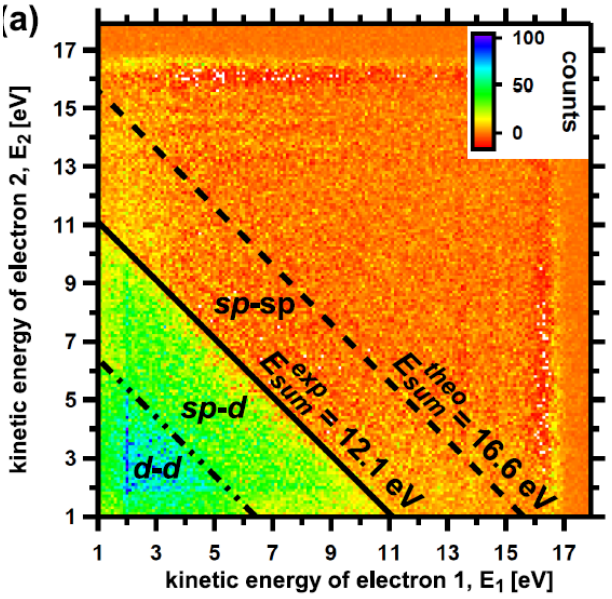

Fig.2: Double photoemission spectrum from Ag(001) at a photon energy of 25 eV, background corrected

Note that the sum kinetic energy for two electrons that originate from near the Fermi level is estimated by the photon energy (25 eV) minus twice the surface work function. In the present case, this corresponds to 16.6 eV as indicated in Fig. 2 by a dashed line. The absence of significant coincidence events for sum energies between 12.1 and 16.6 eV manifests the uncorrelated nature of the Ag sp valence band. On the other hand, we find the highest DPE intensities below sum energies of 7.5 eV. This region might be assigned to d-d electron pairs since the Ag d-band onset is located 4 eV below the Fermi level. However, the data reveal also strong electronic correlations between d and sp electrons that lead to electron pairs with sum energies between 7.5 and 12.1 eV.

To summarize, efficient double photoemission spectroscopy with a high-order harmonic generation light source is demonstrated on Ag(001). The two-dimensional energy distributions show strong electron-electron correlations with a wide energy sharing for d-d and sp-d electron pairs. Contrary, no DPE intensity is found for the energy region of sp-sp electron pairs, which points to the absence of significant electron-electron correlation in the sp band.

References

[1] P. Fulde, “Electron Correlations in Molecules and Solids”; Springer, Berlin (1995).
[2] B. D. Napitu and J. Berakdar ; Phys. Rev. B 81, 195108 (2010).
[3] J. Kirschner, O. M. Artamonov, and S. N. Samarin ; Phys. Rev. Lett. 75, 2424 (1995).
[4] C.-T. Chiang, A. Blättermann, M. Huth, J. Kirschner, and W. Widdra; Applied Physics Letters 101, 071116 (2012).
[5] M. Huth, C. T. Chiang, A. Trützschler, F. O. Schumann, J. Kirschner, and W. Widdra; Applied Physics Letters 104, 061602 (2014).
[6] C.-T. Chiang, M. Huth, A. Trützschler, M. Kiel, F. O. Schumann, J. Kirschner, and W. Widdra; New Journal of Physics 17, 013035 (2015).

Thursday

Sweating the small stuff with the atomic force microscope

Franz J. Giessibl
Experimental and Applied Physics, University of Regensburg, 93053 Regensburg, Germany

Atomic force microscopy (AFM) and scanning tunneling microscopy (STM) provide a direct access to the world of single atoms, allowing to image surfaces with atomic resolution, to perform local spectroscopy of current versus voltage, forces and dissipation. The qPlus force sensor [1] enables to combine STM and AFM capability, providing highly precise imaging and spectroscopy functions and measuring the forces that act during atomic manipulation [2]. Figure 1 below [3] shows an example, where combined AFM/STM reveals two strongly distinct aspects of the atomic structure of matter. The gray veils depict the inverted tunneling currents between a CO molecule adsorbed on Cu(111) and tungsten tips, while the colored surface shows the corresponding force profiles, where the force profiles show a vastly increased spatial resolution over the tunneling current [3]. In contrast to our interpretation published in [3] and based on new experiments [4], we now are quite certain that tips 1, 2 and 3 shown in Fig. 1 are monomer, dimer and trimer tips.

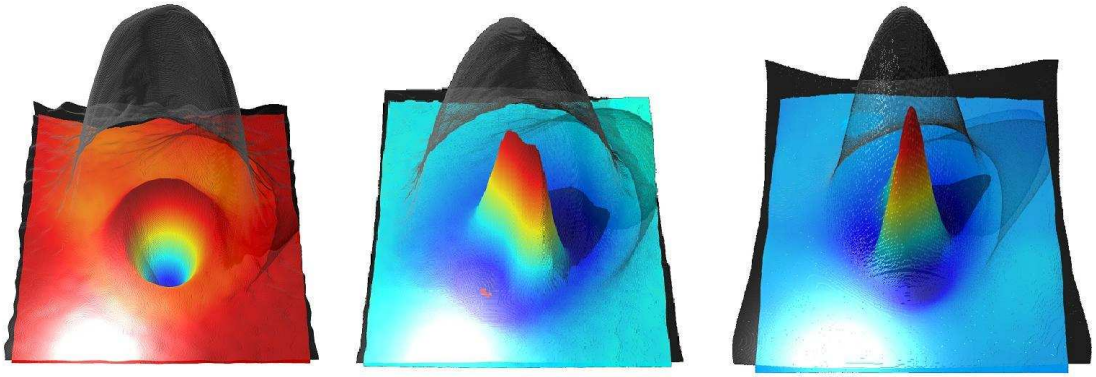

Figure 1 Force profile (colored) and tunneling current (gray) for three different metal tips imaging a CO molecule adsorbed on Cu (111).

Strong angular dependencies of chemical bonding forces have been observed before for Si tips interacting with Si surfaces [5], W tips interacting with graphite [6] and similarities exist between metal tips interacting with CO molecules on Cu and Si adatoms [7]. In the latter two cases, light atoms such as carbon or oxygen interacted with much heavier and much larger metal atoms. Recently, Gross et al. found that CO is an excellent probe for organic molecules. For example, pentacene can be imaged at excellent resolution with CO terminated tips [8], although the softness of CO on tips can lead to image distortions [9,10].

Magnetic exchange force microscopy has allowed to image the antiferromagnetic spin order of NiO (100) by force microscopy [11]. We found that the small amplitude / stiff cantilever technique can dramatically improve the image quality and even enables to perform force spectroscopy on Ni ions with different spin orientation. The force differences are in the piconewton regime. Tips made of permanent magnets such as CoSm allow to resolve the spin order in the antiferromagnetic insulator nickel oxide [12].

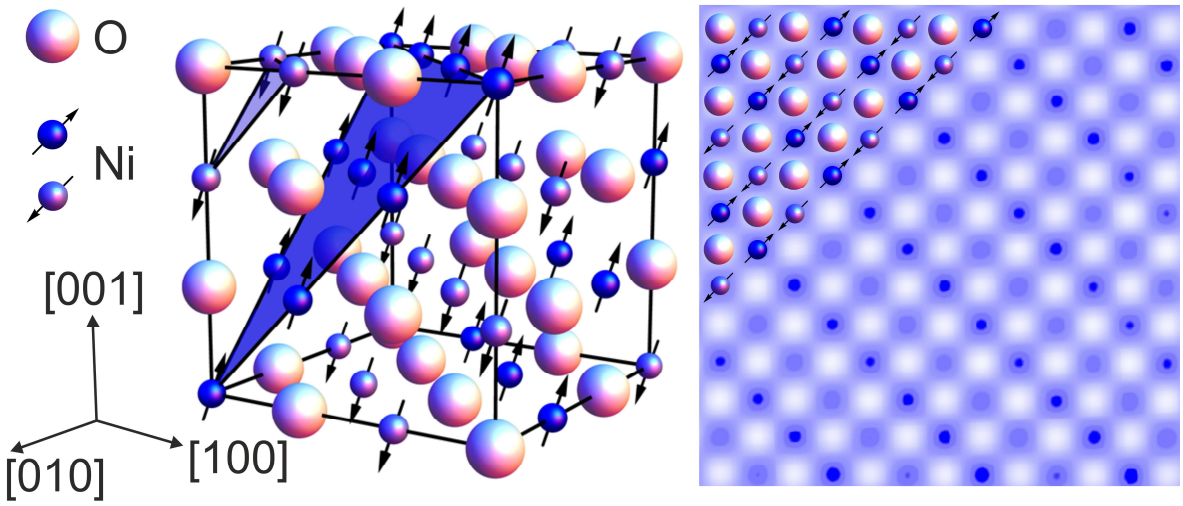

Figure 2 Structure (left) and AFM image (right) of NiO(001).

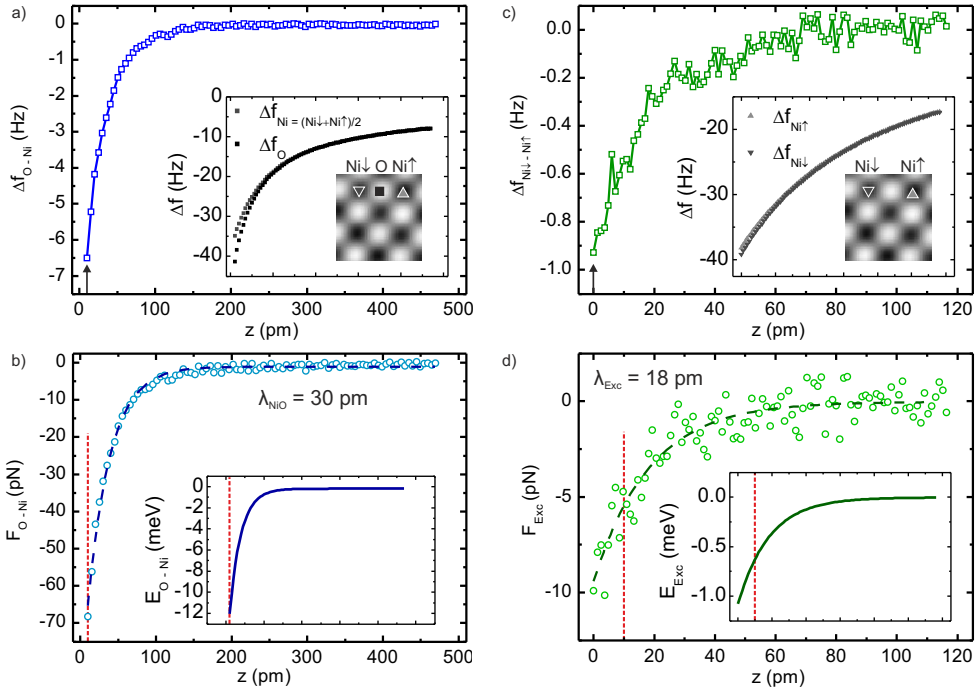

Figure 3 Force spectroscopy on NiO, showing that the spin up/down force contrast amounts to 5 pN.

State-of-the-art force microcopy does sweat the small stuff: it becomes more natural to switch from Angstroms to picometers and from nanonewtons to piconewtons.

[1] F. J. Giessibl, *Appl. Phys. Lett.* **73,** 3956 (1998).
[2] M. Ternes et al., *Science* **319**, 1066 (2008).
[3] J. Welker, F. J. Giessibl, *Science* **336**, 444 (2012).
[4] M. Emmrich et al., submitted.
[5] F. J. Giessibl, S. Hembacher, H. Bielefeldt, J. Mannhart, *Science* **289**, 422 (2000).
[6] S. Hembacher, F. J. Giessibl, J. Mannhart, *Science* **305**, 380, (2004).
[7] J. Welker, J. Weymouth, F. J. Giessibl, *ACS Nano*, DOI: 10.1021/nn403106v (2013).
[8] L. Gross et al. *Science* **325**, 1110 (2009).
[9] A. J. Weymouth, Th. Hofmann, F. J. Giessibl, *Science* **343**, 1120 (2014).
[10] M. Neu et al., Phys. Rev. B **89**, 205407 (2014).
[11] U. Kaiser, A. Schwarz, R. Wiesendanger, *Nature* **446,** 522 (2007).
[12] F. Pielmeier, F. J. Giessibl, *Phys. Rev. Lett.* **110,** 266101 (2013).

STM at the solid-liquid interface

Michiel Coenen, Kunal Bose, Pieter van der Meer, Bas Hendriksen, Hans Elemans, Sylvia Speller
Institute for Molecules and Materials, Radboud University, Nijmegen, The Netherlands

Maxwell Crossley, Jeffrey Reimers
School of Chemistry, University of Sydney, Australia

B.hendriksen@science.ru.nl

The capability of the scanning tunneling microscope to image surfaces and molecules on surfaces in liquids with atomic resolution allows us to study processes, such as the growth molecular monolayers from solution and chemical reactions, under relevant, realistic conditions. Here, I will discuss STM experiments in organic solvents and aqueous solutions.

We used liquid STM to study the formation, structure and electronic properties of tetraundecylcopperporpyrin (CuP) monolayers on a graphite surface. Monolayers of CuP formed at the solid-liquid interface of graphite and octanoic acid show a variety of structural polymorphs. Their relative coverage can be controlled by the concentration of the CuP in the octanoic acid solution, with the higher concentrations leading to higher density structures [1]. Based on high-resolution STM images and DFT calculations we relate each of the polymorphs to a different conformation of each of the alkyl tails. By a combination of STM and AFM experiments we show that the polymorphs have a different electronic structure [2].
We followed the transitions from low density polymorphs into higher density polymorphs by applying higher concentrations of CuP. The structures were found to be kinetically trapped as the exchange of CuP molecules from the supernatant solution with the monolayer was surprisingly small [3]. Only at specific defects CuP molecules from the solution were incorporated in the monolayer, these defect could also be created by STM tip manipulation [4].

Further, I will demonstrate two new methods for STM experiments in liquids, which we recently developed. The first one is STM combined with a micro fluidic cell, which allows the controlled application of liquid droplets and their exchange during STM experiments [5]. The second method is alternating current STM, which allows atomic resolution imaging in aqueous solutions without the need for tip coating [6].

[1] M.J.J. Coenen et al., PCCP 15 (2013) 12451.
[2] M.J.J. Coenen et al., in preparation.
[3] M.J.J. Coenen et al.,Chem. Commun. 47 (2011) 9666.
[4] M.J.J. Coenen et al, Chem. Phys. Chem. 15 (2014) 3484.
[5] K. Bose et al., in preparation.
[6] F. van der Meer & B.L.M. Hendriksen, in preparation.

Magnetic Property of [Co/Nix]y multi-layer with High Brightness and Highly Spin-polarized LEEM

Takanori Koshikawa[1], Masahiko Suzuki[1], Kazue Kudo[2], Kazuki Kojima[3], Tsuneo Yasue[1], Noriko Akutsu[1], Agerico Dino[3], Hideaki Kasai[3], Ernst Bauer[4], Tsutomu Nakanishi[5], Jin[6] and Yoshikazu Takeda[7]

1) Osaka Electro-Communication University and Osaka Univ. Osaka, Japan,
2) Ochanomizu University, Tokyo, Japan,
3) Osaka University, Osaka, Japan,
4) Arizona State University, Tempe, USA
5) School of Science, Nagoya University, Nagoya, Japan
6) KEK, Tsukuba, Japan
7) Aichi Synchrotron Light center, Aichi, Japan

We have already developed a novel very high brightness and high spin-polarized low energy electron microscope (SPLEEM) [1-3]. Our developed SPLEEM can make us the dynamic observation of the magnetic domain images possible. However the size of the spin-polarized electron gun is large and we have developed a new compact spin-polarized electron gun with a new idea. In principle two devices are necessary to operate 3-dimensional spin direction; one is a spin manipulator which changes the out-of-plain spin direction and another one is a spin rotator which can change the in-plain spin direction. We have proposed a multi-pole Wien filter which enables 3-dimensional spin operation with one device [4].

Current induced domain wall motion is a key phenomenon to realize novel spintronics devices such as a race-track memory (IBM) and a domain wall motion magneto-resistive random access memory (NEC). It has been indicated that domain walls in nanowires with perpendicular magnetic anisotropy can move with lower current density than those with in-plane magnetic anisotropy. Multilayer [CoNix] multi-layer is known to exhibit perpendicular magnetic anisotropy and is expected as a material for the devices with low operation current]. We investigated magnetic property during growth of the [CoNix]y multi-layer with our high brightness and highly spin-polarized SPLEEM [1-3]. We will also reproduce the magnetic domain pattern formation of the surface of Co/Ni multilayers by numerical simulations based on the Landau-Lifshitz-Gilbert (LLG) equation, which describes the dynamics of local magnetization. Fig. 1 shows experimental and simulation results of magnetic domain images of multilayers of pairs of [$CoNi_2$] on W(110) [5,6]. The

numerical simulations well reproduce the magnetic domain patterns observed in the experiments.

More detailed experimental results will be shown on the magnetic property for different pairs of Co/Ni systems, i.e., Co/Ni2, Co/Ni3 and Ni2/Co on W(110). Fig.2 shows that the changing angle between the in-plain and the out-of-plain for the same kinds of materials, such as Co and Ni after shifted the abscissa of Ni2/Co pairs. Three systems show the similar property and the contribution of Ni layer is not large. The main contribution to the perpendicular magnetization would cause with the un-isotropy of the interface of Co and Ni layer.

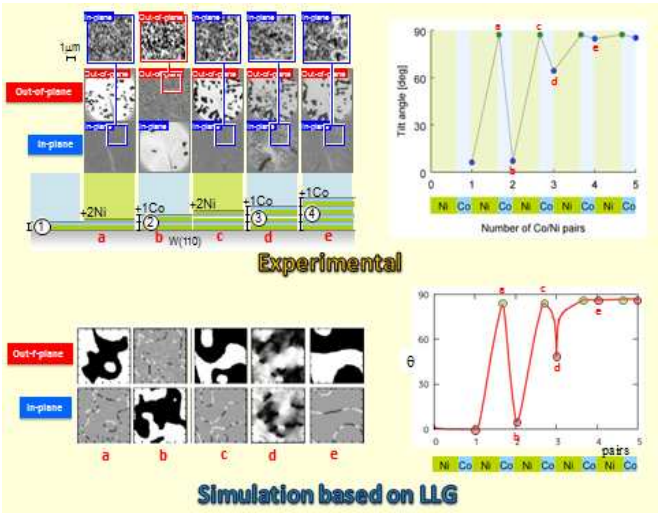

Fig.1 Magnetic domains of Co/Ni multi-layers

[1] N.Yamamoto *et al.*, J. Appl. Phys. **103**, 064905 (2008).

[2] X.G. Jin *et al.*, Appl. Phys. Express **1**, 045602 (2008).

[3] M.Suzuki *et al.*, Appl. Phys. Express **3**, 026601 (2010).

[4] T.Yasue et.al., Rev. Sci. Instrum., 85, 043701 (2014).

[5] M.Suzuki et.al., J.Phys.Condens.Matter. **25**, 406001 (2013). (Short news on the web of IOP and IOPselect)

[6] K.Kudo et.al., J.Phys.Condens.Matter. **25**, 395005 (2013).

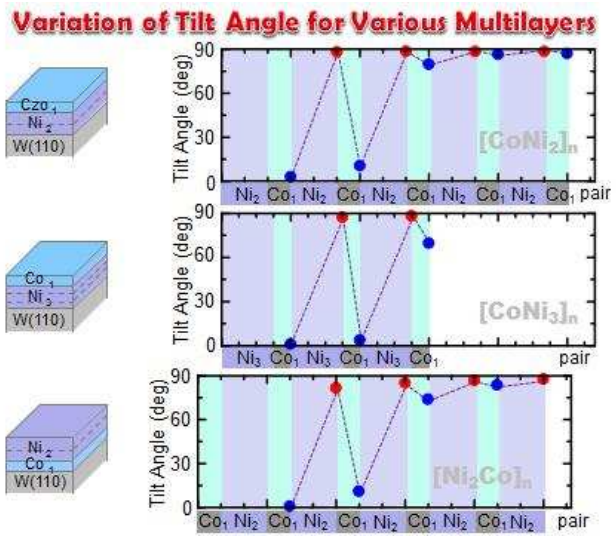

Fig.2 Magnetic direction of Co/Ni2, CoNi3 and Ni2/Co multi-layers on W(110)

Improving the temporal resolution of laser-based photoemission electron microscopy

E. Mårsell[1,*], E. Lorek[1], A. Losquin[1], C. Guo[1], P. Rudawski[1], A. Harth[1], M. Miranda[1], R. Swärd [1], C. L. Arnold[1], J. Mauritsson[1], A. L'Huillier[1], A. Mikkelsen[1]

[1] *Department of Physics, Lund University, P.O. Box 118, 221 00 Lund, Sweden*

E-mail: erik.marsell@sljus.lu.se

Photoemission electron microscopy (PEEM) in combination with femtosecond laser pulses has during the past decade emerged as a powerful technique to study local field enhancement on nanostructured surfaces with subwavelength spatial resolution [1-2]. In combination with interferometric techniques, it has also been used to resolve surface plasmon dynamics with high temporal resolution [3-4]. Most of these studies have used laser pulses with durations of tens of femtoseconds. Here, we discuss ways of utilizing shorter bursts of light in order to further improve the temporal resolution of PEEM.

Interferometric time-resolved PEEM (ITR-PEEM), as described by Kubo *et al.* [3], is based on two equal laser pulses with a variable delay. By acquiring PEEM images for different delays, the near-field dynamics can be studied. We have implemented this technique using 6 fs near-infrared pulses from a broadband oscillator to study the near-field dynamics in a variety of engineered metallic nanostructures. Figure 1a shows an SEM image of an array of gold bow-tie nanoantennae with varying size. Illuminating the array with near-IR laser pulses results in photoemission from hot-spots at the centres of the bow-ties (Fig. 1b). Because of the photon energy being approximately one third of the work function, the photoemission is nonlinear and therefore very sensitive to the local field. Thus, the photoemission signal varies significantly between the antennae. There is, however, a general trend with bow-ties close to the middle of the array emitting more electrons due to their resonance frequency overlapping with the laser spectrum. The photoemission signal from two different areas of the array as a function of the delay between two equal laser pulses is shown in Fig. 1c. The dephasing of the oscillation indicates the different near-field dynamics of the antennae. In brief, the shorter oscillation period for the smaller bow-ties, apparent already at delays of less than 10 fs, indicates a higher resonance frequency. More in-depth information of the exact near-field

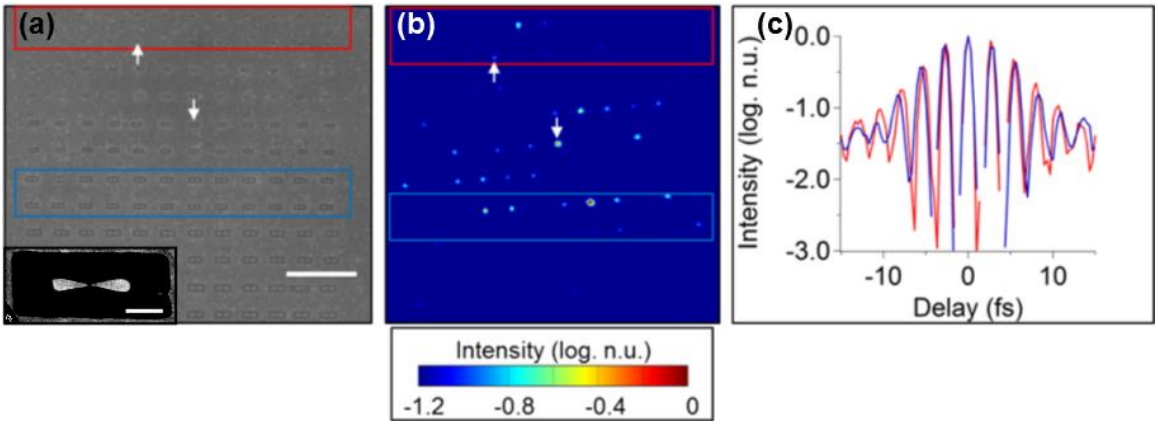

Fig. 1. *ITR-PEEM measurements on gold bowtie nanoantennae. a) SEM image of an antenna array. Scale bar is 5 µm. Inset: Zoom in of a single, resonant bow-tie antenna. Inset scale bar is 200 nm. b) Laser-PEEM image of the array shown in a. The white arrows and coloured squares serve as guides for the eye. c. PEEM autocorrelation traces corresponding to smaller (red) and larger antennae (blue square). The differences between the traces indicate different ultrafast near-field dynamics. The laser beams are incident from the top in the PEEM image, and the electric field vector lies in the sample plane.*

dynamics can be acquired through comparison with finite-difference time domain modelling.

Another way of further improving the temporal resolution of PEEM is to use extreme ultraviolet (XUV) attosecond pulses generated by the interaction of intense near-IR laser pulses with a noble gas [5]. This technique, atto-PEEM, can in principle directly measure the near-field with attosecond temporal and nanometre spatial resolution. However, experiments have shown that it is very challenging to implement in practice [6-8]. The main issue has been the low repetition rate of existing attosecond light sources, which is problematic due to space charge effects blurring the PEEM image when the number of emitted electrons per laser pulse is significantly more than one. In a new setup, we use non-collinear optical parametric amplification to create near-IR pulses of 7 fs duration and 11 µJ energy at a repetition rate of 200 kHz. The pulses are focused by a 5 cm focal length achromat lens into a continuous stream of argon to generate high-order harmonics. A 200 nm thick Al filter is used to block the fundamental beam. The radiation is then re-focused onto the PEEM sample using a toroidal mirror. This new light source is a vast improvement from the previous experimental setup [6,8], which was based on a conventional chirped-pulse amplification system working at 1 kHz. The high-order harmonic spectra from these two light sources are compared in Fig. 2a. Both light sources were used to image Ag nanowires on Au substrates, and the images are shown in Fig. 2b-c. The 200 kHz light source achieves an improvement in resolution of a factor of ~2 while reducing the acquisition time by more than an order of magnitude.

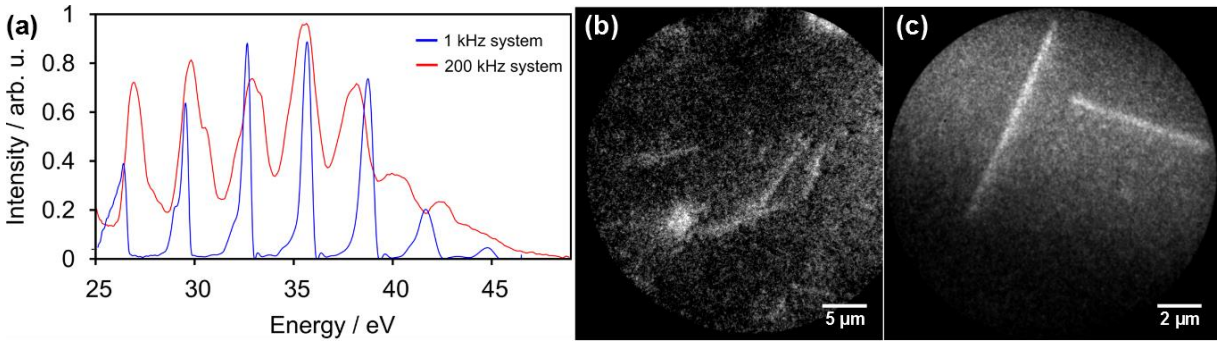

Fig. 2*.Comparison of two different high-order harmonic sources for PEEM applications. a) Spectra of the harmonics from the two laser systems. The difference in the widths of the harmonics is due to the broader spectrum of the IR pulses from the 200 kHz system. b) PEEM image of Ag nanowires using the 1 kHz system and an acquisition time of* ***400 seconds****. c) PEEM image of a similar sample using the 200 kHz system and an acquisition time of* ***30 seconds****.*

As a next step, we plan to do IR-XUV pump-probe experiments using the 200 kHz high-order harmonic source. With this system, we hope to further push the temporal resolution in photoemission electron microscopy down to the attosecond regime.

References

[1] O. Schmidt *et al.*, Appl. Phys. B 74, 223 (2002).
[2] M. Aeschlimann et al., Nature 446, 301 (2007).
[3] A. Kubo et al., Nano Lett. 5, 1123 (2005).
[4] Q. Sun et al., Light Sci. Appl. 2, e118 (2013).
[5] M. I. Stockman et al., Nature Photon. 1, 539 (2007).
[6] A. Mikkelsen et al., Rev. Sci. Instrum. 80, 123703 (2009).
[7] S. H. Chew et al., Appl. Phys. Lett. 100, 051904 (2012).
[8] E. Mårsell et al., Ann. Phys. (Berlin) 525, 162 (2013).

Resent progress in analyser development in the field of high pressure photoelectron spectroscopy

J. Åhlund[1]

1. [1] *VG Scienta AB, Box 15120, 750 15 Uppsala, Sweden*

E-mail: john.ahlund@vgscienta.com

High-pressure Photoelectron Spectroscopy (HP-PES) is a rapidly developing technique with applications in a wide range of scientific fields e.g. catalysis, battery and solar cell research. Here we present resent progress in HP-PES analyser development and in particular the design and performance of a newly developed high pressure photoelectron spectrometer (Scienta R4000 HiPP-3) capable of recording spatially resolved spectra under high pressure.

The Scienta R4000 HiPP-3 analyser is based on the Scienta R4000 HiPP-2 analyser. Both analysers are of hemispherical type and equipped with differentially pumped electrostatic lenses. The HiPP-2 is constructed for operation up to 10 keV whereas the HiPP-3 is optimized for spatial resolution spectroscopy in the XPS energy range.

The HiPP-2 analyser is presented in ref [1]. Here a newly developed lens mode for the HiPp-2 analyser, the "Swift Acceleration Mode", is discussed. With this mode, electrons are accelerated towards the analyser by a large voltage applied to the second aperture of the differential pumping stage. In the Swift Acceleration Mode, the signal decrease due to inelastic scattering is much less severe than for traditional analysers.

The HiPP-3 is tested using a laboratory based system equipped with an Al Kα X-ray anode. The transmission of the analyser is demonstrated by measuring the Ag 3d features on a silver sample in up to 25 mbar of nitrogen using the Swift Acceleration principle. The instrument is demonstrated to be capable of measuring core level spectra as well as valence band spectra with unprecedented transmission. Further, the spatial mode of the analyser is tested using a test sample of well-defined gold stripes on a silicon sample. A spatial resolution of better than 5 μm of the Au $4d_{5/2}$ core level line was demonstrated under vacuum conditions as well as for high pressure measurements of 1 mbar.

Acknowledgements

The HiPP-2 development was supported by the Swedish Governmental Agency for Innovation Systems (VINNOVA).

References

[1] Susanna K. Eriksson, Maria Hahlin, Juhan Matthias Kahk, Ignacio J. Villar-Garcia, Matthew J. Webb, Helena Grennberg, Rositza Yakimova, Håkan Rensmo, Kristina Edström, Anders Hagfeldt, Hans Siegbahn, Mårten O. M. Edwards, Patrik G. Karlsson, Klas Backlund, John Åhlund, and David J. Payne Review of Scientific Instruments 85, 075119 (2014)

New attosecond time-resolved photoemision experiments from surfaces of layered crystals

S. Neb[1], F. Siek[1], M. Hensen[1], S. Fiechter[2], J.-H. Dil[3], N. Müller[1], W. Pfeiffer[1], U. Heinzmann[1]

[1] *Molecular and Surface physics, faculty of physics, Bielefeld University, 33615 Bielefeld, Germany*

[2] *Helmholtz Zentrum Berlin, Hahn-Meitner Platz 1, 14109 Berlin, Germany*

[3] *Institute of Condensed Matter Physics, EPFL, CH-1015 Lausanne, Switzerland*

E-mail: uheinzm@physik.uni-bielefeld. de

We report on recently measured delays for core-level photoelectron emission from different layered materials with and without inversion symmetry.

The availability of single attosecond (as) XUV pulses allows investigating ultrafast electron dynamics on the attosecond timescale. Photoelectron wave packets generated by the XUV pulse interact with a simultaneously present 5fs phase stabilized IR pulse. Measuring the photoelectron streaking for electrons emitted from different initial bands and core-level states as a function of the delay between XUV and IR pulse allows determination of the relative timing of the different processes. The layered structure of the investigated crystals yields element-specific photoelectrons emitted from different depth and thus helps to resolve the physical origin of the temporal delays in photoemission, as studied for the first time in solids by Cavalieri et al [1]. The physical origin of delays between the emitted electrons from different bands is not completely understood and different theoretical models co-exist [2].

Contamination effects can be ruled out for the layered crystals studied, since the delays measured and the photoelectron spectra have been found to be constant for more than 36 hours after preparation of the crystal. Our apparatus, including the laser pulse and its phase stability has been very stable during this period of time. The delay differences measured with accuracies of about 10as provide the feasibility for testing the various theoretical models for the time dynamics of photoemission. In particular crystals with defined layers of different chemical composition allow studies of the influence of electron propagation effects due to the different localization of the bands they come from on the one side and of photoelectron wave phase shifts on the other side [3].

References

[1] A.L. Cavlieri, N. Müller, Th. Uphues, V.S. Yakovlev, A. Baltuska, B. Horvath, B. Schmidt, L. Blümel, R. Holzwarth, S. Hendel, M. Drescher, U. Kleineberg, P. M. Echenique, R. Kienberger, F. Krausz and U. Heinzmann, "Attosecond spectroscopy in condensed matter", Nature 449, 1029 - 1032 (2007)

[2] for a review see U. Heinzmann, "Attosecond Time-Resolved Photoemission Spectroscopy in Condensed Matter – Photoelectron Wave Phase Shifts and Time Delays", Chapter 13 of "Attosecond Physics" Springer Series in Optical Sciences 177 (Eds. L. Plaja et al.), p. 231-253, DOI 10.1007/978-3-642-37623-8, Springer-Verlag Berlin (2013)

[3] U. Heinzmann and J.-H. Dil, topical review, J. Phys. Condens. Matter 24, 173001 (2012)

Origin of Perpendicular Magnetic Anisotropy in Co/Ni(111) superlattices

M. Gottwald[1,4], T. Hauet[1], F. Bertran[2], P. Lefevre[2], A. Taleb[2], P. Ohresser[2], E. Snoeck[3], L. Calmels[3], E. Arenholz[4], S. Mangin[1], E. Fullerton[5] and S . Andrieu[1]

[1]*Institut Jean Lamour, Lorraine University - CNRS, Nancy, France*
[2]*SOLEIL synchrotron, Saclay, France*
[3]*CEMES, CNRS – Toulouse University, Toulouse, France*
[4]*ALS Berkeley USA*
[5]*UCSD, University of California, San Diego, USA*

Manipulating the magnetization of thin layers by using other routes than applied magnetic field is of particular importance for spintronics applications. One way is to use the Spin Transfer Torque (STT) phenomenon in order to switch the magnetization in nanopillars using a current. Perpendicular Magnetic Anisotropy (PMA) is particularly interesting to obtain since the STT critical currents are strongly decreased compared to devices with in-plane magnetization. We observed that magnetization in Co/Ni (111) superlattices grown by Molecular Beam Epitaxy is perpendicular for a Co thickness range between 0.2 and 3.5 ML [1]. As the coercive field depends on the magnetic energy balance and consequently on the Co thickness, spin valves with 2 (Co/Ni)-based magnetic layers separated by an Au spacer can be prepared (see figure 1). Playing with the Co thickness, the coercive magnetic field can be tuned and adapted for each magnetic layer.

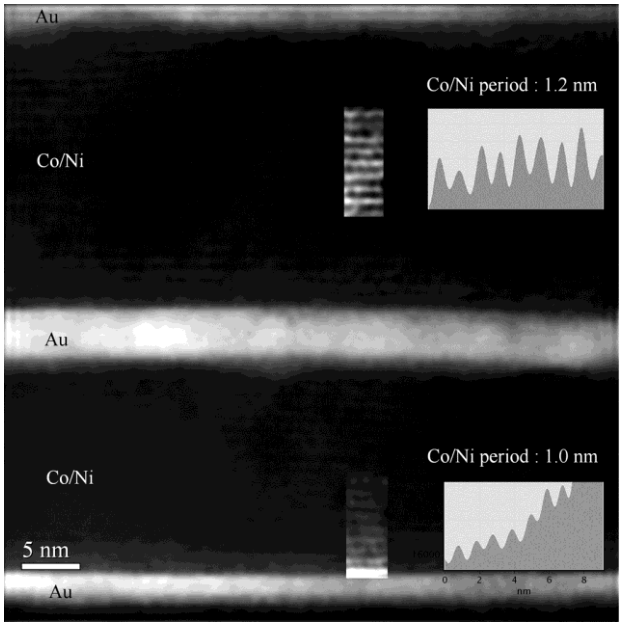

FIG1 : HRTEM image of a spin valve composed of a bottom hard magnetic layer ($Co_{1ML}Ni_{3ML}$)x10 leading to a H_c=500 Oe) and a top soft magnetic layer ($Co_{2ML}Ni_{3ML}$)x10 leading to a H_c=200 Oe) separated by a Au layer (from ref.2)

In this talk, we give a review on the structural and magnetic properties of these Co/Ni(111) single-crystalline layers in order to try to understand in details the origin of this PMA [2]. This perpendicular anisotropy is explained by taking into account a strong interfacial anisotropy as definitely shown by looking at the influence of the Ni capping on a Co layer : without Ni on top, the chosen 3ML thick Co layer has an-in

plane magnetizeation. We thus varied the Ni coverage from 0 to 1.2ML, and measured the hysteresis loop by MOKE for each Ni coverage (see fig.2). We actually observed that the easy magnetization axis turned from in-plane to out-of-plane around 0.6ML Ni. The possibility of a magnetoelastic contribution was also analysed. By using both Transmission Electron Microscopy and X-Ray diffraction, the magnetoelastic contribution in the total magnetic energy is thus estimated and shown to be much smaller than the interface anisotropy. On the other hand, the magnetic properties were also analysed by using synchrotron radiation facilities. Spin polarized photoemission experiments were performed on the CASSIOPEE beamline at SOLEIL synchrotron [3]. The spin polarization at the Fermi level is found to be near 80% for 1ML Co, twice the value measured on a reference Co(111) bulk sample. Finally, recent X-Ray Magnetic Circular Dichroism experiments performed at SOLEIL synchrotron allow us extracting the true spin moment and the in-plane to out-of-plane orbital magnetic moment variation $\Delta m_{\perp}$-$\Delta m_{//}$ responsible for the PMA [3]. Surprisingly, clear orbital moment anisotropy is observed for Co but not for Ni, whereas the PMA was always attributed to Ni in the literature. Moreover, the total magnetic moment of Co is found to be strongly enhanced ($2.5\mu_B$ at 20K) compared to bulk ($1.7\mu_B$) whereas a small increase is expected using DFT calculations (5%). The atomic arrangement of Co on a Ni single-crystal was analysed by using anomalous surface diffraction (working at Co L edge) in order to evidence a special atomic arrangement that could explain this unusual high magnetic moment at the interface. However, no special arrangement was evidenced. The origin of such discrepancies will be discussed.

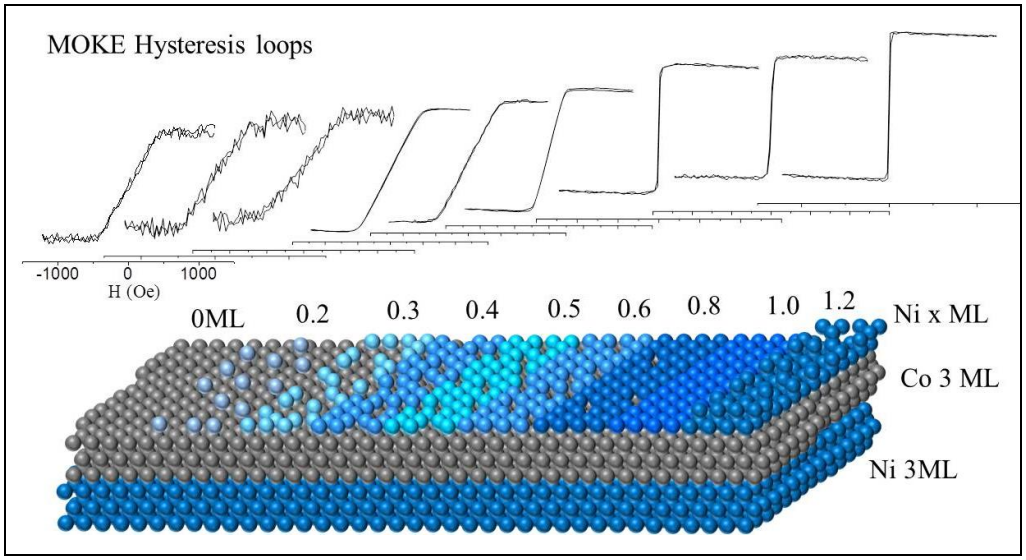

FIG2 : Hysteresis loops measured by Kerr on a 3ML Ni + 3ML Co sample capped by different Ni coverages from 0 to 1.2ML (wedge sample). The magnetic field is applied perpendicular to the film plane. The magnetization thus turns from in plane to out-of plane above 0.6ML Ni.

[1] - *Strong perpendicular magnetic anisotropy in Ni/Co(111) single crystal superlattices* S. Girod *et al*, Appl. Phys. Lett., 94, 262504, (2009)

[2] - *Co/Ni(111) superlattices studied by microscopy, X-ray absorption and ab-initio calculations M. Gottwald et al, Phys. Rev. B 86, 014425 (2012)*

[3] – in preparation

Magnetic Nanostructures

Peter Varga

Institute for Applied Physics, Vienna University of Technology, Austria

CEITEC (Central European Institute for Technology) at Brno University of Technology, Czech Republic

The field of magnetic nanostructures encompasses a wide variety of topics. Spintronics molecular magnets, biomagnetism, new routes to high-density magnetic recording media and magnetic logic devices, magnetic nano-particles and nano-wires. In this presentation two examples for "top down" productions of magnetic nanostructures will be presented. In the first part of the talk growth of non magnetic metastable fcc Fe films on Cu(100) up to a thickness of 40 ML will be demonstrated as well as the transformation of this films into magnetic bcc structures by ion beam bombardement. The lateral size of this magnetic structure is limited by the ion beam diameter down to 30nm with FIB (Focused Ion Beam) [1,2,3,4]. As a second example the production of magnetic nano-disks from permalloy with a diameter in the 100 nm range on a Au wave-guide by using FIB (Focused Ion Beam) technique will be shown. Ultrafast switching of spin circulation in this nano-disks using nanosecond magnetic field pulses is imaged by the process of full-field x-ray transmission microscopy [5,6]. It is planned to use the technique of transforming Fe layers from fcc-non magnetic into bcc-magnetic ones for further experiments in switching of vortex circulation of magnetic nanostructures which will be formed by FIB in metastable nonmagnetic fcc films.

[1] W. Rupp, A. Biedermann, B. Kamenik, R. Ritter, Ch. Klein, E. Platzgummer, M. Schmid, P. Varga, Appl. Phys. Lett. **93** (2008) 063102

[2] S. Shah Zaman, H. Oßmer, J. Jonner, Z. Novotný, A. Buchsbaum, M. Schmid, P. Varga Phys. Rev. B 82 (2010) 235401

[3] S. Shah Zaman, P. Dvorak, R. Ritter, A. Buchsbaum, D. Stickler, H.P. Oepen, M. Schmid, P. Varga J. Appl. Phys. 110 (2011) 024309

[4] J. Gloss, S. Shah Zaman, J. Jonner, Z. Novotny, M. Schmid, P. Varga, M. Urbánek, Appl. Phys. Lett. 103 (2013) 262405

[5] V. Uhlíř, M. Urbánek, L. Hladík, J. Spousta, M.-Y. Im, P. Fischer, N. Eibagi, J. J. Kan, E. E. Fullerton, and T. Šikola, Nature Nanotech. 8, 341 (2013).

[6] M. Urbánek, V. Uhlíř, C.-H. Lambert, J. J. Kan, N. Eibagi, M. Vanatka, L. Flajsman, R. Kalousek, Mi-Y. Im, P. Fischer, T. Sikola, and E. E. Fullerton, submitted Phys.Rev. B

Density of surface states in time-reversal invariant Weyl semimetals

A. P. Protogenov,[1,2] O. A. Shagalova,[3] and E. V. Chulkov[4,5,6]

[1] *Institute of Applied Physics of the RAS, Nizhny Novgorod 603950, Russia; alprot@appl.sci-nnov.ru*
[2] *Donostia International Physics Center (DIPC), 20018 San Sebastián/Donostia, Spain*
[3] *Institute of Applied Physics of the RAS, Nizhny Novgorod 603950, Russia*
[4] *Departamento de Física de Materiales, Facultad de Ciencias Químicas, Uviversidad del País Vasco, Apartado 1072, 20080 San Sebastián/Donostia, Spain*
[5] *Donostia International Physics Center (DIPC), 20018 San Sebastián/Donostia, Spain*
[6] *Centro de Física de Materiales CFM-Materials Physics Center MPC, Centro Mixto CSIC-UPV/EHU, 20018 San Sebastián/Donostia, Spain*

New classes of matter known as topological insulators and Weyl semimetals are characterized by the linear dispersion of low-energy electron excitations on the surface and in the bulk, respectively. The states on the surface of these so-called Dirac materials have a fixed spin orientation for each momentum. The electron states in topological insulators [1, 2] are topologically protected by the time-reversal symmetry. A condition for the existence of Weyl semimetal is breaking of either inversion or time-reversal symmetry. The topological protection manifests itself as massless Dirac modes propagating along the edge or the surface of topological insulators or in the bulk of Weyl semimetals and on their surface in the form of Fermi arc states [3]. Study of the properties of surface electron states, being a hallmark of the topological nature of Weyl nodes, enables one to clarify some features of the topological protection by a symmetry.

Materials for realization of Weyl semimetals include the pyrochlore iridates [3] , topological insulator heterostructures [4] and magnetically doped topological insulators [5]. It should be noted that the topological classification of phase states in topological insulators has been extended to Weyl semimetals [6]. The transport features of Weyl semimetals related to the chiral anomaly as well as the spectrum of collective excitations were recently studied (see reviews [7, 8]). Friedel oscillations due to Fermi arcs in Weyl semimetals have been studied in an interesting paper [9] where the contribution of the bulk and surface states to the density of states for the model of the stacking alternative two-dimensional electron and hole Fermi surfaces was calculated. Oscillations of the density of bulk states in Weyl semimetals in a strong magnetic field and their experimental signatures were analyzed also.

We examine here the properties of Weyl semimetals when the time-reversal symmetry is preserved, while the spatial inversion symmetry is broken [10], focusing on the density of *surface* states. This type of Weyl semimetal is studied in Ref. [11] in which the spectrum of surface states is obtained. It has the form $E(k_x, k_y) = 4t \sin\frac{k_x a}{4} \sin\frac{k_y a}{4}$. Here $\mathbf{k} = (k_x, k_y)$ is the two-dimensional wave vector, t is the integral of nearest-neighbor hopping, and a is the lattice constant.

The density of surface states is defined by the integral over the surface Brillouin zone (BZ) $|k_x \pm k_y| \leq \frac{2\pi}{a}$ of the delta function $\delta[E - E(k_x, k_y)]$ as follows $N(E) = \int\limits_{BZ} \frac{d^2k}{(2\pi)^2} \delta[E - E(k_x, k_y)]$. Having introduced the dimensionless quantities, i.e., the density of surface states $n(\varepsilon) = N(E)/N_0$ with $N_0 = 4/(\pi^2 a^2 t)$, the energy $\varepsilon = E/(2t)$, the wave vector components $(x, y) = (k_x a/4, k_y a/4)$, after changes of variables, we obtain $n(\varepsilon) = \int\limits_0^{\varphi} \frac{d\alpha}{\sqrt{1 - m\sin^2\alpha}} = F(\varphi, m)$. The amplitude $\varphi = \arcsin\sqrt{\frac{2(1-\varepsilon)}{2-\varepsilon}}$ and the parameter $m = 1 - (\varepsilon/2)^2$ of the elliptic integral of the first kind $F(\varphi, m)$ depend on the energy ε in the range $0 < \varepsilon \leq 1$. The density of surface states versus the energy ε in the range $0.1 < \varepsilon \leq 1$ is shown in Fig. 1. It should be noted that the density of surface states in is valid in the energy range until the surface states merge with the bulk electron state continuum [11]. This energy range is smaller than the interval $(0, 1)$.

The density of states is determined by the dispersion of the electron spectrum and the spatial dimensionality d of the considered problem. It is usually a non-decreasing function of energy. The exception is the one-dimensional case with the quadratic spectrum $E_p = p^2/2m_e$ when $N(E) \sim E^{-1/2}$. For comparison, the density of surface states in topological insulators is equal to $N(E) = \frac{E}{2\pi\hbar^2 v_F^2}$, while it equals $N(E) = \frac{E^2}{2\pi^2\hbar^3 v_F^3}$ for the bulk states in Weyl semimetals, where v_F is the Fermi velocity. The restriction of the phase space affects the contribution to thermodynamic characteristics, e. g., by reducing the specific heat $C \sim T^d$ for Dirac materials, where T is the temperature and $d = 2, 3$. In the considered two-dimensional problem, the origin of the decreasing function $n(\varepsilon)$ is the saddle point at the surface Brillouin zone center, which leads to the appearance of the Van Hove singularity for $\varepsilon = 0$, as well as decreasing of the length of the Fermi arcs at $\varepsilon \to 1$.

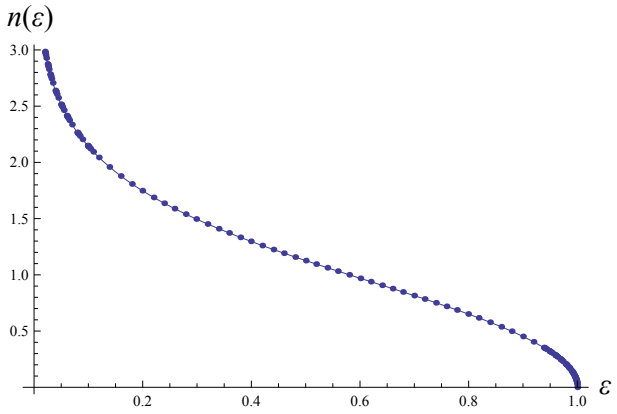

FIG. 1: The density of surface states $n(\varepsilon)$ vs. the energy ε in Weyl semimetal.

The knowledge of $N(\varepsilon)$ and the value $N(\varepsilon_F)$ at the Fermi energy ε_F is important for studying the internal electrostatic effects and the external gate-voltage effects. The quantum capacitance C_Q per unit area of a two dimensional system is given, e. g., by $C_Q = e^2 N(\varepsilon_F)$, where e is the electron charge. This could be used for experimental check of the features of the density of surface states in Weyl semimetals. The density of states also determines the dc conductivity σ_{dc}. Einstein's formula $\sigma_{dc} = e^2 N(\varepsilon_F) D$ expresses σ_{dc} in terms of the density of states and the diffusion constant $D = v_F^2 \tau$, where τ is the transport lifetime. Obviously, we have thereby a contribution of the surface conductivity to the total one in tunneling in Weyl semimetals. As for the distribution of spin degrees of freedom, bulk states for one Dirac node in Weyl semimetal resemble chiral quasi-spin configurations in graphene, while surface states in Weyl semimetal are analogs of helical distributions of spin directions in topological insulators. The energy spectrum and the spin texture of surface states can be experimentally studied using the tunneling spectroscopy technique, for which the behavior of the density of surface states is the key one. To isolate the surface contributions from the bulk ones we have to follow the approach of Ref. [12] for manipulating the surface conditions to distinguish and control the electronic transport of surface carriers of different topological natures.

In conclusion, we have calculated the density of surface states in Weyl semimetals and have shown that it possesses the logarithmic singularity for $\varepsilon \to 0$ decreasing linearly at the intermediate energy of surface electron states and approaching zero as $\sqrt{1-\varepsilon}$ for $\varepsilon \to 1$. It resembles the behavior of the set of two orthogonal one-dimensional Dirac metals embedded in two-dimensional space.

Acknowledgement.– The authors are grateful to V. Ya. Demikhovskii, S. V. Eremeev, E. R. Kocharovskaya, and V. G. Tyuterev for useful discussions. This work was supported in part by RFBR Grant No. 14-02-00174 (O.A.S.) and by the University of the Basque Country UPV/EHU under Grant No. IT-756-13 (E.V.C.).

[1] M. Z. Hasan and C. L. Kane, Rev. Mod. Phys. **82**, 3045 (2010).
[2] X.-L. Qi and S.-C. Zhang, Rev. Mod. Phys. **83**, 1057 (2011).
[3] X.Wan, A.M. Turner, A. Vishwanath, and S.Y. Savrasov, Phys. Rev. B **83**, 205101 (2011).
[4] A.A. Burkov and L. Balents, Phys. Rev. Lett. **107**, 127205 (2011).
[5] G.Y. Cho, Possible topological phases of bulk magnetically doped Bi_2Se_3: turning a topological band insulator into the Weyl semimetal, arXiv: 1110.1939.
[6] B.-J. Yang and N. Nagaosa, Classification of stable three-dimensional Dirac semimetals with nontrivial topology, arXiv: 1404.0754.
[7] P. Hosur and X.-L. Qi, Compt. Rend. Physique **14** (9-10), 857 (2013).
[8] A. M. Turner and A. Vishwanath, Beyond band insulators: topology of semimetals and interacting phases, arXiv: 1301.0330.
[9] P. Hosur, Phys. Rev. B **86**, 195102 (2012).
[10] G. B. Halasz and L. Balents, Phys. Rev. B **85**, 035103 (2012).
[11] T. Ojanen, Phys. Rev. B **87**, 245112 (2013).
[12] H. Cao, C. Liu, J. Tian, Y. Xu, I. Miotkowski, M.Z. Hasan Y.P. Chen, Controlling and distinguishing electronic transport of topological and trivial surface states in a topological insulator, arXiv: 1409.3217.

Friday

Phonon-Mediated Electron Transport through CaO Thin Films

Yi Cui,[1] Sergio Tosoni,[2] Wolf-Dieter Schneider,[1,3] Gianfranco Pacchioni,[2]
Niklas Nilius,[1,4] Hans-Joachim Freund [1]

[1]*Fritz-Haber-Institut der Max-Planck-Gesellschaft, Faradayweg 4-6, 14195 Berlin, Germany*
[2]*Dipartimento di Scienza dei Materiali,*
Università di Milano-Bicocca, via Cozzi 53, 20125 Milano, Italy
[3]*Ecole Polytechnique Fédérale de Lausanne, Institute of Physics,*
CH-1015 Lausanne, Switzerland
[4]*Carl von Ossietzky Universität Oldenburg, Institut für Physik, D-26111 Oldenburg, Germany*
(e-mail: wolf-dieter.schneider@epfl.ch)

Scanning tunneling microscopy has developed into a powerful tool for the characterization of conductive surfaces, for which the overlap of tip and sample wavefunctions determines the image contrast. On insulating layers, as the CaO thin film grown on Mo(001) investigated here, direct overlap between initial and final states is not enabled anymore and electrons are transported via hopping through the conduction-band states of the oxide. Carrier transport is accompanied by strong phonon excitations in this case, imprinting an oscillatory signature on the differential conductance spectra of the system. The phonons show a characteristic spatial dependence and become softer around lattice irregularities in the oxide film, such as dislocation lines [1].

The experiments were performed in an ultra-high vacuum STM operated at liquid-helium temperature. The CaO films were prepared by Ca deposition onto a clean Mo(001) single crystal in 5×10^{-7} mbar of O_2 [2]. Upon vacuum annealing to 1000 K, the initially amorphous films crystallized and developed a sharp square pattern in LEED, indicative for the (001) termination of rocksalt CaO. STM measurements revealed wide and atomically-flat terraces of up to 20 nm diameter, delimited by a network of dislocation lines. The films contained traces of Mo that entered the oxide via atom diffusion from the metal substrate during annealing. The Mo ions are responsible for a strong electron-donor character of the material, which controls its reactivity towards electronegative adsorbates, such as oxygen and gold [3,4].

STM conductance spectra taken at the conduction band onset of a thick CaO film exhibit regular dI/dV oscillations that vary with film thickness and experimental setpoint conditions. After correcting the dI/dV traces for the impact of the tip electric field, a unique energy spacing of (82±10) meV is obtained. The underlying excitations are assigned to CaO

longitudinal optical (LO) phonons [5], being emitted as the electrons move through the oxide lattice. The mode-energy experiences local variations, reflecting the different structural quality of the oxide lattice. Our work demonstrates that new physical phenomena become evident in STM experiments on thin dielectric films with increasing thickness, where the dominant electron-transport scheme changes from a tunneling to a hopping regime.

This work has been supported by the DFG Excellence Project 'UNICAT', the FIRB Project RBAP115AYN and the COST Action CM1104. Y. C. is grateful for a fellowship of the Humboldt Foundation.

[1] Y. Cui, S. Tosoni, W.-D. Schneider, G. Pacchioni, N. Nilius, and H.-J. Freund, Phys. Rev. Lett. (in print).

[2] X. Shao, P. Myrach, N. Nilius, and H.-J. Freund, J. Phys. Chem. C **115**, 8784 (2011).

[3] Y. Cui, X. Shao, M. Baldofski, J. Sauer, N. Nilius, and H.-J. Freund, Angew. Chem. Int. Ed. **52**, 11385 (2013).

[4] X. Shao, S. Prada, L. Giordano, G. Pacchioni, N. Nilius, and H. J. Freund, Angew. Chem. Int. Ed. **50**, 11525 (2011).

[5] D. H. Saunderson and G. E. Peckham, J. Phys. C: Solid State Phys. **4**, 2009 (1971).

In situ observation of Pd(553) surface structure dynamics during CO oxidation

M. Shipilin[1], J. Gustafson[1], C. Zhang[1], L. R. Merte[1], E. Lundgren[1]
[1] *Division of Synchrotron Radiation Research, Lund University, Lund, Sweden*

E-mail: mikhail.shipilin@sljus.lu.se

Over the past decades, vicinal surfaces have been used as model systems for fundamental studies in the field of heterogeneous catalysis, see for example Refs. [1,2]. After low-index single-crystal surfaces, vicinal single-crystal surfaces are used to bridge the materials gap. The inherent property of vicinal surfaces is the simultaneous presence of atomic terraces and steps that expose undercoordinated atoms. Thus, such a surface can mimic to a certain extent the edges between nanoparticles facets.

In this contribution we present results from *in situ* studies of a Pd(553) single-crystal acting as a model catalyst in the process of CO oxidation. It is well known that Pd is a highly efficient material for this process and both chemisorbed and oxide-like structures have been reported to be responsible for the activity.

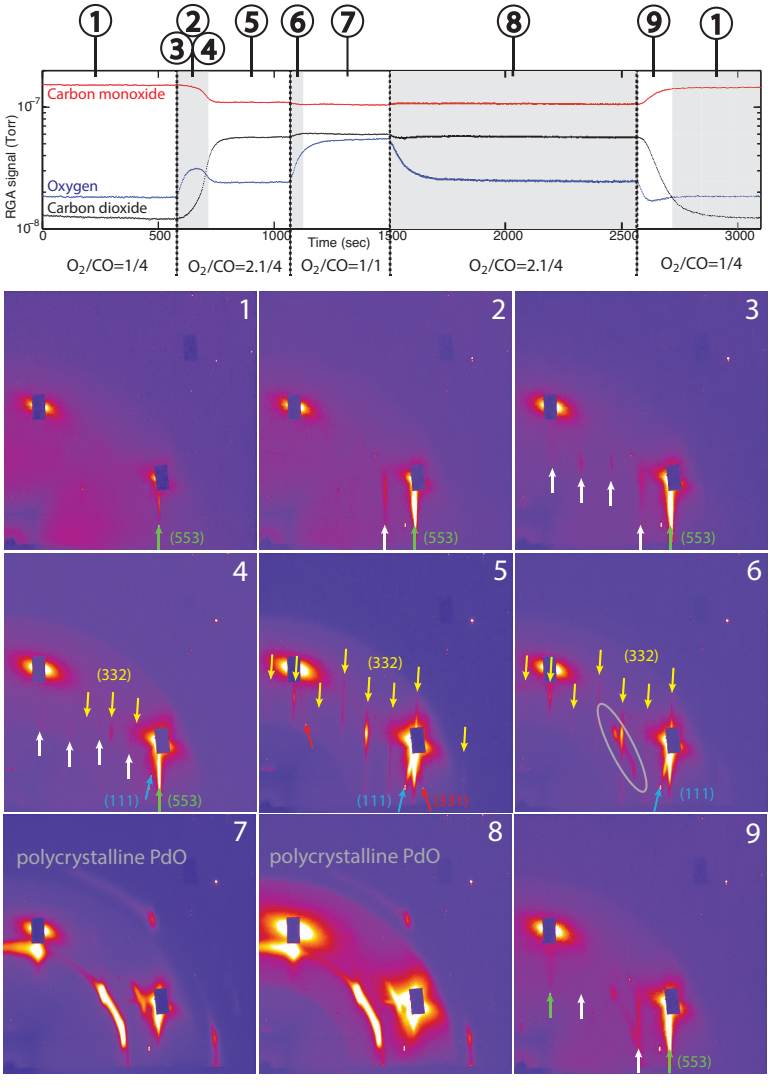

Fig.1 The mass-spectrometer signal showing the partial pressures of CO, O_2 and CO_2 gases detected in the reactor volume reproducing the semi-realistic conditions for catalytic CO oxidation reaction over the Pd(553) crystal (upper panel). Dashed vertical lines show the points where the oxygen flow was changed. Numbers in circles show which diffraction patterns were observed at certain conditions. The corresponding patterns are shown in the lower panel. Arrows of the same colour point to diffraction rods caused by the same surface structure.

We apply a high-energy surface X-ray diffraction experimental technique to investigate the evolution of the surface structure. Due to its photon-in-photon-out nature it allows for probing the structural changes of crystal surfaces under harsh reaction conditions, while the high energy of incoming radiation in combination with a large two-dimensional photon detector makes it possible to achieve a subsecond time-resolution to follow the dynamic surface restructuring [3,4].

The partial gas pressures in the CO and O_2 mixture over the sample are shown in figure 1 in conjunction with the corresponding diffraction patterns. The relative sample-detector orientation was set to the position where the *kl*-plane in reciprocal space can be constantly recorded and visualized. This orientation allows for observation of surface periodicity in the direction perpendicular to the steps on the (553) surface.

For an ingoing gas mixture of 1 mbar O_2 and 4 mbar CO, i.e. an O_2:CO ratio below stoichiometry, the mass-spectrometry reveals a low CO_2 production and the corresponding diffraction pattern is characteristic for a CO poisoned surface. After an increase of the O_2 partial pressure to 2.1 mbar (slightly above stoichiometry), the surface becomes catalytically active, while the diffraction data shows the sequential change of the periodicity of the surface structure. After further increase of the oxygen partial pressure the catalytic activity does not change significantly while the diffraction patterns show the formation of a polycrystalline oxide phase on the surface. Upon reducing the access of oxygen to the initial amount, the surface recovers to the CO poisoned state. Our experimental data obtained under reaction conditions partly correspond to the results presented in the Ref. [5], where the authors study the oxidation states of a Pd(553) crystal exposed to molecular oxygen at different pressures. Using this information we have a fingerprint for the type of oxygen induced surface structures during high-pressure CO oxidation conditions, revealing chemisorbed oxygen, surface oxide and bulk oxide formation. The details of the Pd(553) surface restructuring dynamics will be elucidated in the contribution.

Acknowledgements

This work is done within the Röntgen-Ångström collaboration "Catalysis on the atomic scale". The authors would like to thank the Swedish Research Council (349-2011-6491), the Swedish Foundation for Strategic Research (SSF) (RMA06-0085), the Crafoord foundation (20130825), the Knut and Alice Wallenberg foundation (2003.0217) and the Anna and Edwin Berger foundation.

References

[1] J. G.Wang,W. X. Li, M. Borg, J. Gustafson, A. Mikkelsen, T. M. Pedersen, E. Lundgren, J. Weissenrieder, J. Klikovits, M. Schmid, B. Hammer, and J. N. Andersen, Phys. Rev. Lett. **95**, 256102 (2005).

[2] J. Gustafson, A. Resta, A. Mikkelsen, R. Westerström, J. Andersen, E. Lundgren, J. Weissenrieder, M. Schmid, P. Varga, N. Kasper, X. Torrelles, S. Ferrer, F. Mittendorfer, G. Kresse, Phys. Rev. B **74** 035401 (2006).

[3] J. Gustafson, M. Shipilin, C. Zhang, A. Stierle, U. Hejral, U. Ruett, O. Gutowski, P.-A. Carlsson, M. Skoglundh, and E. Lundgren, Science **343** 758 (2014).

[4] M. Shipilin, U. Hejral, E. Lundgren, L. R. Merte, C. Zhang, A. Stierle, U. Ruett, O. Gutowski, P.-A. Carlsson, M. Skoglundh, J. Gustafson, Surface Science **630** 229 (2014).

[5] R. Westerström, J. Gustafson, A. Resta, A. Mikkelsen, J. N. Andersen, E. Lundgren, N. Seriani, F. Mittendorfer, M. Schmid, J. Klikovits, P. Varga, M. D. Ackermann, J. W. M. Frenken, N. Kasper and A. Stierle, Phys. Rev. B **76**, 155410 (2007).

Revisiting the CO chemisorption on stepped Pt(111) with a curved crystal surface: step-density dependent properties

A. L. Walter[1], J. Lobo-Checa[2], F. Schiller[2], L. Merte[3], J. Gustafson[3], E. Lundgren[3], D. Sánchez-Portal[2], M. Corso[4], and J. E. Ortega[1,2,4]

[1] *Donostia International Physics Center DIPC, San Sebastian, Spain*
[2] *Centro de Física de Materiales, CFM-CSIC, San Sebastian, Spain*
[3] *Department of Physics, Lund University, Sweden*
[4] *Departamento de Física Aplicada I, Univ. del País Vasco, San Sebastian, Spain*
E-mail: enrique.ortega@ehu.es

Stepped surfaces featuring arrays of atomic steps (of lattice constant *d*) are known to strongly influence relevant surface phenomena, such as chemical reactions. In fact, step atoms, due to their lower coordination, are preferred adsorption places and chemically active sites. However, it is not a-priori clear whether stepped surfaces promote or disturb a given physical-chemical process. One key parameter is the step density *1/d*, which may be critical, e.g., to enhance gas/surface heterogeneous catalysis. Using surfaces with curved shape one can smoothly vary the surface crystal orientation, i.e., the step-density *1/d* on a single sample, allowing a rational assessment of the influence of steps on surface chemical reactions.

Here we utilize a curved Pt(111) surface to revisit the chemisorption of CO on stepped Pt(111) [1]. We demonstrate the enormous potential of the curved surface approach, not only to study molecule/surface chemistry problems, but also to reveal subtle *1/d* properties of stepped surfaces, which straightforwardly arise by scanning the curved surface with spectroscopic and microscopic probes. In particular, we combine Scanning Tunnelling Microscopy (STM) and high-resolution X-ray Photoemission Spectroscopy (XPS), the latter using the small (100 micron) spot size beam provided in synchrotron facilities.

Our systematic *1/d* STM analysis is focused on the statistical distribution of the step array across the bare curved surface, at an atomic scale. Such study allows the striking, direct observation of the transition from entropic-repulsion to energetically-interacting steps. This transition was predicted time ago on the grounds of the elastic theory of stepped crystals [2], but it was never observed in a single sample. The entropic regime applies in sparse step lattices ($1/d<<1$), whereas at higher *1/d* values the elastic strain field of contiguous steps overlaps, effectively leading to a mutual repulsive interaction. The increasingly accumulating strain in surface (terrace) atoms is, in fact, evidenced in the *1/d* -dependent shift of the Pt 4f surface core-level, which is nicely imaged by a direct XPS scan on the curved surface (Fig. 1).

For the CO adsorption problem the curved surface allows one to immediately identify the hierarchy of the different surface sites [3]. On the one hand, the step preference versus the terrace on stepped surfaces, and on the other hand, the preferred on-top chemisorption for B-type steps versus the on-top and bridge for A type. Focusing on the very early adsorption stage, the *1/d* XPS scan on the curved surface directly reflects a remarkable property, namely a *1/d*-dependent, rapid transition from CO-covered to CO-free terraces. An abrupt sweep of CO molecules from terraces and their attachment to steps can only be explained by a dramatically increasing on-terrace diffusion length for CO away from the (111) direction. Our theory reveals that such behaviour is also explained by the *1/d*-increasing lattice strain that characterizes stepped surfaces, which directly influences the adsorption energy [4], and hence the CO diffusion length.

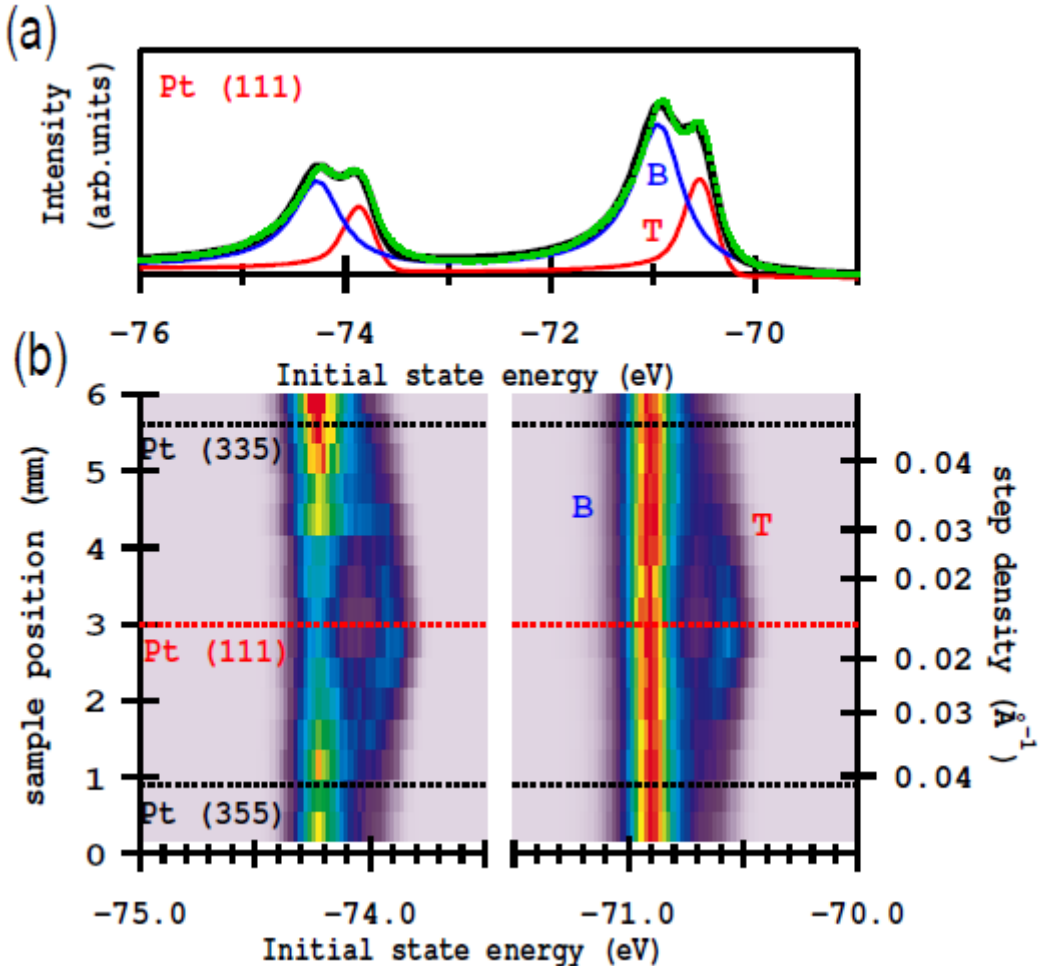

Fig. 1 (a) Pt 4f XPS spectra taken from the (111) plane of the curved Pt(111) crystal. A least-squares fitting to the spectra is shown, which indicates two components, one (B, blue) associated with bulk atoms and another one (T, red) associated with surface atoms. (b) XPS image showing the evolution of the Pt 4f spectra across the curved surface. A characteristic step-density-dependent shift is observed in the surface component, which is explained as due to the 1/d-dependent increasing strain at the surface plane.

Acknowledgements

We acknowledge financial support from the Spanish Ministry of Economy (MAT2013-46593-C6-4-P), Basque Gouvernment (IT621-13). ALW acknowledges support from the Donostia International Physics Centre in San Sebastian, Spain and the Director, Office of Science, Office of Basic Energy Sciences, of the U.S. Department of Energy.

References

[1] Curved crystals are provided by *Bihurcrystal Ltd.* (http://www.bihurcrystal.com/)
[2] H. C. Jeong and E. D. Williams, Surf. Sci. Rep. **34**, 171 (1999).
[3] See for example B. Tränkenschuh, C. Papp, T. Fuhrmann, R. Denecke, and H. P. Steinrück, Surf. Sci. **601**, 1108 (2007).
[4] M. Gsell, P. Jakob, and D. Menzel, Science **280**, 717 (1998); A. Schlapke, M. Lischka, A. Groß, U. Käsberger, and P. Jakob, Phys. Rev. Lett. **91**, 016101 (2003).

Ceria on Cu(110): formation of nanostripe strain defects

[1]Liying Ma, [1]Nassar Doudin, [1]Svetlozar Surnev, [2]Giovanni Barcaro, [2]Luca Sementa, [1]Venu Makad, [2]Alessandro Fortunelli, [1]Falko P. Netzer

[1]Surface and Interface Physics, Institute of Physics, Karl-Franzens University, A-8010 Graz, Austria

[2]CNR-ICCOM & IPCF, Consiglio Nazionale delle Ricerche, I-56124 Pisa, Italy

(falko.netzer@uni-graz.at)

The growth morphology and atomic geometry of ceria nanostructures on Cu(110) have been investigated by STM, LEED, XPS, and DFT calculations. Ceria grows epitaxially in a two-dimensional (2-D) hexagonal layer, which is associated with a CeO_2(111)-type trilayer structure forming a (3x11) coincidence lattice. An important experimental parameter is the oxygen pressure during growth: it influences the stoichiometry of the ceria overlayer as well as the Cu surface oxide phase, which coexists with the ceria for coverages below the full monolayer. For oxygen pressures in excess of 10^{-7} mbar, stoichiometric CeO_2 and coexisting CuO-c(6x2) surface oxide are formed, whereas for lower oxygen pressures, in the 10^{-8} mbar range, slightly substoichiometric ceria ($CeO_{\sim 1.9}$) and a CuO-(2x1) surface oxide are observed. The DFT + U calculations have been performed on a somewhat simplified (3x2) overlayer lattice. They reveal that the most stable situation is a single CeO_2(111)-type trilayer on a strongly reconstructed Cu-O interfacial layer (figure 1b). The measured STM height of the ceria overlayer with respect to the substrate depends on the bias voltage, but converges to ~ 4.25 Å for bias values beyond the ceria conduction band edge. This is compatible with the geometry parameters derived from the DFT model (figure 1b).

The ceria overlayer grows essentially 2-D, but displays a peculiar nanostripe pattern, with varying periodicities ranging from 4-8 nm and a corrugation amplitude of 0.2-0.3 nm (figure 1a). This nanostripe pattern is interpreted as due to a topographic modulation of the overlayer, caused by the frustration of the overlayer-substrate bonding as a result of the epitaxial mismatch at the ceria-Cu interface, as it has been postulated recently for a 2-D NaCl layer on Cu(110) [1]. Detailed STM investigations with ultrahigh resolution reveal that the ceria lattice is distorted in the transition region between dark (low) and bright (high) stripes, which gives rise to periodic regions of anisotropic lattice strain - socalled "lattice strain defects". It is speculated that these lattice strain defects may support a particular surface chemistry.

[1] M. Wagner, F.R. Negreiros, L. Sementa, G. Barcaro, S. Surnev, A. Fortunelli, F.P. Netzer, Phys. Rev. Lett. 110, 216101 (2013)

Work supported by the ERC Advanced Grant "SEPON", by the FWF Project P26633-N20, and by the COST Action CM1104

Figure 1:

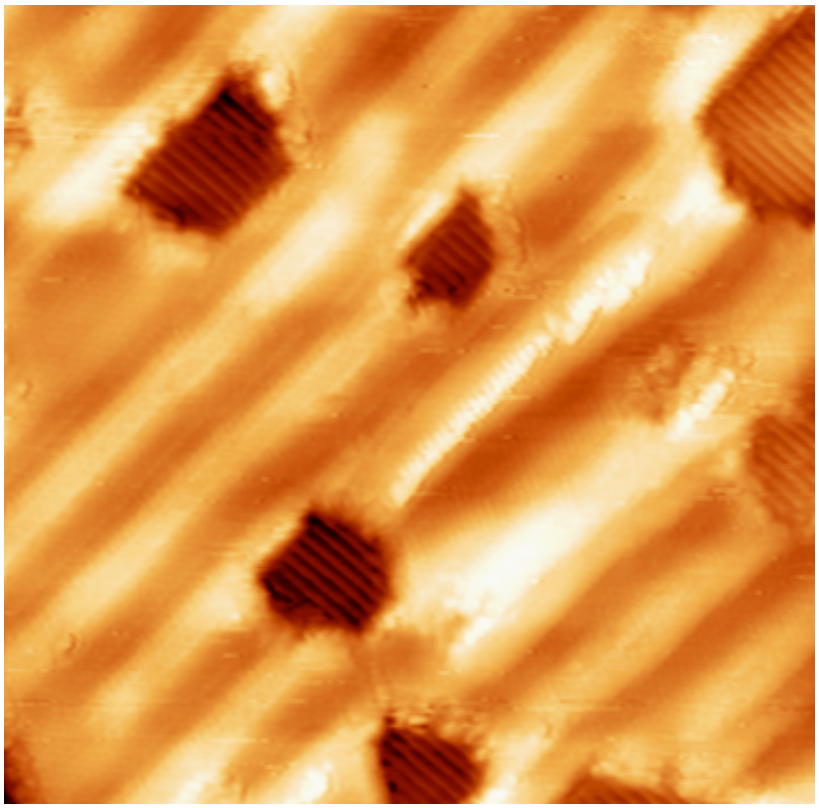

(a) STM image of ~1 ML ceria on Cu(110) (29 x 29 nm^2; +1.45 V; 0.1 nA). Note the CuO-(2x1) surface oxide structure in the dark vacancy holes.

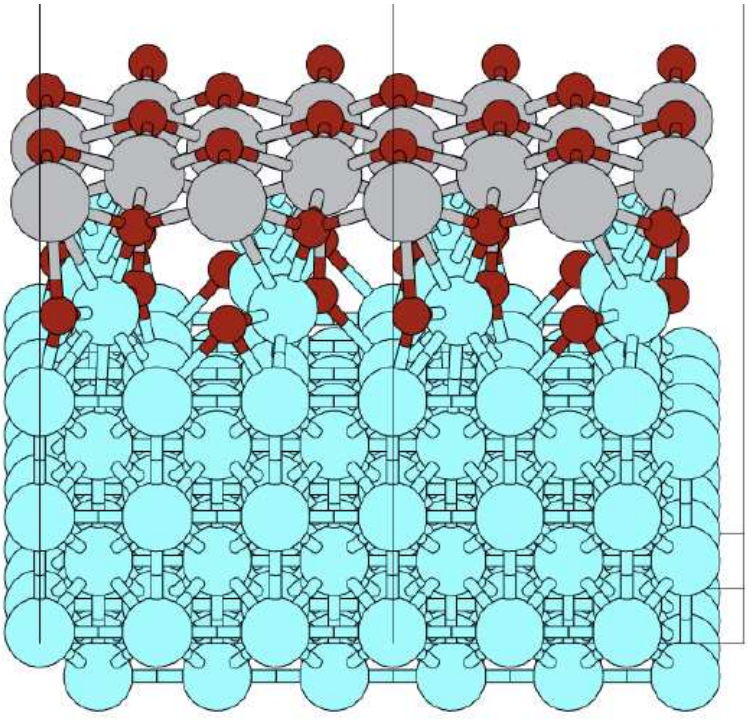

(b) DFT model of a CeO_2 (111) trilayer on a CuO_x interface on Cu(110) (light blue: Cu; grey: Ce; red: O).

Recent Advances In High Resolution Real And Reciprocal Space Photoelectron Emission Microscocopy

Konrad WINKLER[1], Nicholas BARRETT[2], Claire Mathieu[2], Nils Weber[3], Matthias Escher[3]

Email: k.winkler@omicron.oxinst.com

[1]*Omicron NanoScience, Germany,* [2]*CEA/DSM/IRAMIS/SPCSI, F-91191 Gif-sur-Yvette, France,* [3]FOCUS GmbH, *Germany*

Conventional electron spectroscopy methods are limited in providing simultaneous real and reciprocal or k-space information from small areas under laboratory conditions. Therefore, the characterization of materials with only micron scale sample homogeneity requires new instrumentation. Recent improvements in aberration compensated energy-filtered photoelectron emission microscopy (PEEM) can overcome the known limitations in both synchrotron and laboratory environments.

We present first results from real and reciprocal space photoelectron emission microscopy (PEEM) e.g. on Ag (111) showing high k and high energy resolution using a laboratory based He I and II radiation at room temperature and temperatures below 40K [1]. The combination of a recently developed LHe cooled sample stage [2] with an improved aberration compensated energy-filter allows 30 meV energy resolution while a new type of event counting detector improves the signal to noise ratio of the detector.

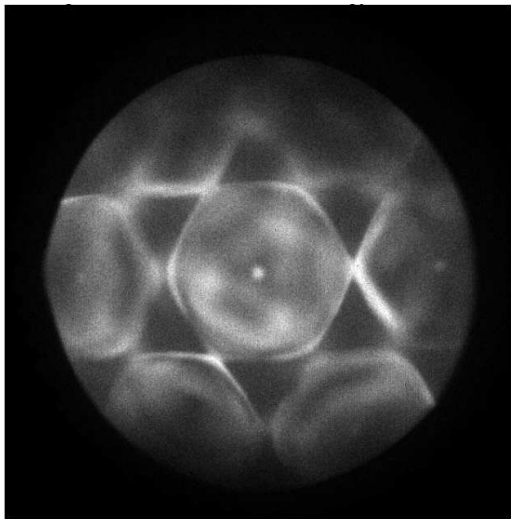

Figure 1: Photoemission data excited by a laboratory VUV light source (He II) from a Ag(111) surface at room temperature. The photoemission horizon (±90° start angles) corresponds to 6.0 (±0.1) $Å^{-1}$. The surface state visible in the centre of the image surrounded by six neighboring surface states defines a circle with a diameter of 5.02 $Å^{-1}$ used to scale this image.

References

[1] C. Mathieu et all, Breakthrough in high energy resolution photoelectron emission microscopy, submitted to Ultramicroscopy 2014

[2] N. Barrett et all, Laboratory-based real and reciprocal space imaging of the electronic structure of few layer graphene on SiC(000-1) using photoelectron emission microscope, Ultramicroscopy, 130 (2013), 94.

3D atomic structure analysis around active-site atoms

Fumihiko Matsui[1], Tomohiro Matsushita[2], Koichi Hayashi[3], Hiroshi Daimon[1]
[1] *Graduate School of Materials Science, Nara Institute of Science and Technology (NAIST), Japan*
[2] *Japan Synchrotron Radiation Research Institute, SPring-8, Sayo, Hyogo 679-5198, Japan*
[3] *Institute for Materials Research, Tohoku University, Sendai 980-8577, Japan*
E-mail: daimon@ms.naist.jp

An active-site atom plays an important role in a functional material, such as a dopant boron atom in a p-type Si semiconductor. However the 3D atomic structure analysis around this kind of specific atom has been impossible by a standard structure analysis method such as an x-ray diffraction because this kind of active site has no translational symmetry. Several methods to analyse the 3D atomic structure around this kind of specific atoms with no translational symmetry have been developed around 1990's such as "photoelectron holography" [1,2], and "fluorescent x-ray holography" [3]. Their accuracy to reproduce the atomic positions, however, has not been enough to investigate their structure in detail. Recently their accuracy improved dramatically by the development of analysis code [4] and sensitive detectors for fluorescent x-ray holography [5]. A new technique of direct 3D atomic structure analysis method "stereo photograph of atomic arrangement" has also developed [6]. These techniques received renewed attention recently because of its theoretical interest and potential technological applications. Hence we started a project of "3D active-site science" supported by JSPS Grant-in-Aid for Scientific Research on Innovative Areas: Grant Number 26105001. Main subjects in this project are ranging from inorganic materials to bio-materials, such as the dopant in semiconductor or oxides, the active-centre in catalysis, the interface structure in organic devices, the photochemical centre of photosynthesis proteins and so on.

In this presentation some example of recent "stereo photograph of atomic arrangement" (Fig.), "photoelectron holography" [7], and "fluorescent x-ray holography" [8] will be demonstrated.

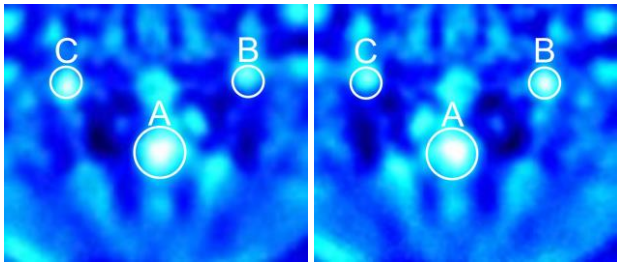

Fig. Stereo photograph of atomic arrangement around In atom in InP crystal.

References

[1] A. Szo¨ke: AIP Conf. Proc. 147 (1986) 361.
[2] J. J. Barton: Phys. Rev. Lett. 61 (1988) 1356.
[3] M. Tegze, G. Faigel, Europhys. Lett. 16 (1991) 41.
[4] T. Matsushita, A. Yoshigoe, and A. Agui: Europhys. Lett. 71 (2005) 597.
[5] K. Hayashi, N. Happo, S. Hosokawa, W. Hu, and T. Matsushita, *J. Phys.: Condens. Matter* **24** (2012) 093201.
[6] H. Daimon: Phys. Rev. Lett. 86 (2001) 2034.
[7] F. Matsui, T. Matsushita and H. Daimon, J. Phys. Soc. Jpn 81 (2012) 114604.
[8] K. Hayashi, N. Happo, S. Hosokawa, J. Electr. Spectr. Relat. Phenom. 195 (2014) 337.

List of Participants

Participants	Email	Country	Institution
Andrieu, S.	stephane.andrieu@univ-lorraine.fr	France	*Université de Lorraine*
Arnau, A.	andres.arnau@ehu.es	Spain	*Universidad del Pais Vasco*
Aumayr, F.	aumayr@iap.tuwien.ac.at	Austria	*TU Wien*
Auwärter, W.	wau@tum.de	Germany	*Technische Universität München*
Åhlund, J.	john.ahlund@vgscienta.com	Sweden	*VG Scienta*
Barth, J.	jvb@tum.de	Germany	*TUM*
Bauer, P.	peter.bauer@jku.at	Austria	*Johannes Kepler University*
Berghaus, T.	t.berghaus@nanoscore.de	Germany	*Nanoscor gmbh*
Bichara, C.	xtof@cinam.univ-mrs.fr	France	*CNRS*
Buck, M.	mb45@st-andrews.ac.uk	UK	*University of St Andrews*
Cheynis, F.	cheynis@cinam.univ-mrs.fr	France	*Aix-Marseille University*
Chulkov, E.	waptctce@ehu.es	Spain	*Basque Country University*
Coraux, J.	johann.coraux@neel.cnrs.fr	France	*Université Grenoble Alpes*
Curiotto, S.	curiotto@cinam.univ-mrs.fr	France	*Aix-Marseille Université*
Daimon, H.	daimon@ms.naist.jp	Japan	*Nara Inst. of Science and Technology*
de Oteyza, D.	d_g_oteyza@ehu.es	Spain	*Donostia International Physics Center*
Diebold, U.	diebold@iap.tuwien.ac.at	Austria	*TU Wien*
Dil, H.	hugo.dil@epfl.ch	Switzerland	*Ecole Polytechnique Fédérale de Lausanne*
Eberhardt, D.	eberhard@physik.tu-berlin.de	Germany	*TU Berlin*
Eberhardt, W.	wolfgang.eberhardt@cfel.de	Germany	*DESY-CFEL*
Ernst, K.	karl-heinz.ernst@empa.ch	Suisse	*Empa*
Filimonov, S.	filimon@phys.tsu.ru	Russia	*Tomsk State University*
Garreau,Y.	garreau@synchrotron-soleil.fr	France	*Université Paris-Diderot*
Gölzhäuser, A.	ag@uni-bielefeld.de	Germany	*University of Bielefeld*
Günther, S.	sebastian.guenther@tum.de	Germany	*Technische Universität München*
Giessibl, F.	franz.giessibl@ur.de	Germany	*Universitaet Regensburg-Physik*
Gustafson, J.	johan.gustafson@sljus.lu.se	Sweden	*Lund University*
Heinzmann, U.	uheinzm@physik.uni-bielefeld.de	Germany	*University of Bielefeld,*
Hendriksen, B.	b.hendriksen@science.ru.nl	The Netherlands	*Radboud University Nijmegen*
Johansson, L.	lars.johansson@kau.se	Karlstad	*Karlstad University*
Klappenberger, F.	florian.klappenberger@tum.de	Germany	*Physik Department E20*
Koshikawa, T.	kosikawa@isc.osakac.ac.jp	Japan	*Osaka Electro-Communication Univ.*
Krylov, S.	krylov@physics.LeidenUniv.nl	Russia	*Russian Academy of Sciences*
Le Lay, G.	guy.lelay@univ-amu.fr	France	*Aix-Marseille University*
Leroy, F.	leroy@cinam.univ-mrs.fr	France	*Aix-Marseille University*
Libuda, J.	joerg.libuda@fau.de	Germany	*University Erlangen-Nuernberg*
Lineke, B.	maria.messing@sljus.lu.se	Sweden	*Lund University*
Lundgren, E.	edvin.lundgren@sljus.lu.se	Sweden	*Lund University*
Maier, M.	markus.maier@oxinst.com	Germany	*Omicron NanoTechnology GmbH*
Marbach, H.	hubertus.marbach@fau.de	Germany	*Friedrich-Alexander-Univ.*
Margraf, R.	romarg@arcor.de	Germany	*Naturheilpraxis Margraf*
Mårsell, E.	erik.marsell@sljus.lu.se	Sweden	*Lund University*
Messing, M.	maria.messing@ftf.lth.se	Sweden	*Lund University*
Müller, P.	muller@cinam.univ-mrs.fr	France	*Aix-Marseille University*
Navarro-Paredes, V.	navarro@physics.leidenuniv.nl	Netherlands	*Leiden University*

Netzer, F.	falko.netzer@uni-graz.at	Austria	*Karl-Franzens University*
Ortega, E.	enrique.ortega@ehu.es	Spain	*Universidad del Pais Vasco*
Protogenov, A.	alprot@appl.sci-nnov.ru	Russia	*Institute of Applied Physics of the RAS*
Renaud, G.	gilles.renaud@cea.fr	France	*CEA INAC/SP2M*
Repain, V.	vincent.repain@univ-paris-diderot.fr	France	*Université Paris Diderot*
Resta, A.	andrea.resta@synchrotron-soleil.fr	France	*Synchrotron Soleil*
Roncin, P.	philippe.roncin@u-psud.fr	France	*CNRS*
Schneider, W.	wolf-dieter.schneider@epfl.ch	Switzerland	*Ecole Polytechnique de Lausanne*
Setvin, M.	setvin@iap.tuwien.ac.at	Austria	*Vienna University of Technology*
Shipilin, M.	mikhail.shipilin@sljus.lu.se	Sweden	*Lund University*
Silkin, V.	waxslavas@ehu.es	Spain	*Donostia Int. Physics Center*
Taglauer, E.	edmund.taglauer@web.de	Germany	*Max-Planck-Institut für Plasmaphysik*
Thornton, G.	g.thornton@ucl.ac.uk	UK	*UCL*
van Baarle, D.	baarled@physics.leidenuniv.nl	Netherlands	*Leiden University*
Varga, P.	varga@iap.tuwien.ac.at	Austria	*Vienna University of Technology*
Widdra, W.	wolf.widdra@physik.uni-halle.de	Germany	*Martin-Luther-Universität Halle*
Widmer, R.	roland.widmer@empa.ch	Switzerland	*Empa*
Woell, C.	Christof.woell@kit.edu	Germany	*Karlsruhe Institute of Technology*
Wutte, U.	ursula.wutte@gmx.at	Austria	*Vienna University of Technology*
Yuhara, J.	j-yuhara@nagoya-u.jp	Japan	*Nagoya University*

VG SCIENTA

DEVELOPMENT NOTE

Scienta HiPP-3 performance

The Scienta HiPP-3 analyser features a newly developed, patent pending, technology for outstanding imaging XPS as well as a newly developed Swift Acceleration Mode enabling unparalleled transmission.

Unparalleled transmission

The HiPP-3 analyser features a new and improved version of the Swift Acceleration Mode. With this mode, electrons are accelerated towards the analyser by a large voltage applied to the second aperture of the differential pumping stage, see figure 1. With this feature, transmission is increased by more than an order of magnitude.

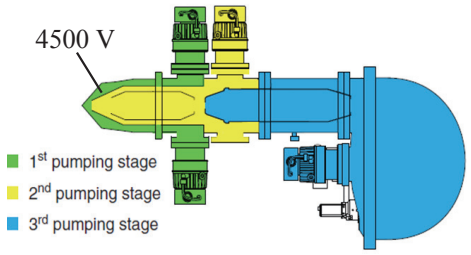

Figure 1: Differential pumping stages in Scienta R4000 HiPP-3. The arrow indicates where a high voltage is applied to accelerate electrons into analyser.

Transmission tests have been performed with the Scienta MX650 HP Al Ka x-ray source. The resulting pressure dependence can be seen in figure 2. The figure shows a pressure series of Ag 3d from vacuum up to 25 mbar of N_2.

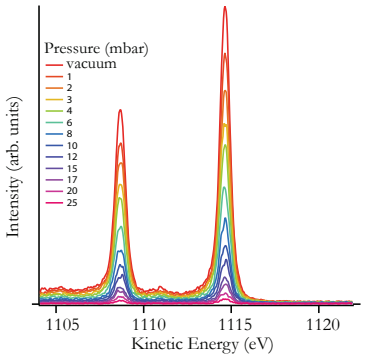

Figure 2: Ag 3d spectra recorded in different pressure of N_2. The measurement time for each spectrum was 60 seconds.

For more information, please contact one of our sales offices

SWEDEN OFFICE
+46 (0)18 480 58 00
Info@vgscienta.com

USA OFFICE
+1-720 350 5000
Bill. Gerace@vgscienta.com

JAPAN OFFICE
+81 (0)3 5842 5885
Japansales@vgscineta.com

CHINA OFFICE
+86 (0) 10 5815 6051
Chinasales@vgscienta.com

or visit

www.vgscienta.com

Outstanding imaging mode

The HiPP-3 analyser features a revolutionary imaging mode. This mode enables parallel imaging in one direction with a guaranteed resolution of better than 10 µm in a field of view of up to 0.8 mm. This mode is avaliable in both UHV and at ambient conditions.

Figure 3 show test data of the imaging mode. Test measurements have been performed at a dedicated development system at VG Scienta using the Scienta MX650 HP, which is an Al a monochromatic x-ray source adapted for high pressure, and a special test sample with narrow gold lines on silicon. In this study, gold lines with the width of 40 µm have been used. Measurements have been performed for the Au 4d core level. The bottom figure show a cut out of the detector image. From the slope of the curve, a spatial resolution of better than 5 µm has been demonstrated.

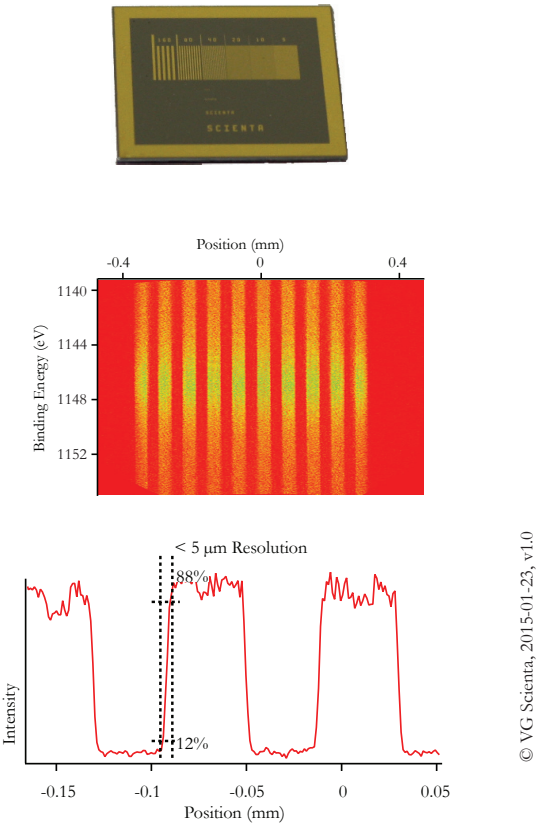

Figure 3: Demonstration of spatial resolution. **Top:** A special test sample consisting of narrow lines of Au on Si, with the sample region magnifiifed to the right. **Center:** Detector image showing parallel detection of kinetic energy and emission position. **Bottom:** Integrated spectrum showing a spatial resolution of better than 5 µm. This resolution is acheived by a new patent pending imaging technology.

3S'15 Symposium on surface science

	Monday	Tuesday	Wednesday	Thursday	Friday	
8h15	***Welcome***	*Chair: Filimonov*	*Chair: Leroy*	*Chair: Schneider*		*Chair: Diebold / Koshikawa*
	Chair: Thornton					
8h20	01-Dil	13-Barth	25-Yuhara	34-Giessibl	**8h20**	43-Schneider
8h40	02-Le Lay	14-Buck	26-Resta	35-Hendriksen	**8h40**	44-Shipilin
9h00	*Discussion time*	*Discussion time*	*Discussion time*	***Slalom race***	**9h00**	45-Ortega
12h00	***Lunch***	***Lunch***	***Lunch***	***Lunch***	**9h20**	46-Netzer
14h00	*Discussion time*	*Discussion time*	*Discussion time*	*Discussion time*	**9h40**	47-Maier
16h15	*Chair: Andrieu / Lundgren*	*Chair: Buck / Varga*	*Chair: Netzer / Renaud*	*Chair: Bauer / Garreau*	**10h00**	48-Daimon
16h20	03-Repain	15-Ernst	27-Curiotto	36-Koshikawa	**10h 20**	***Award Ceremony*** *Chair: Aumayr*
16h40	04-Coraux	16-Auwärter	28-Garreau	37-Marsell	**11h00**	*Discussion time*
17h00	05-Bichara	17-Klapenberger	29-Gustafson	38-Åhlund	**12h00**	**Lunch**
17h20	06-Renaud	18-Marbach	30-Widmer	39-Heinzman	**14h00**	*Discussion time*
17h40	07-van Baarle	19-Filimonov	31-Navarro	40-Andrieu	**17h00**	**2nd Poster session**
18h00	08-Günther	20-Arnau	32-Lundgren	41-Varga		
18h20	09-Roncin	21-Diebold	33-Brummel	42-Protogenov		
19h00	***Dinner***	***Dinner***	**Poster presentation** *Chair: Le Lay*	***Dinner***	**19h00**	***Dinner***
	Chair: Bichara	*Chair: Arnau*				
20h20	10-Aumayr	22-Wöll	**Conference dinner**	**1st Poster session**		
20h40	11-Gölzhäuser	23-Setvin				
21h00	12-Bauer	24-Thornton				
21h20	*Discussion time*	*Discussion time*				

Sunday	
15h	Reception
19h	**Dinner**
20h	Free time